THESIS FOR THE DEGREE OF DOCTOR OF PHILOSOPHY

Interplay of the Electrical and Mechanical Properties of Conjugated Polymers

Improving the Mechanical Properties of Polythiophenes with Oligoethylene Glycol Side Chains

Sepideh Zokaei

Department of Chemistry and Chemical Engineering

CHALMERS UNIVERSITY OF TECHNOLOGY

Gothenburg, Sweden 2022

Department of Chemistry and Chemical Engineering
Chalmers University of Technology
SE-412 96 Gothenburg
Sweden
Telephone + 46 (0)31-772 1000

Cover:
Illustration of different strategies for tuning the properties of the materials. If the right strategy is selected, the product material will possess characteristics that are suitable for the desired application. The cover is designed by Mariza Mone.

Interplay of the Electrical and Mechanical Properties of Conjugated Polymers

Improving the Mechanical Properties of Polythiophenes with Oligoethylene Glycol Side chains

SEPIDEH ZOKAEI

Department of Chemistry and Chemical Engineering

Chalmers University of Technology

ABSTRACT

Knowledge about organic semiconductors has drastically developed in the past decades. They have a myriad of applications in areas such as energy harvesting and storage, bioelectronics and wearable electronics. For most of these applications, mechanical flexibility is desirable. Conjugated polymers, a class of organic semiconductors, tend to be brittle and rigid. The latter is a consequence of their planar-aromatic backbones that endow them with a high glass transition temperature and a tendency to strongly aggregate. Polythiophenes with oligoethylene glycol side chains, on the contrary, tend to be soft materials with a low glass transition temperature and low degree of crystallinity, which limit their use as a bulk free-standing material. At the same time, they can feature high ionic and electrical conductivity. This thesis explores different strategies to modulate the mechanical properties of polythiophenes with polyethylene glycol side chains without unduly affecting their electrical properties.

This thesis will compare the mechanical and electrical properties of a soft polythiophene and a copolymer of the same material with hard urethane blocks, which enable the formation of a reversible network. Then, blending of a doped soft conjugated polymer with melt-processable insulating polymers such as polycaprolactone is explored with the goal to prepare thermally stable blends for melt-processing. Conducting stretchable fibers of a doped conjugated polymer and a polyurethane elastomer are demonstrated that feature a high degree of electrical and mechanical stability. Further, the properties of composites with cellulose nanomaterials are described. The nanocomposites feature a high elastic modulus, and the presence of cellulose nanofibrils does not affect the electrical conductivity. Finally, the impact of molecular doping, which is an essential step for rendering the conjugated polymers conductive, on the nanostructure and thermomechanical properties of polythiophenes with oligoethylene glycol side chains is explored. In particular, doping is found to strongly increase the elastic modulus of the polymer. Evidently, a wide range of methods such as copolymerization, blending, the use of a reinforcing agent as well as molecular doping itself can be used for the which may facilitate the design of mechanically robust electrical conductors.

keywords: organic electronics, conjugated polymers, mechanical properties, electrical properties, blends, composites, copolymers, doping, conducting fibers

To my parents,
Fariba and Jafar

NOMENCLATURE

Symbols and Abbreviations

A	Absorbance
ε	Strain
μ	Charge carrier mobility
σ	Electrical conductivity
σ	Stress
ν	Poisson ratio
ω	Angular velocity
CNC	Cellulose nanocrystal
CNF	Cellulose nanofibril
DSC	Differential scanning calorimetry
DMA	Dynamic mechanical analysis
E	Elastic modulus
E′	Tensile storage modulus
$E^{"}$	Tensile loss modulus
E^{*}	Complex modulus
E-textile	electronic textiles
FFF	Fused filament fabrication
FTIR	Fourier transform infrared
G'	Shear storage modulus
$G"$	Shear loss modulus
GIWAXS	Grazing-incidence wide-angle X-ray scattering
HOMO	Highest occupied molecular orbital
IE	Ionization energy
M_n	Number average molar mass
MFC	Microfibrillated cellulose
n	Charge carrier density
LUMO	Lowest unoccupied molecular orbital
M_n	Molecular weight

OECT	Organic electrochemical transistor
OLED	Organic light-emitting diode
P	Polymer
PDI	Polydispersity index
q	Electric charge of the charge carrier
R	Resistance
SEM	Scanning electron microscopy
PDI	Polydispersity index
T_g	Glass transition temperature
TGA	Thermogravimetric analysis
WAXS	Wide-angle X-ray scattering

Chemicals

[EMIM][BF$_4$]	1-ethyl-3-methylimidazolium tetrafluoroborate
AcN	Acetonitrile
BDT	Benzodithiophene
BR	Butyl rubber
CB	Chlorobenzene
CH$_3$Cl	Chloroform
DDQ	2,3-dichloro-5,6-dicyano-1,4-benzoquinone
DMF	N,N-dimethylformamide
DMSO	Dimethyl sulfoxide
DPP	Diketopyrrolopyrrole
EAA	Poly(ethylene-*co*-acrylic acid)
F$_4$TCNQ	2,3,5,6-tetrafluoro-7,7,8,8-tetracyanoquinodimethane
FC	Ferrocene
Fc$^+$	Ferrocenium
Fe(Tos)$_3$	Iron (III) p-toluenesulfonate
H-TFSI	Bistriflimidic acid
ITO	Indium tin oxide
LiF$_4$TCNQ	Lithium salt of 2,3,5,6-tetrafluoro-7,7,8,8-tetracyanoquinodimethane
Magic Blue	Tris(4-bromophenyl)ammoniumyl hexachloroantimonate
Mo(tfd-COCF$_3$)$_3$	Molybdenum tris(dithiolene) complex
MWCNT	Multi-walled carbon nanotubes
p(g$_x$2T-T)	Thiophene based copolymer with oligoethylene glycol side chains
p[p(g$_4$2T-T)-*co*-U]	Copolymer of p(g$_4$2T-T) and urethane blocks
P3AT	Poly(3-alkylthiophene)
P3DDT	Poly(3-dodecylthiophene)
P3HT	Poly(3-hexylthiophene-2,5-diyl)
P3OT	Poly(3-octylthiophene)
PA	Polyacetylene
PANI	Polyaniline
PCBM	(6,6)-phenyl-C61-butyric acid methyl ester

PCL	Polycaprolactone
PDMS	Poly(dimethylsiloxane)
PDSA	1,3-propanedisulfonic acid
PEDOT:PSS	Poly(3,4-ethylenedioxythiophene):poly(styrenesulfonate)
PEO	Poly(ethylene oxide)
PET	Polyethylene terephthalate
PU	Polyurethane
SBS	Styrene-butadiene-styrene
SEBS	Styrene-ethylene-butylene-styrene
SWCNT	Single-walled carbon nanotube
TAZ	Benzotriazole
THF	Tetrahydrofuran
U	Urethane

PUBLICATIONS

This thesis consists of an extended summary of the following appended papers:

Paper I   **Toughening of a Soft Polar Polythiophene through Copolymerization with Hard Urethane Segments**

<u>Sepideh Zokaei</u>, Renee Kroon, Johannes Gladisch, Bryan D. Paulsen, Wonil Sohn, Anna I. Hofmann, Gustav Persson, Arne Stamm, Per-Olof Syrén, Eva Olsson, Jonathan Rivnay, Eleni Stavrinidou, Anja Lund and Christian Müller
Advanced Science, 2021, 8, 2002778

Paper II   **Conducting Elastomeric Fibers with High Stretchability and Stability**

<u>Sepideh Zokaei</u>, Mariavittoria Craighero, Claudia Cea, Lucas M. Kneissl, Renee Kroon, Dion Khodagholy, Anja Lund and Christian Müller
Small, 2021, 2102813

Paper III   **Tuning of the Elastic Modulus of a Soft Polythiophene through Molecular Doping**

<u>Sepideh Zokaei</u>, Donghyun Kim, Emmy Järsvall, Abigail M. Fenton, Albree R.Weisen, Sandra Hultmark, Phong H. Nguyen, Amanda M. Matheson, Anja Lund, Renee Kroon, Michael L. Chabinyc, Enrique D. Gomez, Igor Zozoulenko and Christian Müller
Materials Horizon, 2022, 9, 433-443

Paper IV   **Decoupling of the Electrical and Mechanical Properties of a Polythiophene through Doping with Bistriflimidic Acid**

Sandra Hultmark, Mariavittoria Craighero, <u>Sepideh Zokaei</u>, Donghyun Kim, Emmy Järsvall, Furqan Farooqi, Sara Marina, Renee Kroon, Jaime Martin, Igor Zozoulenko and Christian Müller
Manuscript in preparation

CONTRIBUTION REPORT

Paper I   Shared first author together with R.K, who designed and synthesized the co-polymer. Planned the study with C.M. and R.K. Carried out sample preparation, electrical measurements, spectroelectrochemistry, spectroscopy, fitting UV-vis spectra and determining charge carrier density. Performed mechanical measurements and WAXS together with A. L. Performed electrochemical swelling experiments with J. G., who analyzed them. OECTs were tested and analyzed by B. D. P., W. S., and J. R. Imaging was done by G. P. and E. O. Was responsible for data compilation. Conducted data analysis and interpretation and wrote main part of the paper together with C.M., R.K. and A. L.

Paper II   First author. Planned the experiments with A. L., C. M. and R. K. Performed mechanical and electrical characterization of fibers with M. C., who prepared the fibers with A. L. Strain sensor devices were designed by C. C. and D. R. Was responsible for data compilation. Conducted data analysis and interpretation and wrote main part of the paper together with A. L. and C. M.

Paper III   Shared first together with D. K. and E. J., and corresponding author with C. M. Led and planned the study and experimental design with C.M. Performed thermomechanical measurements and their analysis. D. K. and I. Z. performed molecular dynamics. E. J. did spectroscopy, and calculated oxidation levels. S. H. carried out fast scanning calorimetry measurements. A. F., A. W. and E. D. G. performed oscillatory shear rheometry measurements. A. L. carried out WAXS. P. N. and M. C. carried out the GIWAXS characterization. Compiled data, did data analysis and interpretation and wrote the paper together with C. M.

Paper IV   Carried out mechanical, electrical and thermal characterization together with S. H., M. C., F. F., and E. J. Contributed to data analysis and writing of the paper with C. M., S. H., and M. C.

RELATED PUBLICATIONS NOT INCLUDED IN THIS THESIS

Paper V   **Chemical Doping of Conjugated Polymers with the Strong Oxidant Magic Blue**

Anna I. Hofmann, Renee Kroon, <u>Sepideh Zokaei</u>, Emmy Järsvall, Claudia Malacrida, Sabine Ludwigs, Till Biskup and Christian Müller
Advanced Electronic Materials, 2020, 202000249

Paper VI   **Robust PEDOT:PSS Wet-Spun Fibers for Thermoelectric Textiles**

Youngseok Kim, Anja Lund, Hyebin Noh, Anna I. Hofmann, Mariavittoria Craighero, Sozan Darabi, <u>Sepideh Zokaei</u>, Jae Il Park, Myung-Han Yoon and Christian Müller
Macromolecular Materials and Engineering, 2020, 201900749

TABLE OF CONTENTS

1

INTRODUCTION

Polymers are omnipresent in our daily life and examples can be found everywhere from kitchen appliances to synthetic textiles in our clothes. Composed of many small repeating units linked together to form chains, polymers are usually colourless and electrical insulators. Polyethylene, the most common polymer, is used in power cables providing excellent insulating layers for preventing electricity leakage. However, there exists a peculiar class of polymers possessing color and electrical properties, so called conjugated polymers.

Ferdinand Runge introduced the oxidation of aniline for generating materials with colors. Later Henry Letheby developed that further and demonstrated the electrochemical oxidation of aniline in 1862.[1] However, The conductive properties of the reaction product, which was likely polyaniline, a type of conjugated polymer, were not discovered until a century later. Heeger, MacDiarmid, Shirakawa and their research teams discovered that oxidation of polyacetylene (PA) with iodine, bromine, or chlorine will produce an electroconductive material. This discovery was not only awarded the Nobel Prize in Chemistry in 2000 but also initiated the development of organic electronics using polymeric materials.[2]

Organic electronics have drastically developed during the past decades and are commercialized with organic semiconducting materials as the main element in light-emitting diodes (OLEDs) in displays.[2-6] There are many additional application areas being developed in academia and industry such as energy harvesting,[7-10] energy storage,[11, 12] bioelectronics[13-15] and wearable electronics.[4, 16-18] Organic electronics offer many advantages compared to their inorganic counterparts such as low cost, large-area fabrication, ease of processing and mechanical flexibility. Additionally, their properties can be tailored by chemical modification.[19]

Stretchable electronics, *i.e.,* electronic devices or materials with high deformability, have gained attention for wearable electronics[20-22] that can be used for electronic skin and health care applications. Wearable electronics can be in the format of electronic textiles (e-textiles)[23-27] offering advantages such as breathability and shape conformation.

Several strategies have been introduced to fabricate electronic materials or devices from organic semiconductors that feature reversible or irreversible stretchability. These strategies will later be described in this thesis.

1.1 Conjugated Polymers

Organic semiconductors can be small molecules or polymers. Conjugated polymers feature alternating single and double bonds along the backbone. The alternating bonds bring about overlapping π-orbitals, where the π-electrons can delocalize along the backbone.[28]
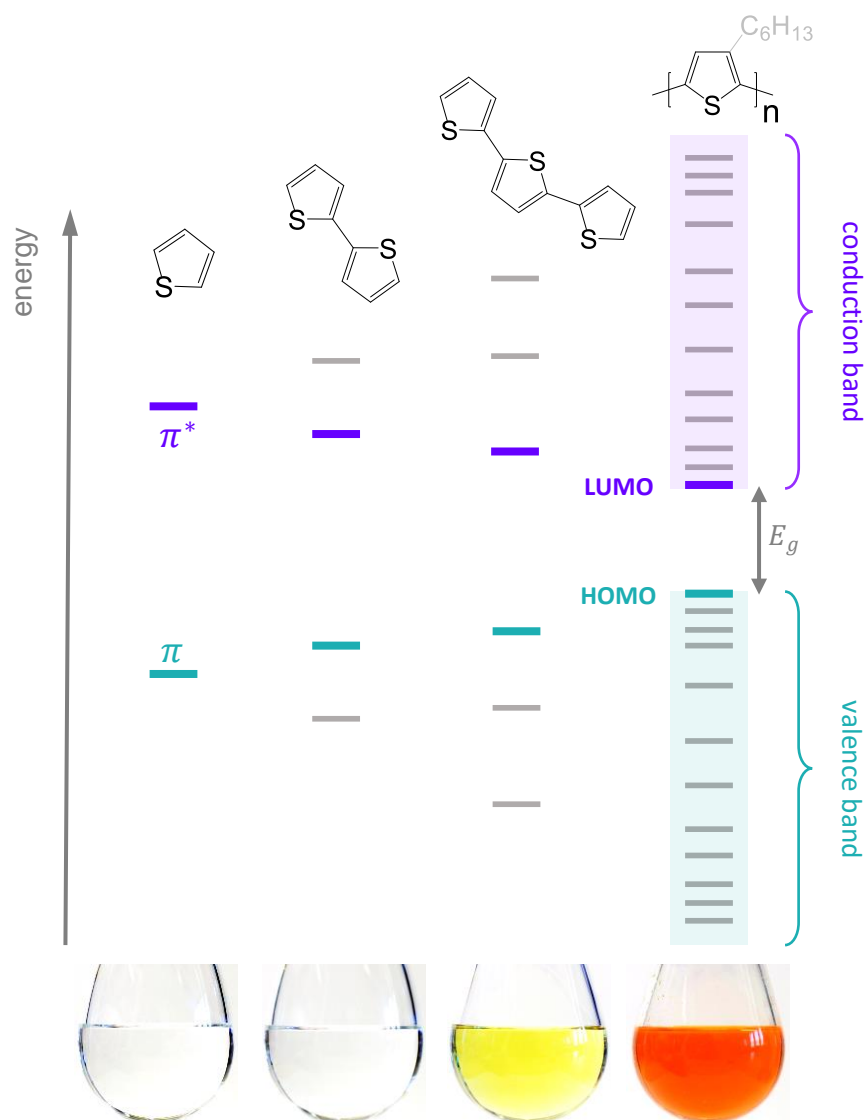
Figure 1.1 Evolution of the HOMO and LUMO levels as well as the band gap E_g with increasing number of thiophene repeat units, resulting in valence and conduction bands for polythiophene. Reproduced with permission from ref. [29] published by The Royal Society of Chemistry.

Energy level splitting of π-bonds gives rise to bonding π- and anti bonding π*-orbitals, composing the highest occupied molecular orbital (HOMO) and lowest unoccupied molecular orbital (LUMO), respectively (illustrated in Figure 1.1). The difference of the HOMO and LUMO energy levels is defined as the band gap (E_g). As the conjugation length of these polymers increases, E_g is narrowed down, giving rise to semiconducting behaviour. The E_g of conjugated polymers is typically in the range of 1 – 3 eV. Charge carriers (electrons or holes) can be injected into a conjugated polymer and transported through the π-orbitals. This process is called doping.[29, 30]

1.2 Molecular Doping of Conjugated Polymers

The electrical conductivity (σ) of a material is proportional to the charge carrier concentration (n) and charge carrier mobility (μ) (eq. 1.1).

$$\sigma = q\,n\,\mu$$

(eq. 1.1)

q = *electric charge of the charge carriers*

Doping takes place through two main mechanisms: (1) redox doping, *i.e.,* the partial or complete transfer of electrons, to form a donor–acceptor charge-transfer complex or ion pair, and (2) acid-base doping, *i.e.,* the transfer of a proton or hydride to the polymer backbone. The presence of a counter ion maintains charge neutrality. The illustration in Figure 1.2 shows the basic principles of acid-base and redox doping.

In redox doping, oxidizing agents accept electrons from the highest occupied molecular orbital, HOMO, of a conjugated polymer, resulting in the formation of holes on the conjugated polymer (p doping). Reducing agents, act as electron donners and give electrons to the lowest unoccupied molecular orbital, LUMO, level of a polymer (n doping). The produced holes or electrons increase the number of charges.[31] Upon doping, polarons, *i.e.,* delocalized radical cations or anions, emerge and bipolarons, *i.e.*, delocalized dications or dianions, start to appear with increasing doping concentration.[29, 30]
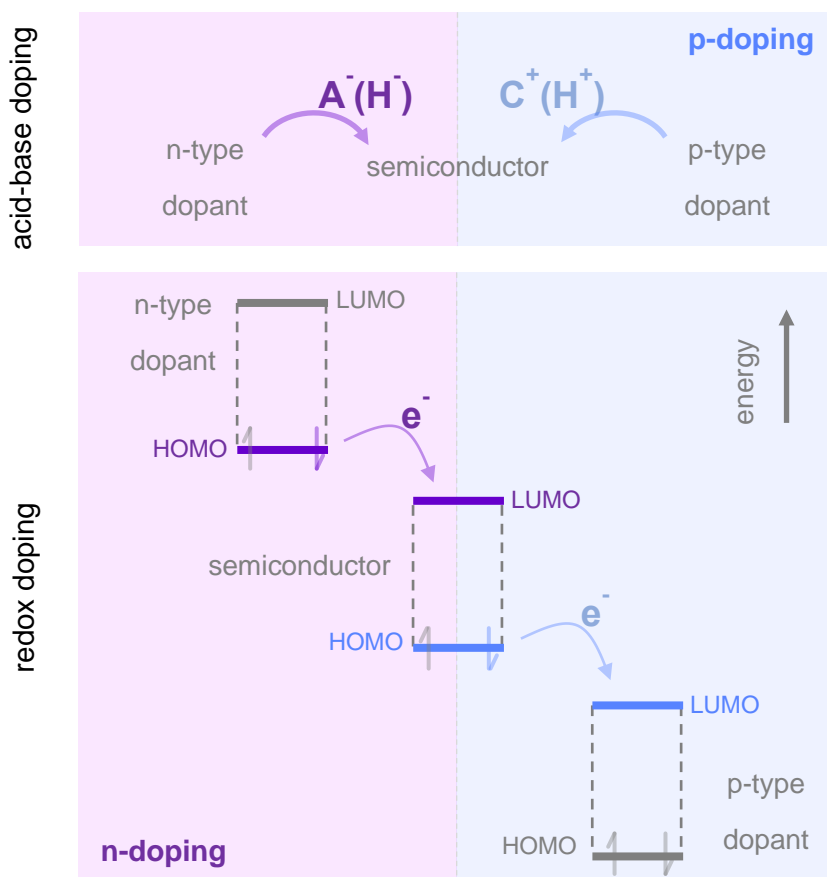
Figure 1.2 Basic principles of acid-base and redox doping. Reproduced with permission from ref.[29] published by The Royal Society of Chemistry.

1.2.1 p-type Molecular Doping

In p-type molecular doping, the dopant molecule must undergo a reversible electron or proton transfer reaction followed by insertion of its negative ion into the polymeric material to retain its charge neutrality. Some examples of molecular dopants are displayed in Figure 1.3.

The doping reactions of a conjugated polymer (P) with 2,3,5,6-tetrafluoro-7,7,8,8-tetracyanoquinodimethane (F$_4$TCNQ) and iron (III) p-toluenesulfonate (Fe(Tos)$_3$) are described by eq. 1.2 and eq. 1.3, respectively. The dopants undergo a redox reaction and transfer an electron to the polymer.

$$P + F4TCNQ \rightleftarrows P^+ + F4TCNQ^-$$ (eq. 1.2)

$$P + Fe(Tos)_3 \rightleftarrows P^+ + Tos^- + Fe(Tos)_2$$ (eq. 1.3)
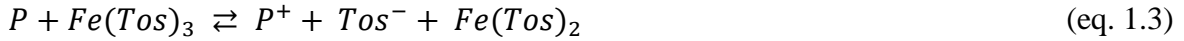
Bistriflimidic acid (H-TFSI) does not dope the polymer through acid/base mechanism. Its doping mechanism is acid mediated doping by oxygen (O_2), which transfers an electron to the polymer. eq. 1.4 to 1.6 show the different steps in reacting with O_2 and doping the polymer as proposed by Mammone and MacDiarmid.[32] The overall reaction is described in eq. 1.7

$$2\,P + O_2 \rightleftarrows 2\,P^+ + O_2^-$$ (eq. 1.4)

$$2\,P^+ + 2\,O_2^- + 2\,HTFSI \rightleftarrows 2\,P^+ + 2\,TFSI^- + H_2O_2$$ (eq. 1.5)

$$2\,P + H_2O_2 + 2\,HTFSI \rightleftarrows 2\,P + 2\,TFSI^- + 2\,H_2O$$ (eq. 1.6)

$$2\,P + O_2 + 2\,HTFSI \rightleftarrows 2\,P^+ + 2\,TFSI^- + H_2O$$ (eq. 1.7)
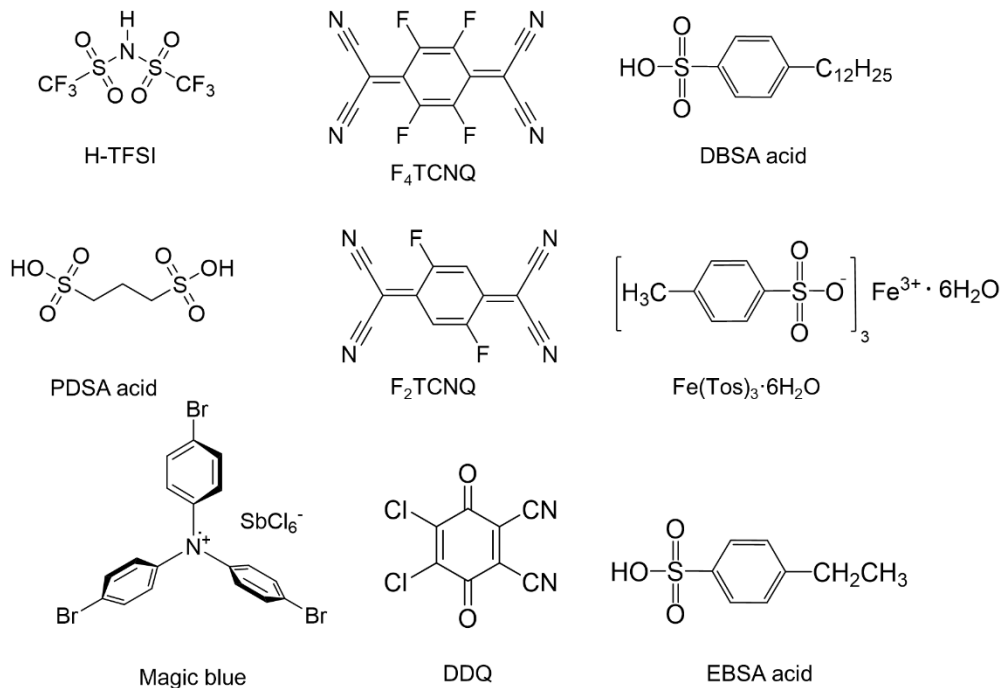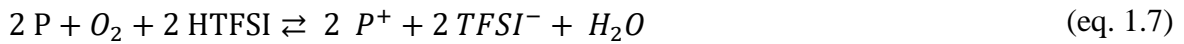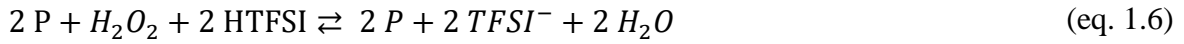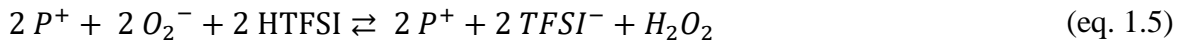
Figure 1.3 Chemical structures of some commonly used p-type molecular dopants.

Molecular Doping Processes

There are two main methods to molecularly dope a polymer: coprocessing and sequential doping (illustrated in Figure 1.4). The method has an impact on the ionization efficiency and nanostructure of the doped polymer. In the case of sequentially doping, the polymer film is subjected to a dopant in solution (using an orthogonal solvent to the polymer) or vapor phase (Figure 1.4). Sequential doping of bulk structures is limited by slow dopant diffusion into the polymer. Yu et al, have shown that F_4TCNQ has diffused only a few hundreds of micrometers into 1 mm^3 sized cubes of poly(3-hexylthiophene) (P3HT) after 2 weeks.[33]

Coprocessing involves mixing of the dopant and polymer in a common solvent before solidification. The advantage of the latter method is the exact control over the amount of added dopant. However, dopant:polymer interactions may give rise to precipitation or phase separation. While this phenomenon occurs for P3HT doped with F_4TCNQ and results in low electrical performance, swapping alkyl side chains with oligoethylene glycol ones makes the polythiophene suitable for coprocessing with the same dopant, resulting in a conductivity of up to 340 S cm^{-1} (see section 4.2 of the thesis). The use of polar oligoethylene glycol side chains increases the polarity of the polymer and enables its dissolution in polar solvents, which are suitable for dissolving polar molecular dopants such as F_4TCNQ.[34]
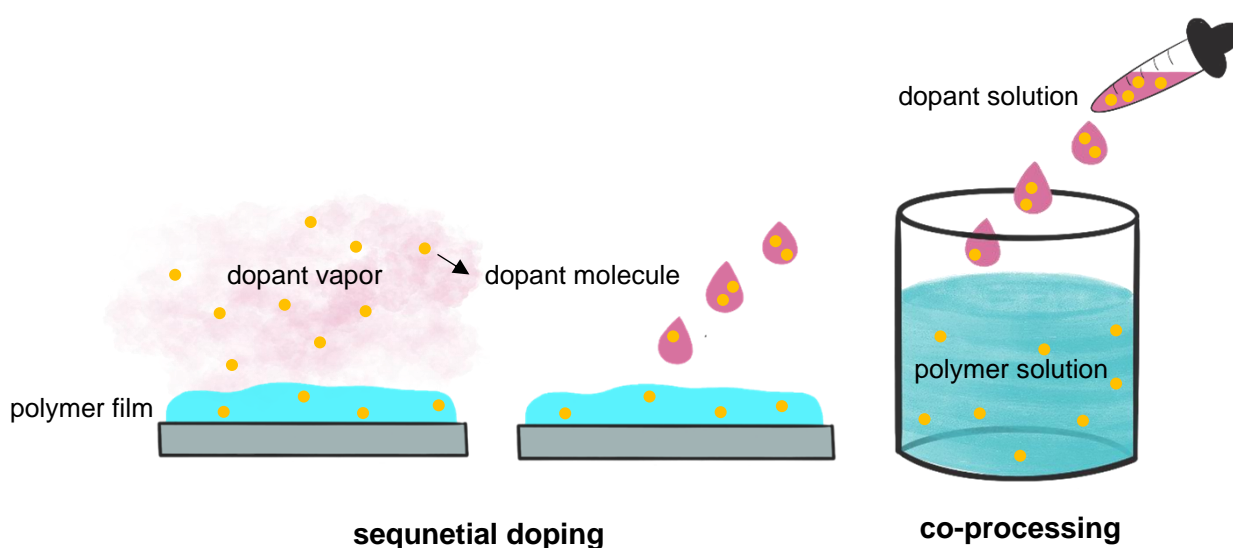
Figure 1.4 Schematic of different doping processes: sequential doping with dopant vapor or solution (left) and coprocessing from solution, which leads to gelation (right).

1.3 Electrochemical Doping

Electrochemical doping involves a polymer coated on an electrode such as indium tin oxide (ITO) and a counter electrode, for allowing the charges to flow, in contact with an electrolyte. Usually, a third electrode, denoted as reference electrode, is added that acts as a reference in measuring and controlling the working electrode potential without passing any current. In electrochemical p-type doping, upon applying a large enough voltage to the working electrode, the polymer gets oxidized and loses an electron to the underlying working electrode. Concomitantly, a negative ion from the electrolyte ingresses into the polymer so that the overall system maintains charge neutrality (Figure 1.5).[35, 36]
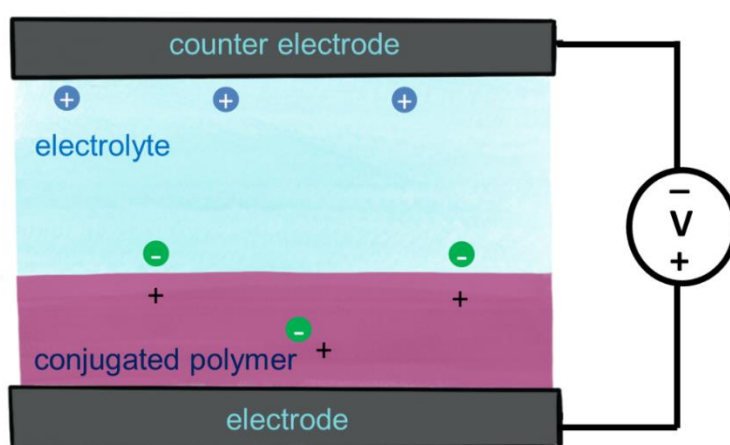
Figure 1.5 Schematic of electrochemical doping. Charge transfer occurs through the working electrode upon application of a voltage. The electrolyte ions (green) are absorbed and diffuse into the conjugated polymer (pink).

1.4 Ion-exchange Doping

The ion-exchange doping method involves subjecting the polymer film to a combined concentrated electrolyte and a molecular dopant solution. Charge transfer takes place between the molecular dopant and the polymer. Then, the dopant ion exchanges with an electrolyte anion, which diffuses into the polymer. Similar to electrochemical oxidation, there will only be electrolyte anions in the film providing that the ion exchange is efficient.[36]

2

THERMOMECHNICAL PROPERTIES OF POLYMERS

Polymers cover a wide span of mechanical properties, from being stretchable and ductile (like low density polyethylene in plastic bags) to stiff but brittle (like poly(methyl metacrylate) in plexiglass) or from being soft (like natural rubber) to being rigid (like polyoxymethylene in gears). They can show a wide range of elastic modulus (E) values, defined as the ratio of stress (σ) to strain (ε) in the linear elastic region. In tensile testing, where the sample is elongated at a fixed strain or force rate, elastic modulus is called Young's modulus.[37] Typical stress-strain curve (Figure 2.1) of a ductile polymer consists of a linear elastic region followed by a plastic deformation region until failure. A polymer can exhibit a yield point, which marks the end of elastic region and beginning of plastic deformation. While the deformation in the former region is reversible, it is permanent in the plastic region.[37] Some polymers become stiffer during the plastic deformation and strain hardening occurs. Both E and strength increase with the deformation rate as well as a decrease in temperature.[38]
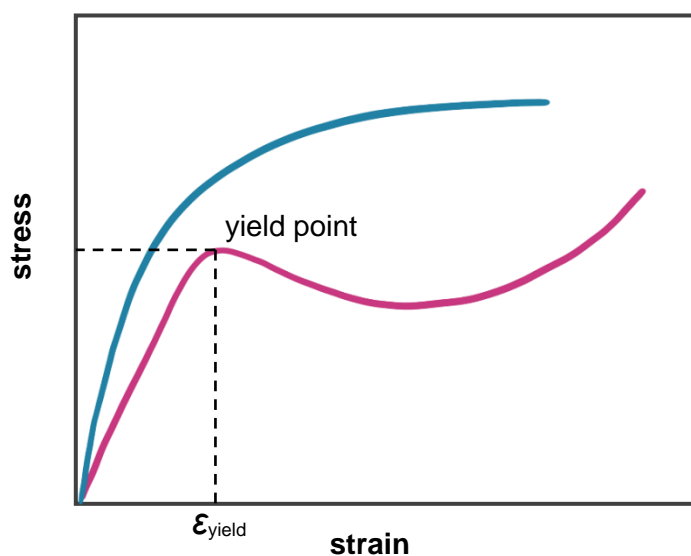
Figure 2.1 Typical tensile deformation stress-strain curve of ductile polymers. The yield point is marked on the pink curve. Blue curve corresponds to a polymer that shows a uniform extension and pink curve is a typical of a polymer showing strain softening after yield point followed by a strain hardening until fracture.[37]

2.1 Dynamic Mechanical Analysis (DMA)

Polymers are viscoelastic materials, featuring both elastic and viscous characteristics. Applying an oscillating sinusoidal strain, $\varepsilon(t)$, (eq. 2.1) to a viscoelastic material in dynamic testing using a DMA gives rise to stress, $\sigma(t)$ (eq. 2.2). $\sigma(t)$, which is out of phase by δ from the strain, (Figure 2.2) comprises of a viscous component, which is $\pi/2$ out of phase with the strain and an elastic component, which is in phase with the strain (Figure 2.2). The ratios of the stress components to $\varepsilon(t)$ are called the storage and loss moduli, E' and E'' respectively (eq. 2.3 - 2.4). The former modulus is known as the real and the latter as the imaginary component of the complex modulus (E^*) (eq. 2.5).[37, 39]

$$\varepsilon(t) = \varepsilon_0 \sin (\omega t) \qquad \text{(eq. 2.1)}$$

$\omega = angular\ velocity$

$$\sigma(t) = \sigma_0 \sin (\omega t + \delta) \qquad \text{(eq. 2.2)}$$

$$E' = \frac{\sigma_0}{\varepsilon_0} \cos \delta \qquad \text{(eq. 2.3)}$$

$$E'' = \frac{\sigma_0}{\varepsilon_0} \sin \delta \qquad \text{(eq. 2.4)}$$

$$E^* = E' + iE'' \qquad \text{(eq. 2.5)}$$
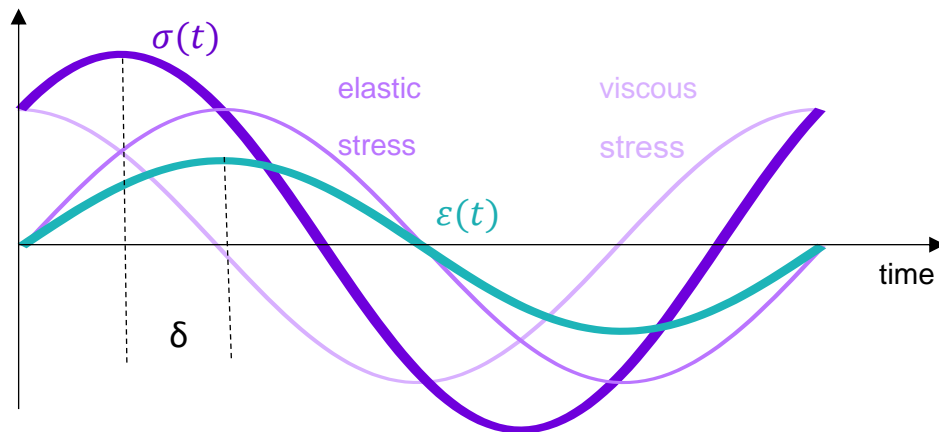
Figure 2.2 Applying an oscillating sinusoidal strain $\varepsilon(t)$ (green) to a viscoelastic polymer gives rise to a stress $\sigma(t)$ (dark purple), which has a phase difference of δ from $\varepsilon(t)$ and is comprised of elastic and viscous stress components (light purple).

The dynamic loss modulus (E'') corresponds to the energy of plastic deformation of a polymer and is proportional to the energy dissipated in the form of heat, while the dynamic storage modulus (E') is related to the energy of elastic deformation and describes the stiffness of the material.[40] The ratio of loss modulus to storage modulus is called *tan δ*, which is the damping factor.

Figure 2.3 illustrates the mechanical behaviour of an amorphous polymer under oscillatory strain as a function of temperature. Increasing the temperature gives rise to higher mobility of the polymer chains. Hence the tensile storage modulus (E') of the polymer decreases with temperature. The region with the highest modulus (1-3 GPa) is called the glassy state (region 1), where the polymer shows very little segmental mobility, and the deformation is limited to stretching of secondary bonds and bond angle changes.[39] In the transitional state (region 2), the storage modulus significantly drops due to the start of large-scale molecular motions,[37, 41] the polymer reaches the glass transition temperature (T_g), and exhibits damping.[39] Therefore, E'' shows a peak followed by a more prominent peak of *tan δ* at a slightly higher temperature. Increasing the frequency of the measurement shifts these peaks to higher temperatures. Therefore, T_g will increase with frequency. At temperatures above T_g (region 3), the rubbery plateau is reached, where E' is constant. The length of the plateau increases with molecular weight and cross-linking.[37] In region 4 long range entanglements start to slip and the polymer starts to behave like a viscous material and flows (region 5).[42] While E' shows another drop, E'' increases and takes on a larger value than E', which means the applied force is now higher than intermolecular forces and the material starts to flow, unless cross-linked.[40]

The influence of crystallinity on the modulus of an amorphous polymer is demonstrated in Figure 2.4. As a result of the reinforcing effect of the crystallites due to their higher moduli compared to amorphous segments, the modulus increases above T_g and drops after the melting temperature.
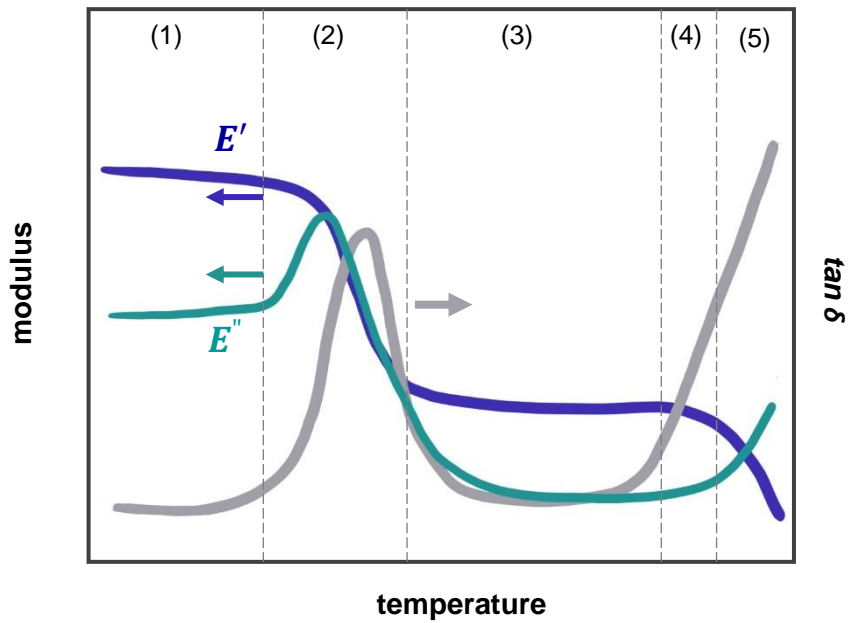
Figure 2.3 Representative variation in storage modulus (E') (blue), loss modulus (E'') (green) and tan delta (grey) of a fully amorphous polymer with temperature. The marked regions are: (1) glassy state, (2) transitional state, (3) rubber plateau, (4) rubbery flow and (5) viscose flow states.
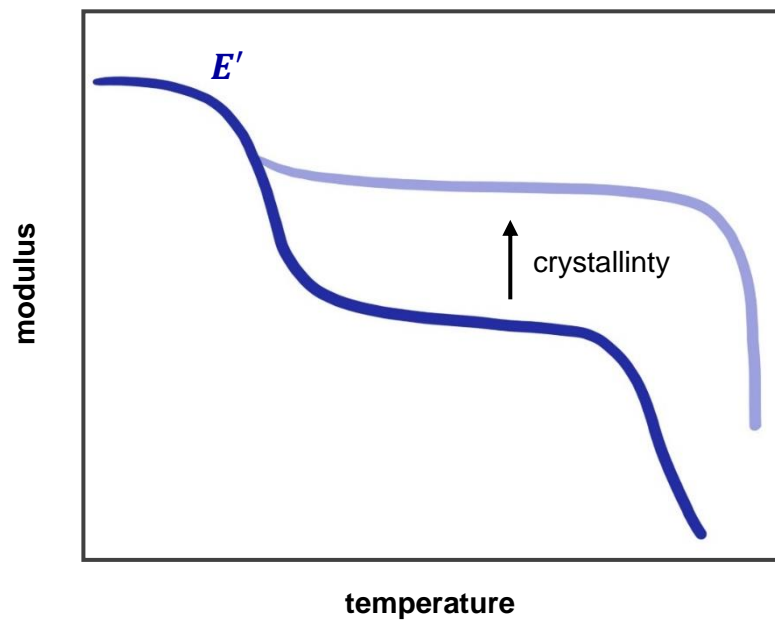
Figure 2.4 Influence of crystallinity on storage modulus (E').

2.2 Deformability of Polymers

For a polymer to be robust and withstand a high level of strain without failure, the following conditions are required:

1) An operating temperature above the T_g of the polymer

2) A reinforcement mechanism *e.g.*, having crystallites or cross-links, to hold the integrity of the material, so that it keeps its shape as a solid substance.

2.3 Thermomechanical Properties of Conjugated Polymers

Conjugated polymers are usually rigid because of their planar-aromatic backbones that generally endow them with a tendency to strongly aggregate and a high T_g. Therefore, they can be brittle at room temperature .[43] Figure 2.5 shows an Ashby plot depicting the room-temperature elastic modulus vs. T_g of a variation of conjugated polymers. p(g$_4$2T-T) with T_g= -46 °C exhibits a modulus of ~ 8 MPa due to a very low crystallinity,[44] while regio-random poly(3-butylthiophene-2,5-diyl) (P3BT) with a $T_g \approx$ +45 °C is in the glassy state (shear storage modulus (G') $\approx$ 700 MPa).[45]

While a stiffer main chain and bulkier side chains lead to a higher T_g, an increase in alkyl side chain length decreases the T_g.[45] Generally, bulky side chains, depending on their weight fraction, also show relaxations in DMA. The side chain as well as local sub-T_g relaxations are indicated by peaks in the loss modulus or tan δ prior to the main peak associated with the relaxation of backbone.[45] In some conjugated polymers such as benzothiadiazole-quarter thiophene based copolymer (PffBT4T-2OD) with T_g= 28 °C and G'= 60 MPa at room temperature (RT), the main increase in toughness and drop in storage modulus occurs after the sub-T_g.[45, 46] This explains the relatively low modulus (compared to the values in glassy state) for some of the conjugated polymers for which RT< T_g in the Ashby plot (Figure 2.5).
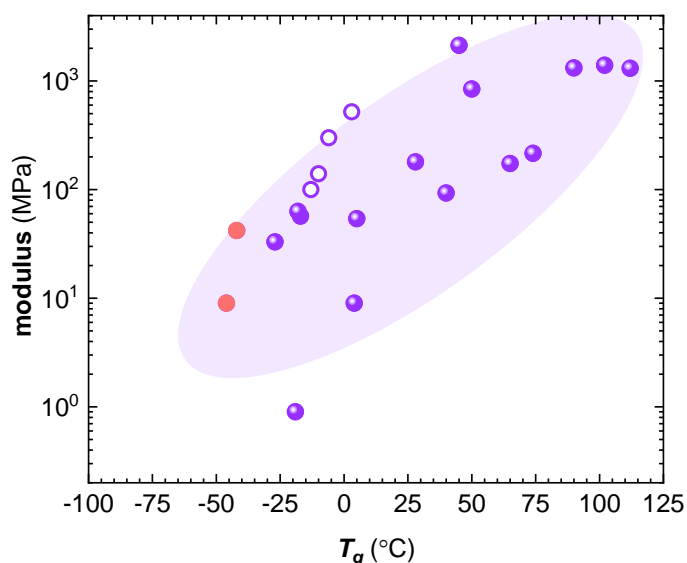
Figure 2.5 Tensile modulus (at 25 °C to 30 °C) vs. the T_g of conjugated polymers from ref. [47]. (open circles) and ref. [45], for which the tensile modulus is calculated from $E = G/2(1 + \nu)$, where G is shear modulus and the Poisson ratio is taken to be $\nu \approx 0.5$ (filled purple circles). Red filled circles belong to the Young's moduli measured in this thesis.

2.4 Modulating the Mechanical Properties of Conjugated Polymers

The main approaches to impart the desired mechanical properties, such as stretchability, to organic electronic materials and devices based on conjugated polymers are listed below:

1) structural engineering, 2) synthetic design, 3) blending with polymers, and small molecules as well as making composites with nanomaterials and 4) doping.

2.4.1 Structural Engineering

Structural engineering is based on designing and modifying the geometry of the electronic device so that it can feature stretchability and flexibility. Such efforts include spin coating of stiff P3HT:(6,6)-phenyl-C61-butyric acid methyl ester (PCBM) on pre-strained polyethylene terephthalate (PET)[48] and polydimethylsiloxane (PDMS)[49] substrates for organic solar cells.

2.4.2 Synthetic Design

Fabrication of electronic materials that exhibit both a high degree of deformability and mixed ion-electron transport can be achieved through synthetic modification.[50] This approach provides the possibility of adding different functionalities and tuning of the mechanical and electrical properties, as well as solution processability. These possibilities make conjugated polymers perfect candidates for stretchable electronics, even though the electrical conductivity and charge transport properties of inorganic materials are still superior. [51, 52]

Examples of synthetic methods for modulating mechanical properties are: copolymerization with a non-conjugated polymer such as polyurethane,[53-55], the introduction of non-conjugated flexible linker units[52, 56-63] and change in the length and grafting density of the side chains.[64, 65]

An increase in the length of alkyl side chains leads to a reduction of T_g. At the same time, ordered domains in conjugated polymers, caused by intermolecular π-stacking, can reinforce the polymers further.[52] As an example, increasing the alkyl side chain length from butyl to dodecyl in regio-random poly(3-alkylthiophene)s (P3AT)s leads to a strong reduction in T_g from +45 to -18 ºC giving rise to a significant drop in G' at room temperature from 1 GPa to about 100 kPa. [66] Carrying out the same change in the length of alkyl side chains of a regio-regular P3AT increases the crack onset strain and reduces the modulus, but to lower extent (from 1 GPa to 160 MPa)[67] due to the presence of more crystallites than its regio-random counterpart. [64, 65]

2.4.3 Blending and Preparing Composites

Synthetic methods for adjusting the mechanical properties of conjugated polymers can be time-consuming and expensive.[68] A simpler and more cost-effective approach for modulating the mechanical properties of conjugated polymers is to blend them with insulating polymers and small molecules or by forming composites with nanomaterials. The main challenge in blending and preparation of composites is to ensure the presence of conductive pathways for charge transport.[69]

Blends with insulating polymers

Blending a conjugated polymer with elastomers or flexible insulating polymers is an intriguing approach to combine the desired electrical properties of the former with the mechanical properties of the latter materials. In addition to fine-tuning mechanical properties, incorporation of insulating polymers may enhance environmental stability as well.[70]

Blends of an organic semiconductor and insulating polymers have been successfully used in many organic electronic devices including field effect,[26, 71-74] and electrochemical transistors,[75] solar cells,[76] thermoelectrics[77, 78] and conducting fibers.[79-81]

This method is very comprehensive since polymers with a wide range of molecular weight and mechanical properties are available.[71] Phase separation, which occurs in blending immiscible polymers, is desired in a way that a continuous path of the conducting material in the insulating matrix is ensured. In this way, not only less conductive material is used, and cost will reduce, but also electrical performance will be preserved. There are reports that describe how using nanoconfinement of conducting materials resulted by phase separation in stretchable insulating matrix is advantageous to ensure a conductive path for good charge transport and high crack strain due to large interface between the conjugated polymer and the matrix.[68, 74, 82] Blending of a styrene-ethylene-butylene-styrene (SEBS) elastomer with conjugated polymers such as poly(indacenodithiophene-co-benzothiadiazole) has improved crack onset and flexibility with minor loss of charge carrier mobility in field effect transistors at 100% strain.[68] Blends of P3HT with poly(dimethylsiloxane) (PDMS) elastomer, not only exhibit high ductility but also their charge mobility in field effect transistors has been improved compared to pristine P3HT.[83, 84] There are other rubbers like butyl rubber (BR)[85] that have been used for improving mechanical ductility and crack onset. Parameters such as crystallinity,[68] molecular weight[86] and processing solvents[68] strongly influence the final properties of the blends.

There are studies that have employed synthetic modification to control the microstructure of the blend for more enhanced mechanical and electrical properties. For instance, non-conjugated moieties capable of cross-linking with each other have been added to a Diketopyrrolopyrrole (DPP) based copolymer and PDMS elastomer prior to blending to boost stretchability.[26]

Composites with nanomaterials

Compounding conjugated polymers with conductive nanofillers usually aims to improve their electrical performance.[87-89] For instance: The addition of natural graphite and single-walled carbon nanotube (SWCNT) to undoped PA results in the injection of charge carriers from filler particles. Hence PA becomes conductive.[87] Also, integration of 2D materials like graphene[88] and graphene oxide[89] to conjugated polymers such as P3HT[89] improves their charge mobility. Besides conductive nanofillers, the incorporation of cellulose nanocrystals during electrochemical deposition of polyaniline (PANI) and poly(3,4-ethylenedioxythiophene), resulted in enhanced ion transport in the composites.[90] Since compounding commodity polymers with nanomaterials is widely employed to improve the polymer's mechanical properties, they can also be employed to fine-tune the mechanical properties of conjugated polymers. For instance, incorporation of a few percent of multi-walled carbon nanotubes (MWCNT) to films of cellulose and poly(3,4-ethylenedioxythiophene):poly(styrenesulfonate) (PEDOT:PSS) resulted

in improvement of both the mechanical properties (modulus and ductility) as well as the electrical conductivity.[90] Further, increasing the cellulose nanocrystals in PANI/camphorsulfonic acid from ~67% to ~95%, increased the modulus of the nanocomposite from 1 GPa to 9 GPa.[91]

2.4.4 Doping

Doping is an essential step for adjusting the number of charge carriers in the conjugated polymers. Doping not only increases the electrical conductivity of a conjugated polymer, but also impacts its microstructure[92] and thermomechanical properties.[44]

The electrical transport in doped organic semiconductors is increasingly studied. In comparison, the impact of doping on the mechanical properties has attracted little attention. Impact of doping on mechanical properties of conjugated polymers, can be harnessed for designing organic electronics with desirable mechanical and electrical properties. Molecular doping can either plasticize the polymer due to the presence of counterions or can stiffen it. It has been shown that doping of stiff conjugated polymers, which can be isotropic [93, 94] or aligned, [93, 95-97] can lead to a deterioration of modulus while doping of soft materials tends to have the reverse effect by increasing the modulus.[44] Table 2.1 shows the figure of merit $\eta = \log (E_{doped}/E_{neat})$, *i.e.*, the ratio of the elastic modulus of the doped material E_{doped} and the neat polymer E_{neat}, of a handful of conjugated polymers.

For instance, doping a P3HT with regio-regularity of 95%, which has a T_g of ~ 23 ℃ and modulus of ~340 MPa at room temperature, with 9 mol% Mo(tfd-COCF$_3$)$_3$ resulted in a similar T_g (~ 21 ℃) but slight decrease of the modulus to 270 MPa.[93] The addition of 1 wt% F4TCNQ to a DPP based copolymer, which has a modulus of 374 MPa, [98] led to decrease in T_g from 55 ℃ to 27 ℃ as well as a higher crack onset strain.[94] Conclusively, upon doping the stiff conjugated polymers, plasticization appears to occur, which impacts mechanical properties by reducing the stiffness.

Table 2.1 Elastic moduli at room temperature before and after doping, E_{neat} and E_{doped}, as well as a figure of merit $\eta = \log{(E_{doped}/E_{neat})}$ reported for isotropic polythiophenes. Tthe dopant concentration is calculated per repeat unit, which is composed of one thiophene ring in case of the P3HTs but three thiophene rings in case of p(g$_4$2T-T); [a]poly(ethylene oxide) (PEO), [b]polycaprolactone (PCL). Reprinted with permission from ref. [44], published by The Royal Society of Chemistry.

| polymer	dopant	mol% dopant	wt% dopant	E_{neat} (MPa)	E_{doped} (MPa)	η	ref.
P3HT	Mo(tfd-COCF$_3$)$_3$	9	30	340	270	-0.1	93
P3HT	EBSA	9	16	900	345	-0.4	99
P3HT	F$_4$TCNQ	4	6	340	560	0.2	93
3:7 P3HT:PEO[a]	F$_4$TCNQ	20	29	80	188	0.4	77
P3HT	FeCl$_3$	20	20	230	900	0.6	100
P3OT	FeCl$_3$	18	15	60	470	0.9	101
P3OT	I$_2$	7	9	60	80	0.1	101
2:8 p(g$_4$2T-T):PCL[a]	LiF4TCNQ	25	12	130	184	0.2	this thesis
P3DDT	FeCl$_3$	20	14	50	300	0.8	100
P3DDT	F$_4$TCNQ	7	8	45	80	0.2	this thesis
p(g$_4$2T-T)	F$_4$TCNQ	58	35	8	232	1.5	this thesis
p(g$_4$2T-T)	F$_2$TCNQ	43	21	8	377	1.7	this thesis

On the contrary, it is argued that molecular doping of comparably softer polymers such as Poly(3-octylthiophene) (P3OT, $E \approx 60$ MPa) and poly(3-dodecylthiophene) (P3DDT, $E \approx 50$ MPa) and p($g_4$2T-T) ($E \approx 8$ MPa) gives rise to a higher modulus, for instance up to 470 MPa for the former polymer doped with 18 mol% $FeCl_3$. The reason for the increase in stiffness of conjugated polymers is arguably associated with increased π-stacking, upon doping.[44, 100, 101] Blending p($g_4$2T-T) with 80% polycaprolactone (PCL) increases the modulus up to 130 MPa, hence doping with 25 mol% LiF_4TCNQ results in a lower figure of merit ($\eta \approx 0.2$, Table 2.1) compared to doping of the neat polymer ($\eta \approx 1.3$) with the same amount of F_4TCNQ.[44] Further details about the p($g_4$2T-T):PCL blends will be discussed in *chapter 6*.

As a conclusion, depending on the stiffness of the pristine polymer, molecular doping can be utilized to modulate the glass transition and mechanical properties of the final product.

2.5 Techniques for T_g Measurement

Differential scanning calorimetry (DSC) and DMA are prominent techniques for measuring the glass transition temperature of polymers. However, DSC is not a suitable technique for determining the T_g of many conjugated polymers,[46] and is often unable to detect the related transitions[102] due to the semicrystalline nature and rigid backbone of most of conjugated polymers.[45]

The fabrication of free-standing bulk films of conjugated polymers for DMA measurements can be challenging due to their brittleness in case of a high T_g or softness in case of polymers with low crystallinity and T_g, and the fact that they are usually synthesized in very low quantities. Therefore, different strategies have been utilized to detect with sufficient sensitivity the glass transition of thin polymer films using DMA. These include coating stripes of glass mesh with polymer solution, in a way that the strands are cut at 45° to avoid any continuous glass fibers along the length of the sample, which would impact the DMA response (Figure 2.5),[103] and enclosing of the polymer powder in a metallic pocket.[104] These methods are not suitable for measuring absolute modulus values because the geometry of the sample is not defined. The Glass mesh strategy has been vastly used in this thesis. A glass mesh with a length of 20 mm- 30 mm and width of a few mm is homogeneously coated with a polymer solution.[103] During the experiment, a sinusoidal tensile strain ($\varepsilon_{max} < \varepsilon_{yield}$) is applied and the mechanical response (resulting σ) is measured as a function of temperature at a constant frequency.
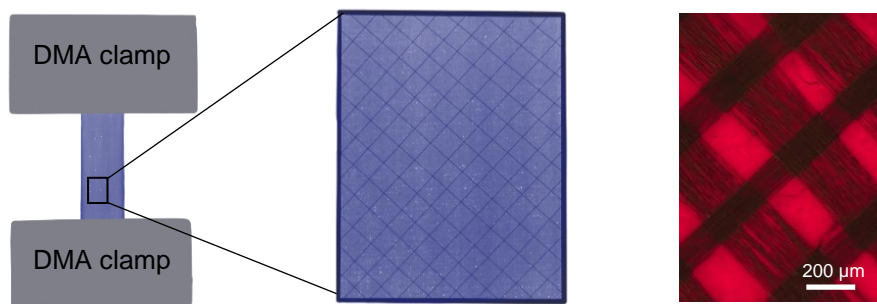
Figure 2.5 Schematic of a polymer film supported by glass mesh with strands cut at 45° mounted in DMA clamps (left). An optical microscopy image of a glass mesh coated with P3HT (chlorobenzene, 20 g L^{-1}) (right).

2.6 Preparation of Free-standing Films for DMA

To measure the absolute modulus of conjugated polymers with DMA, free-standing films are required. In this thesis, less than 10 mg of polymer solution is drop-cast onto a glass substrate using a layer-by-layer method. Pieces with a width of 0.5 mm – 1 mm are cut from the glass using a sharp blade. In case of soft polymers, the samples are supported by a paper frame after peeling off (Figure 2.6). The paper frame is then mounted in a DMA instrument, which has undergone mass calibration considering the weight of the paper. Prior to the test, the paper is cut (Figure 2.6). If the sample is too soft so that it is prone to be damaged during the peeling off process, it can be cooled prior to handling by first immersing the sample in liquid N$_2$. After mounting the frozen piece onto a paper frame, the sample must be allowed to return to room temperature.

Figure 2.6 A rectangle is cut out from a sticky paper frame with the same height as the desired gauge length. After supporting the sample with a paper frame, the frame + sample are mounted in a DMA instrument followed by cutting the sides of the frame prior to measurement.

3

AIMS OF THIS THESIS

Motivated by the need for organic semiconductors with a variety of mechanical properties for wearable electronic and bioelectronic applications, in this thesis different strategies are explored for modulating the mechanical properties of a polythiophene with tetraethylene glycol side chains. this polymer is used as a model for soft polythiophenes to study the interplay of mechanical and electrical properties. The following research questions are explored in this thesis:

1) How does the length of oligoethylene glycol side chains impact the electrical and thermomechanical properties?

2) Can copolymerizing of urethane blocks with a polythiophene with tetraethylene glycol side chains allow to create hard domains in the soft polymer matrix with the goal to increase the elastic modulus yet maintaining the electrical properties to a high extent?

3) What are the considerations for melt-processing of conductive polymer blends and how does phase separation affect the electrical conductivity of the material?

4) How can stretchable conducting fibers, suitable for e-textile applications, be prepared with high electrical and mechanical stability?

5) Can the addition of a low amount of nanocellulose to a polythiophene with tetraethylene glycol side chains improve the stiffness of the material without compromising the electrical conductivity?

6) How does molecular doping alter the nanostructure and thermomechanical properties of a polythiophene with tetraethylene glycol side chains?

4

# CONJUGATED POLYMERS WITH OLIGOETHYLENE GLYCOL SIDE CHAINS

The polarity of conjugated polymers is essential for ionic conductance to facilitate the ingression and transport of ions. Ionic conductance is for instance required in organic electrochemical transistors (OECTs) that are the basic building blocks of many types of chemical and biological sensors.[105] OECTs allow to convert ionic fluxes into electronic signals, which is sought after because it allows to interface electronics with biological systems, where low amplitude ionic fluctuations can be amplified and transconducted.[106]

More polar side chains of conjugated polymers are widely employed to improve the capability to store and transport ions.[107] Conjugated polymers with oligoethylene glycol side chains have received widespread attention for energy storage[108-110], energy harvesting[111-115] and bioelectronics.[116-119] In addition to ionic conductivity due to polarity, compared with ubiquitous apolar alkyl side chains, oligoethylene glycol side chains enhance properties such as swellability,[120] flexibility and polarity, the latter of which imparts processability in polar solvents.[114, 121]

4.1 Polythiophenes with Oligoethylene Glycol Side Chains, p(g_x2T-T)

Substitution of alkyl with oligoethylene glycol side chains (Figure 4.1) results in polythiophenes with low crystallinity, a sub-zero glass transition temperature T_g and a low elastic modulus.[34, 122] Moser et al have shown that increasing the side-chain length from two to six ethylene glycol units lowers crystallinity and increases the ionization energy (IE) from 4.50 eV to 4.66 eV.[107] Triethylene glycol was found to be the optimum length giving rise to the highest charge storage capacity and electronic mobility in OECTs.[107, 117]
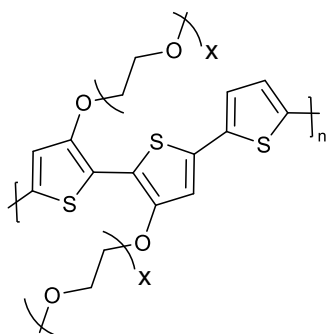
Figure 4.1 Chemical structure of polythiophenes of type p(g$_x$2T-T) with oligoethylene glycol side chains.

4.2 Thermomechanical and Electrical Properties of p(g$_3$2T-T) and p(g$_4$2T-T)

To study the influence of the length of oligoethylene glycol side chains on the T_g, the change in modulus as a function of temperature was analyzed using glass mesh supported polymer films deposited from 10 g L^{-1} p(g$_4$2T-T) (synthesis by Dr. Renee Kroon according to ref. [34]) in chlorobenzene (CB), 10 g L^{-1} p(g$_3$2T-T) (synthesized by Sophie Griggs according to ref. [107]) in 2:8 CB:chloroform (CH$_3$Cl) and 10 g L^{-1} p(g$_6$2T-T) (synthesized by Junfu Tian according to ref. [107]) in CB. The chemical structures of these polymers are displayed in Figure 4.2 a-c. The DMA thermograms reveal a similar T_g of -42 °C, -46 °C and -44 °C ($E^{''}$ peak), for oligoethylene glycol length x= 3, 4 and 6, respectively (Figure 4.2 d-f). Xie et al have demonstrated that besides segmental backbone relaxation revealing itself in a peak in shear loss modulus ($G^{''}$), side-chain relaxation tends to occur with another maximum in the loss modulus at lower temperatures. It has been shown that a poly(benzodithiophene-alt-dithienyl difluorobenzotriazole) type copolymer with tri and tetraethyelene glycol side chains on the benzodithiophene (BDT) donor and benzotriazole (TAZ) acceptor moieties, respectively, exhibits a relaxation process around -40 °C dominated by side chains followed by relaxations of the backbone at 21 °C.[123] Having the same backbone, p(g$_x$2T-T) polymers should show similar T_g, corresponding to the relaxation of the backbone. At the same time, since the loss modulus peak of p(g$_x$2T-T) occurs at the relaxation temperature of oligoethylene side chains, it is feasible that the backbone and side chain relaxation of p(g$_x$2T-T) polymers overlap.
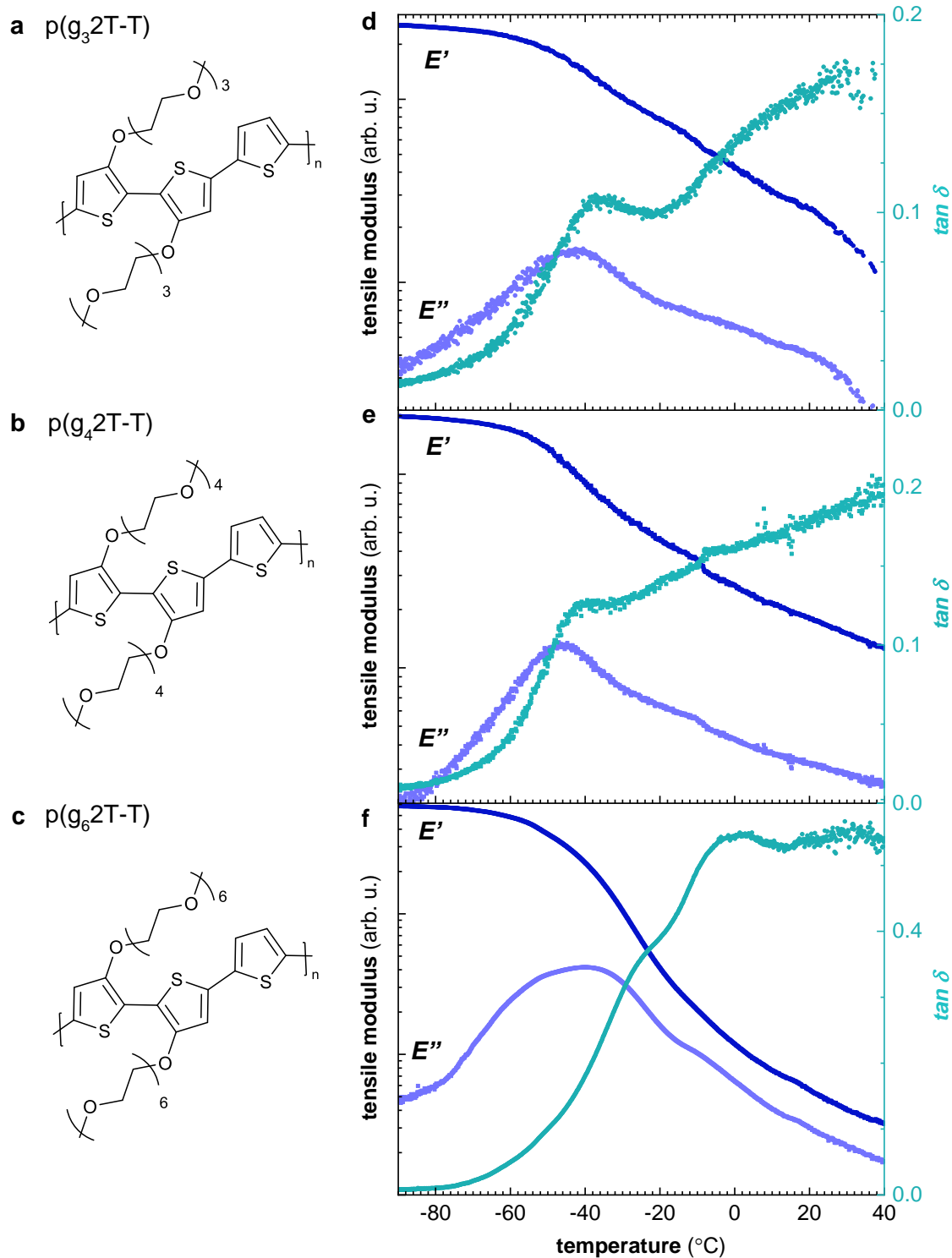
Figure 4.2 Chemical structures of (a) p($g_3$2T-T), (b) p($g_4$2T-T) and (c) p($g_6$2T-T) and (d-f) corresponding DMA thermograms showing the storage modulus (*E'*, dark blue), loss modulus (*E''*, light blue) and *tan δ* (green) measured for glass mesh supported films.
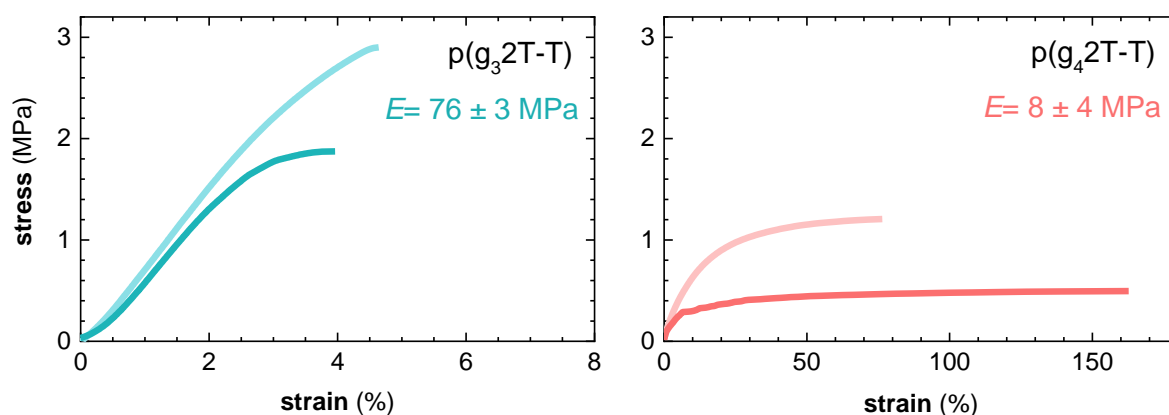
Figure 4.3 Tensile deformation stress-strain curves of p(g$_3$2T-T) (drop cast from 2:8 CB:CH$_3$Cl, green) and p(g$_4$2T-T) (drop cast from CH$_3$Cl, red).
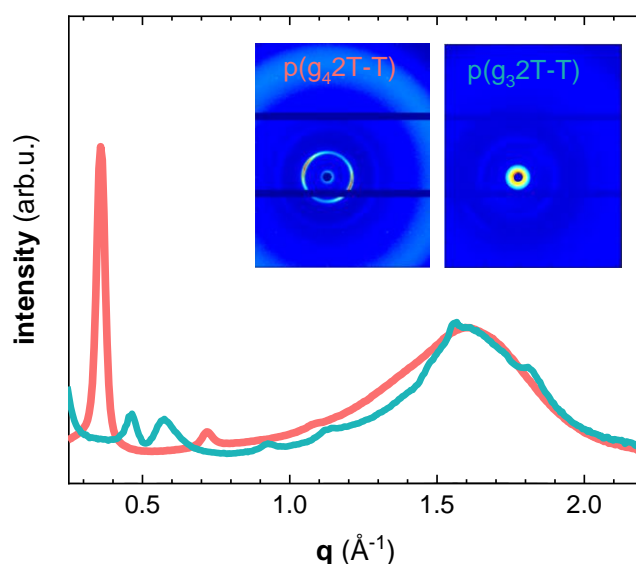
Figure 4.4 Wide angle X-ray scattering (WAXS) patterns and diffractograms of a piece of p(g$_4$2T-T) (red) and a drop cast film of p(g$_3$2T-T) from 2:8 CB:CH$_3$Cl (green). The diffractograms are normalized to the intensity of the halo at 1.6 Å^{-1}.

Tensile deformation on p(g$_4$2T-T) and p(g$_3$2T-T) films was carried out by mounting the material cooled with liquid nitrogen (cf section 2.8). A Young's modulus of (76 ± 3) MPa and (8 ± 4) MPa[44] was measured for p(g$_3$2T-T) and p(g$_4$2T-T), respectively (Figure 4.3). Considering the similar T_g values, the difference in modulus likely arises because of a higher crystallinity in p(g$_3$2T-T). It has been previously reported that p(g$_3$2T-T) and p(g$_4$2T-T) are both able to π-stack.[107] However, according to the WAXS

diffractograms in Figure 4.4, p(g$_3$2T-T) features a peak at 1.81 Å^{-1} associated with π-stacking, while p(g$_4$2T-T) exhibits hardly any π-stacking, indicating a low degree of order.

Doping the polymers with 20 mol% F$_4$TCNQ (cf. experimental section in *paper III*) results in a conductivity of (342 ± 27) S cm^{-1} and (42 ± 1) S cm^{-1} in case of p(g$_3$2T-T) and p(g$_4$2T-T), respectively.

5

COPOLYMER OF p(g₄2T-T) AND URETHANE BLOCKS

5.1 Design Inspiration for p(g₄2T-T) Reinforced with Urethane Blocks

Tough (robust + ductile) materials such as styrene-butadiene-styrene (SBS), consist of hard domains embedded in a soft matrix, that are responsible for connectivity and stretchability, respectively (Figure 5.1). Inspired by this nanostructure, a copolymer of p(g₄2T-T) segments and urethane blocks was designed by Dr. Renee Kroon. Unlike the majority of reported copolymers of rigid conjugated and soft non-conjugated segments,[53-56] such as a copolymer comprising DPP-based blocks and PCL,[56] here, the copolymer design has been inverted by using *soft* conjugated segments of p(g₄2T-T) and *hard* urethane blocks. Urethane blocks were chosen due to their ability to form a hydrogen-bonded network (Figure 5.1).
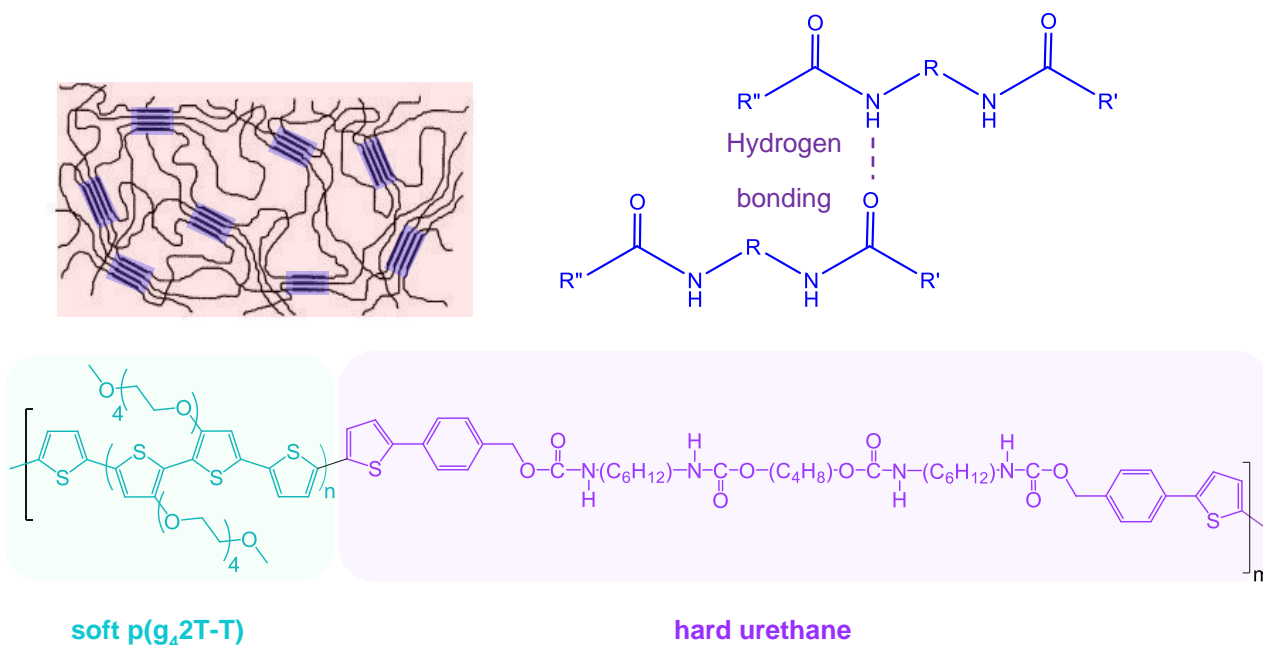
Figure 5.1 Schematic of the nanostructure of polymers composed of hard domains, providing connectivity and soft domains, responsible for stretchability (top left), a hydrogen bond connecting two urethane groups (top right), and the p[p(g₄2T-T)-*co*-U] copolymer composed of soft p(g₄2T-T) (green) and hard urethane blocks (purple) with a molar ratio of 7:1 g₄2T-T:U (bottom).

The here reported copolymer p[p(g₄2T-T)-*co*-U], (see Figure 5.1 for chemical structure, and *paper I* for detailed synthesis procedure) features a molar ratio of 7:1 of g₄2T-T repeat unit and the urethane block, *i.e.*, a 6:1 weight ratio of p(g₄2T-T) and the urethane block. The molecular weight of the copolymer is measured to be $M_n \sim 13.5$ kg mol^{-1} (PDI ~ 2.5).

5.2 Hydrogen Bonding Network in p[p(g₄2T-T)-*co*-U]

To assess whether a hydrogen bonded network exists, transmission FTIR spectroscopy was employed to investigate the presence of hydrogen bonding and to study the impact of temperature (Figure 5.2). The FTIR absorbance (*A*) of NH and C=O stretch vibrations in urethanes will shift to lower energies if hydrogen-bonded.[124] For instance, the infrared absorption of a C=O bond in a polythiophene with urethane side-chains exhibits two peaks at 1705 cm^{-1} and 1725 cm^{-1}, the latter corresponds to free and the former to hydrogen-bonded units.[125] Consequently, the C=O stretch vibrations peak of p[p(g₄2T-T)-*co*-U] at 1683 cm^{-1} and the broad shoulder in 1720 cm^{-1} can be attribute to the respective free and hydrogen bonded urethane groups. Further, it was found that the existing hydrogen bonding network tends to dissociate upon heating to 220 °C revealed by the shift in C=O absorption peak to 1726 cm^{-1}. The hydrogen bonds partially reform after cooling down to room temperature.
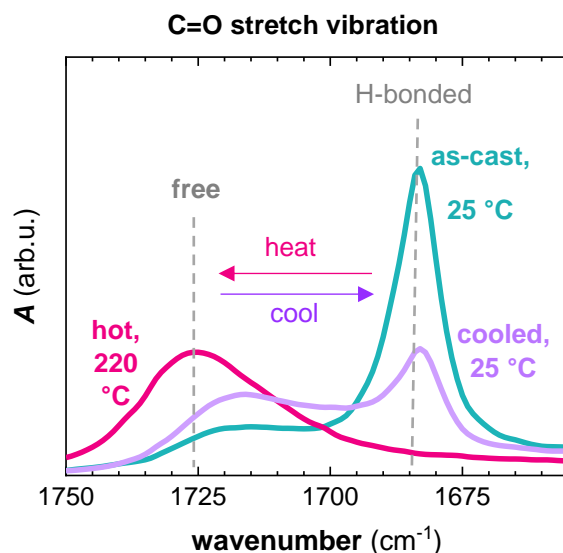
Figure 5.2 FTIR absorbance *A* of the carbonyl stretch vibration, part of the urethane linkage, recorded at 25 °C for a p[p(g₄2T-T)-*co*-U] film cast from dimethyl sulfoxide (DMSO) at 25 °C (green), heated to 220 °C (pink) and after cooling from 220 to 25 °C (purple). Reproduced with permission from ref. [126] published by WILEY.

5.3 Thermomechanical Properties

Free-standing films of p[p(g$_4$2T-T)-*co*-U] (Figure 5.3 a) could be readily obtained. Instead, neat p(g$_4$2T-T) films are soft at room temperature but can form free-standing robust films once cooled. To quantify the impact of copolymerization on the modulus, storage modulus values of the free-standing p[p(g$_4$2T-T)-*co*-U] and p(g$_4$2T-T), recorded at frequency of 1 Hz and a heating rate of 3 °C min^{-1} at 20 °C, are compared. The copolymer features a higher storage modulus ($E' \approx$ 71 MPa) than pristine p(g$_4$2T-T) ($E' \approx$ 37 MPa) (Figure 5.3 c).
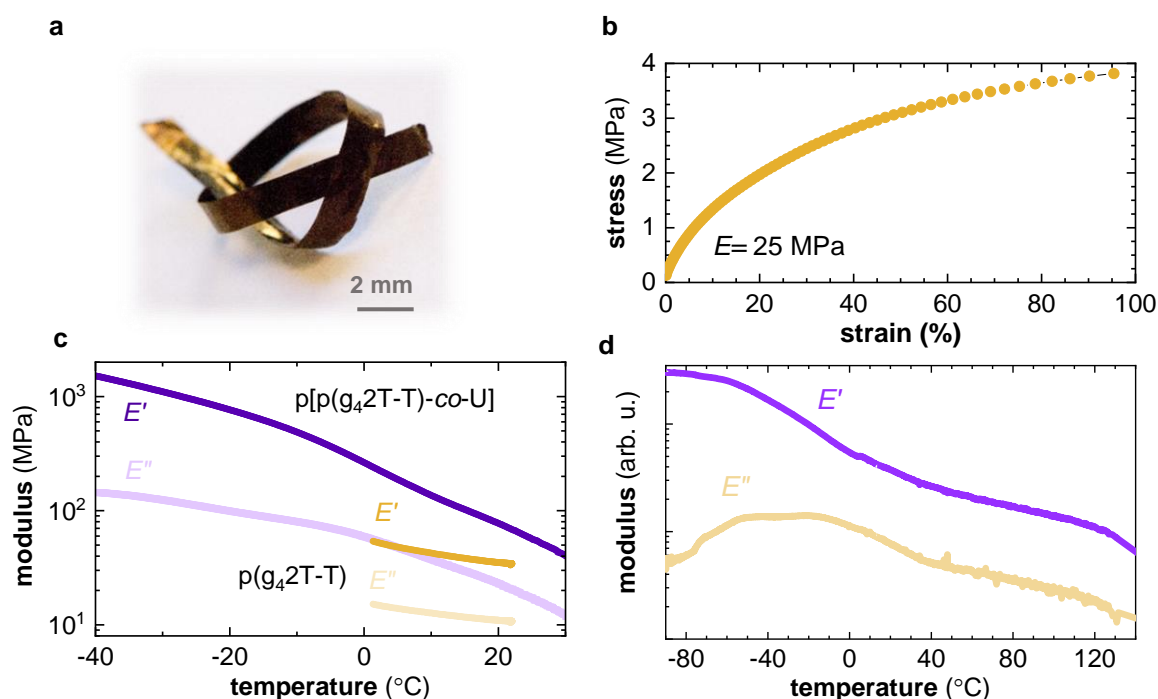
Figure 5.3 (a) Photograph of p[p(g$_4$2T-T)-*co*-U], (b) tensile stress/strain curves recorded for p[p(g$_4$2T-T)-*co*-U]. DMA thermograms of (c) free-standing p[p(g$_4$2T-T)-co-U] and p(g$_4$2T-T) as well as (d) p[p(g$_4$2T-T)-*co*-U] supported by a glass mesh. Reproduced with permission from ref. [126] published by WILEY.

To Probe the ductility of the copolymer, tensile deformation was carried out at 0.5 N min^{-1} resulting in a strain at break of about 100% (Figure 5.3 b). The introduction of urethane blocks also impacts the thermal transitions of p(g$_4$2T-T). DMA thermograms of p[p(g$_4$2T-T)-*co*-U] supported by a glass mesh (Figure 5.3 d) feature one transition at -44 °C as indicated by a maximum in E'', which is very similar to that of neat p(g$_4$2T-T). A second transition emerges at -20 °C, which appears as a broad shoulder in p(g$_4$2T-T) (cf. Figure 4.2 *chapter 4*).

5.4 Molecular Doping

Sequential doping of p($g_4$2T-T) and p[p($g_4$2T-T)-*co*-U] films with F$_4$TCNQ (described in experimental section of *paper I*) results in a conductivity of (48 ± 8) S cm^{-1} and (20 ± 5) S cm^{-1}, respectively.
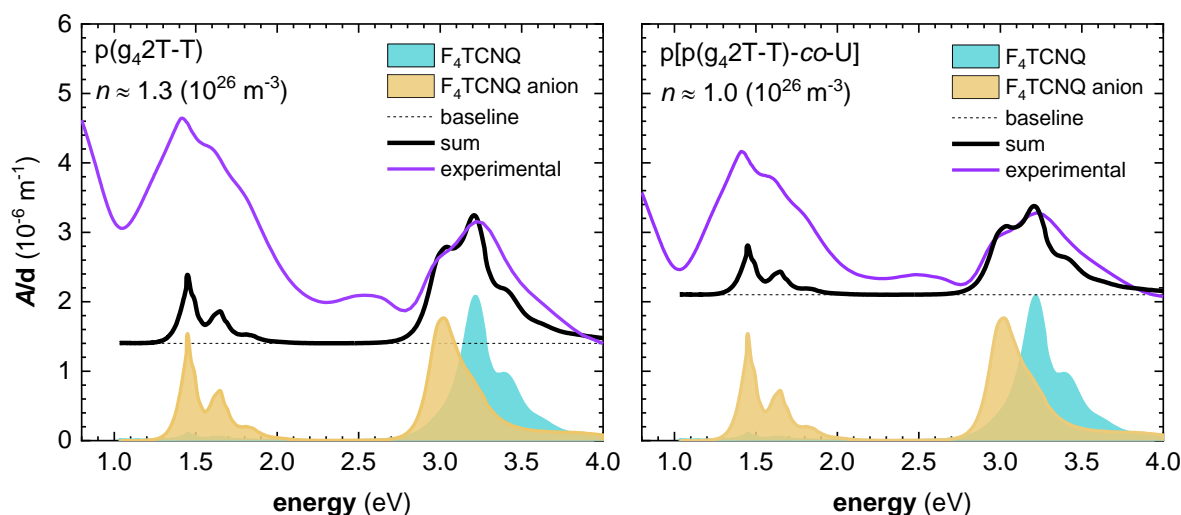
Figure 5.4 Film thickness normalized UV-vis-NIR absorbance (*A*/d) spectra of p[p($g_4$2T-T)-*co*-U] (left) and p($g_4$2T-T) (right) sequentially doped with F$_4$TCNQ (purple), spectra of neat F$_4$TCNQ (blue) and the F$_4$TCNQ anion (yellow) in AcN from ref. [127], and best fits in the UV region (black) including a horizontal baseline (dashed black). The charge-carrier density values from these fits differ from the ones reported in *paper I,* since there is an error in the calculation reported in the paper. However, the ratio of ~1.3 of the charge-carrier density of p($g_4$2T-T) to that of p[p($g_4$2T-T)-*co*-U] is comparable to the one reported in *paper I*. Reproduced with permission from ref. [126] published by WILEY.

It is speculated that the charge-carrier density in case of the copolymer should be lower than for the homopolymer due to the presence of non-conjugated urethane segments. To investigate this hypothesis, the number of charge carriers in p($g_4$2T-T) and p[p($g_4$2T-T)-*co*-U] was estimated through comparison of the UV-vis-NIR absorbance spectra of the F$_4$TCNQ-doped polymers with those of the neutral F$_4$TCNQ and the F$_4$TCNQ anion, as described by Kiefer et al. (Figure 5.4).[127] Due to the high dopant concentration, the presence of dianions is negligible. The decrease in dianion concentration at high oxidation levels is shown in *chapter 8*. The charge-carrier concentration (*n*) is estimated to be ~1.3×10^{26} m^{-3} and ~1.0×10^{26} m^{-3} for the homopolymer and copolymer, respectively. The number of charge carriers has slightly decreased for the copolymer. Taking into account that 14 wt% of the

copolymer is composed of urethane segments, the $p(g_42T\text{-}T)$ fraction has nearly the same capability of charge uptake as in the neat film. Through eq. 1.1 (*chapter 1*), charge-carrier mobility of (2.3 ± 0.4) cm^2 V^{-1} s^{-1} and (1.3 ± 0.3) cm^2 V^{-1} s^{-1} is obtained for the copolymer and homopolymer, respectively. Comparison of the mobility values shows that the incorporation of urethane blocks, which gives rise to a reduction in the degree of order of $p(g42T\text{-}T)$ segments (see WAXS diffractograms in *paper I*), only does not significantly impact the charge-carrier mobility.

5.5 Electrochemical Doping

Electrochemical oxidation of the polymers was compared by performing spectroelectrochemistry. To do so, cyclic voltammograms of the polymer films on ITO/glass, which functioned as the working electrode, were recorded using an electrochemical cell comprised of a platinum (Pt) wire counter electrode and a silver (Ag) wire pseudo-reference electrode. The electrodes were submerged in an electrolyte solution of 0.1 M 1-ethyl-3-methylimidazolium tetrafluoroborate ([EMIM][BF$_4$]) in dry and degassed AcN (cf. experimental section in *paper I* for details). Then, the polymer films were oxidized to different degrees by applying a series of constant potentials between -0.53 V and +0.37 V vs. ferrocene/ferrocenium (Fc)/Fc$^+$ and the corresponding UV-vis-NIR absorbance spectra were recorded (Figure 5.5 a-b). A bias of -0.53 V was applied prior to each oxidation step to ensure there is no charge accumulated in the films. The absorbance (A) of neutral $p(g_42T\text{-}T)$ at ~600 nm weakens with increasing potential due to gradual oxidation of the conjugated backbone. Concurrently, polaronic absorbance bands at 900 nm and in the infrared region emerge (Figure 5.5 a-b). $p[p(g_42T\text{-}T)\text{-}co\text{-}U]$ displays the same behavior upon increasing the oxidation potential. To evaluate the change in associated spectra upon oxidation, the absorbance related to the spectrum of neat polymer at -0.53 V (ΔA) was plotted versus oxidation potential at selected wavelengths (Figure 5.5 c-d). In case of both materials, ΔA at 600 nm decreases with increasing oxidation potential and nearly reaches a plateau at +0.37 V, indicating that the conjugated backbone is fully oxidized. It is concluded that the urethane segments do not significantly impact the ability of the copolymer to take up charge. Polaronic absorption at 2000 nm and 900 nm first increase with oxidation level in case of both materials. However, ΔA at the latter wavelength drops at higher potentials. This is associated with the presence of bipolarons, which are argued to increasingly form at higher charge concentrations.
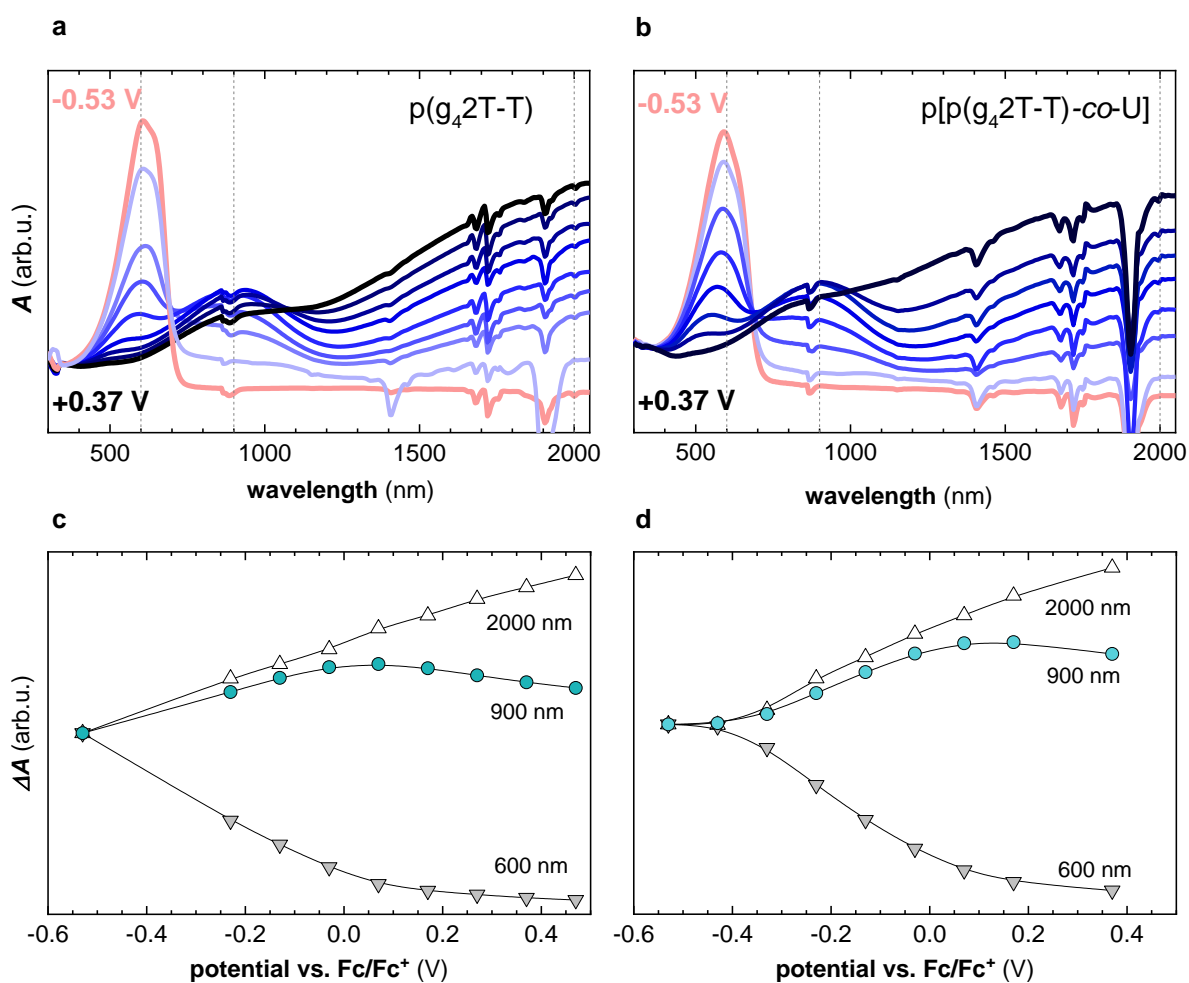
Figure 5.5 UV-vis-NIR absorbance (*A*) spectra of (a) p(g$_4$2T-T) and (b) p[p(g$_4$2T-T)-*co*-U] recorded at various electrochemical potentials starting from -0.53 V (pink) to 0.37 V (black) (c) absorbance related to the spectrum of neat polymer at -0.53 V (Δ*A*) at 600 nm, 900 nm, and 2000 nm (marked by dashed lines vs. oxidation potential. Reproduced with permission from ref. [126] published by WILEY.

6

BLENDS OF p(g₄2T-T) AND INSULATING POLYMERS

6.1 Molecularly Doped Blends of p(g₄2T-T) and Melt-processable Insulating Polymers

Generally, fabrication of 3-dimensional (3D) bulk polymeric structures with a variety of geometries is facilitated using melt processing techniques such as extrusion and fused filament fabrication (FFF), which is a type of 3D printing.

Many conjugated polymers such as P3ATs are melt-processable in their pristine form[33, 128, 129] as well as when blended with melt-processable polymers.[130, 131] In order to render them conductive, the polymer must be doped. Sequential doping takes time since the dopant diffusion into thick structures is slow.[33] Instead, the conjugated polymers can be doped prior to melt processing. To do so, both the dopant and polymer:dopant complex must be thermally stable. Some dopants like F_4TCNQ that are toxic and sublime at high temperatures can make melt processing potentially hazardous. At the same time, the loss of the dopant leads to a reduction in the electrical conductivity as observed for F_4TCNQ:P3HT films.[132] Other doped polymers such as p(g₄2T-T) and PANI doped with sulfonic acids or bistriflimidic acid feature greatly improved thermal stability.[133, 134] However, acid dopants are not suitable for techniques such as melt extrusion since they may corrode the steel barrel of a compounder at elevated temperatures.

This chapter explores blending of p(g₄2T-T) with melt-processable polymers such as PEO, poly(ethylene-*co*-acrylic acid) (EAA copolymer) and PCL (see chemical structures in Figure 6.1). The requirement for the insulating polymers was that they are polar, their melting temperature is low (<100 °C) and they must be processable from the same solvents as p(g₄2T-T) to facilitate a solution-compounding step. The blends are doped via co-processing with the lithium (Li) salt of F_4TCNQ, which is more thermally stable than F_4TCNQ (Figure 6.2 b). The aim was to fabricate electronic materials from these 3-component blends via melt-extrusion and 3D-printing.
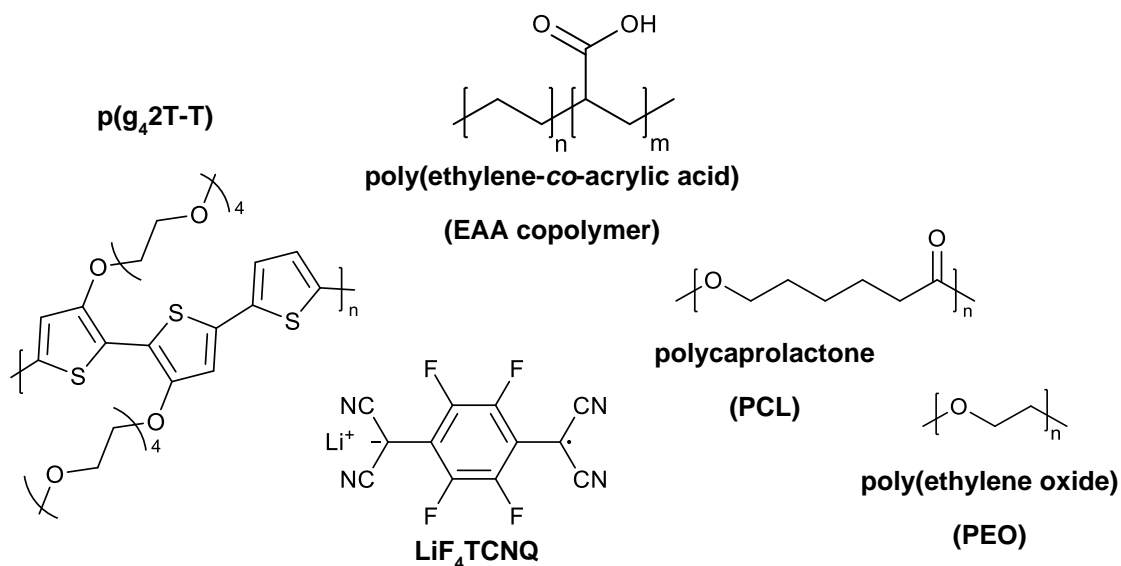
Figure 6.1 Chemical structures of the blend components p(g$_4$2T-T), LiF$_4$TCNQ and the insulating polymers EAA copolymer, PCL and PEO.

6.1.1 Materials and Methods

Materials

The synthesis of p(g$_4$2T-T) is described elsewhere.[34] PEO (M$_n$ = 1000 kg mol^{-1}) and PCl (M$_n$ = 80 kg mol^{-1}) and EEA copolymer containing 20 wt% acrylic acid were purchased from Sigma Aldrich. F$_4$TCNQ was purchased from TCI chemicals. LiF$_4$TCNQ was synthesized according to ref. [127].

For making the blends, p(g$_4$2T-T) was dissolved in CH$_3$Cl (10 g L^{-1}, 50 °C) and tetrahydrofuran (THF, 10 g L^{-1}, 50 °C). The former solution was mixed with solutions of PEO and PCL in 1:1 CH$_3$Cl:AcN (10 g L^{-1}, 50 °C) and the latter was added to a solution of EAA copolymer in THF (10 g L^{-1}, 50 °C) at desired ratios. LiF$_4$TCNQ and F$_4$TCNQ were dissolved in AcN at a concentration of 2 g L^{-1} at 50 °C and 30 °C, respectively, and added to the mixed polymer solutions at the desired molar fraction with regard to the thiophene rings of p(g$_4$2T-T).

Thin films of doped p(g$_4$2T-T) with thickness of 50 - 100 nm were prepared by mixing the solutions of p(g$_4$2T-T) and the dopant followed by spin-coating at 1000 rpm. Thick blend films of p(g$_4$2T-T), insulating polymers and LiF$_4$TCNQ were prepared by drop casting the mixtures at 40 °C on clean glass slides. The films were then peeled off and hot-pressed at 100 °C for DMA analysis.

Dynamic Mechanical Analysis

DMA and tensile deformation were performed using a Q800 dynamic mechanical analyzer from TA Instruments. DMA was carried out at a frequency of 1 Hz while ramping the temperature from -100 °C to 60°C at a heating rate of 3 °C min^{-1} using a dynamic strain of 0.04% and a preload force of 0.005 N. Tensile deformation was performed in a controlled force mode with a force rate of 1 N min^{-1}.

Thermal Gravimetric Analysis

Thermal stability measurements were performed by Thermal Gravimetric Analysis (TGA) with a Mettler Toledo TGA / DSC 3+ under a 20 mL min^{-1} air flow at a scan rate of 2 °C min^{-1}.

UV-vis and FTIR transmission spectroscopy

UV-vis-NIR absorption spectra of the films were performed with a PerkinElmer Lambda 900 spectrophotometer. Transmission FTIR spectra were recorded with a PerkinElmer FTIR Spectrometer 'Frontier' using samples drop-cast onto CaF$_2$. Variable-temperature transmission FTIR was done by heating from 20 to 100 °C followed by cooling down to 20 °C using a Specac electrical heating jacket equipped with a Specac 4000 series temperature controller (West 6100$^+$).

Electrical Conductivity

The electrical resistivity of doped p(g$_4$2T-T):PCL and p(g$_4$2T-T):PEO films was measured with a 4-point probe setup from Jandel Engineering (see experimental section of *paper I* for more details) and a U1253B handheld multimeter in 2-point configuration was used to measure the resistivity of thick doped p(g$_4$2T-T):EAA copolymer films (see experimental section of *paper II* for more details).

Optical Microscopy and Scanning Electron Imaging (SEM)

Transmission optical micrographs were recorded with a Zeiss Axio Scope A1. Samples for SEM were freeze-fractured in liquid nitrogen, and then sputtered with palladium. SEM imaging was done with a JSM-7800F (JEOL Ltd., Japan) or LEO Ultra 55 (Zeiss, Germany) at an acceleration voltage of 2-3 kV.

Melt-extrusion and FFF 3D Printing

Melt extrusion was performed using an Xplore MC5 micro-compounder. EAA, PCL and PEO were compounded for 5 min at 100 °C, 100 °C and 140 °C, respectively and extruded through a nozzle with respective diameter of 1.75 mm, 1 mm and 1 mm. The blend was compounded for 5 min at 100 °C and extruded through a nozzle with a diameter of 1.5 mm. FFF with the extruded PCL filament was performed with a Massportal Pharaoh XD20, with a nozzle temperature of respective 110 °C and a printing surface with a temperature of 30 °C.

6.1.2 Electrical Conductivity of p(g$_4$2T-T) Doped with LiF$_4$TCNQ and F$_4$TCNQ

In a first set of experiments the electrical properties of p(g$_4$2T-T) co-processed with LiF$_4$TCNQ was studied. The conductivity of p(g$_4$2T-T) doped with 10 mol% of LiF$_4$TCNQ reaches (6 ± 2) S cm^{-1} and displays similar values at higher dopant concentrations (Figure 6.2 a). Kroon et al have reported that the electrical conductivity of p(g$_4$2T-T) doped with 10 mol% F$_4$TCNQ reaches ~100 S cm^{-1} and shows similar values at higher dopant concentrations.[34] In this study, an electrical conductivity of (30 ± 2) S cm^{-1} was measured for p(g$_4$2T-T) doped with 10 mol% F$_4$TCNQ.
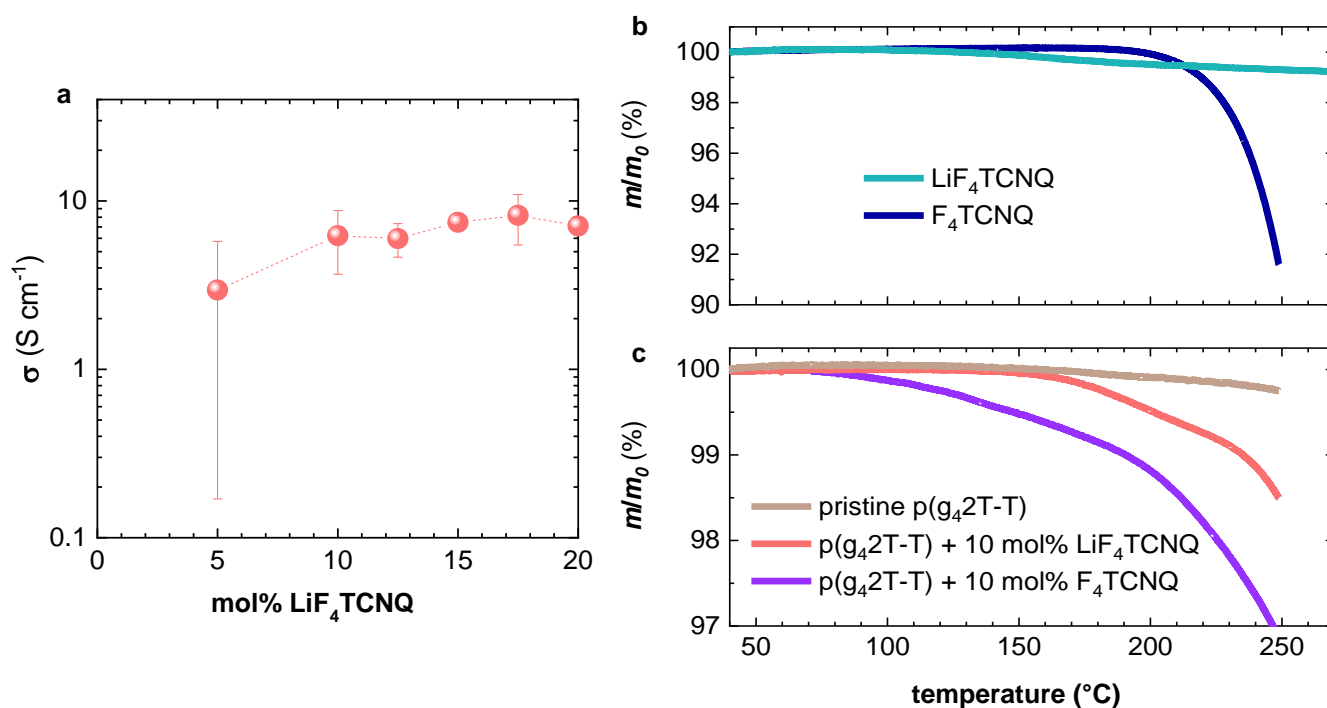
Figure 6.2 (a) Electrical conductivity σ of p(g$_4$2T-T) as a function of LiF$_4$TCNQ molar fractions. TGA curves of (b) pristine LiF$_4$TCNQ (green) and F$_4$TCNQ (blue) and (c) p(g$_4$2T-T) (beige) before and after doping with LiF$_4$TCNQ (pink) and F$_4$TCNQ (purple). m/m_0 is a measure of mass loss, indicating the ratio of the mass (m) of the material at a corresponding temperature to its initial mass (m_0).

6.1.3 Thermal Stability of p(g$_4$2T-T) Doped with LiF$_4$TCNQ and F$_4$TCNQ

TGA was used to gain information about the thermal stability of the neat dopants and doped polymer films. While F$_4$TCNQ shows a 9% drop in mass, LiF$_4$TCNQ has lost only 1% of its mass up to ~250 °C (Figure 6.2 b). The loss of mass in F$_4$TCNQ is presumably due to sublimation. Pristine p(g$_4$2T-T) shows almost no mass loss up to 250 °C. Comparing the thermal stability of the p(g$_4$2T-T) doped with 10 mol% LiF$_4$TCNQ and F$_4$TCNQ up to 250 °C, even though the absolute mass loss is not large (< 3%), a trend can be observed that the mass loss for p(g$_4$2T-T) doped with 10 mol% F$_4$TCNQ and LiF$_4$TCNQ starts at 90 °C and 160 °C, respectively (Figure 6.2 c).

Further, the impact of heating on the electrical properties of p(g$_4$2T-T) doped with F$_4$TCNQ and LiF$_4$TCNQ was explored. The resistance (R) at elevated temperatures relative to the resistance at 30 °C (R_{30}) is shown in Figure 6.3 a. R/R_{30} of p(g$_4$2T-T) doped with 10 mol% LiF$_4$TCNQ remains unchanged up to 130 °C. p(g$_4$2T-T) doped with 10 mol% F$_4$TCNQ shows a similar trend. However, the resistance of p(g$_4$2T-T) doped with LiF$_4$TCNQ increases by cooling the films to 30 °C. In order to probe the influence of time on the electrical stability of F$_4$TCNQ and LiF$_4$TCNQ, the doped polymer films were subjected to 120 °C and the change in resistance was recorded relative to the initial measured resistance at 120 °C (R_{120}) (Figure 6.3 b). p(g$_4$2T-T):LiF$_4$TCNQ shows an increase after 30 min, while p(g$_4$2T-T):F$_4$TCNQ appears stable.
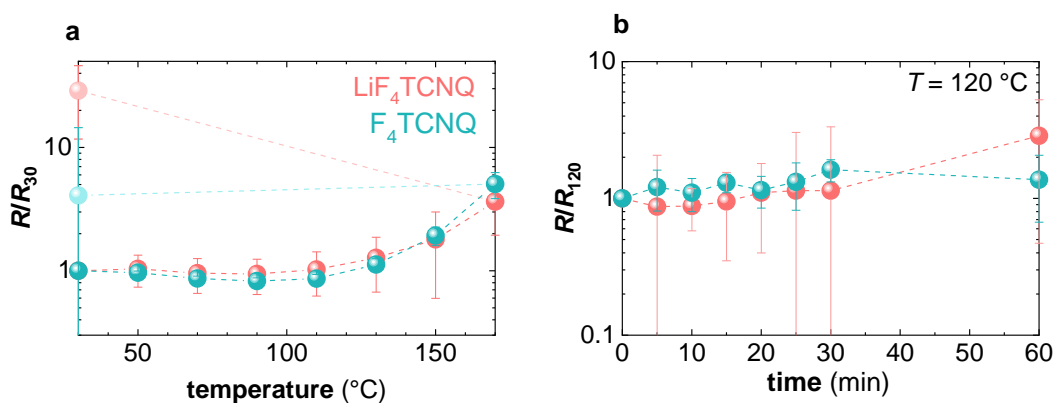
Figure 6.3 (a) Electrical resistance R of p(g$_4$2T-T) doped with LiF$_4$TCNQ (pink) and F$_4$TCNQ (green) relative to their electrical resistance at 30 °C, R_{30}, as a function of temperature. (b) R of p(g$_4$2T-T) doped with LiF$_4$TCNQ and F$_4$TCNQ at 120 °C related to their initial resistance at 120 °C (R_{120}) as a function of time.
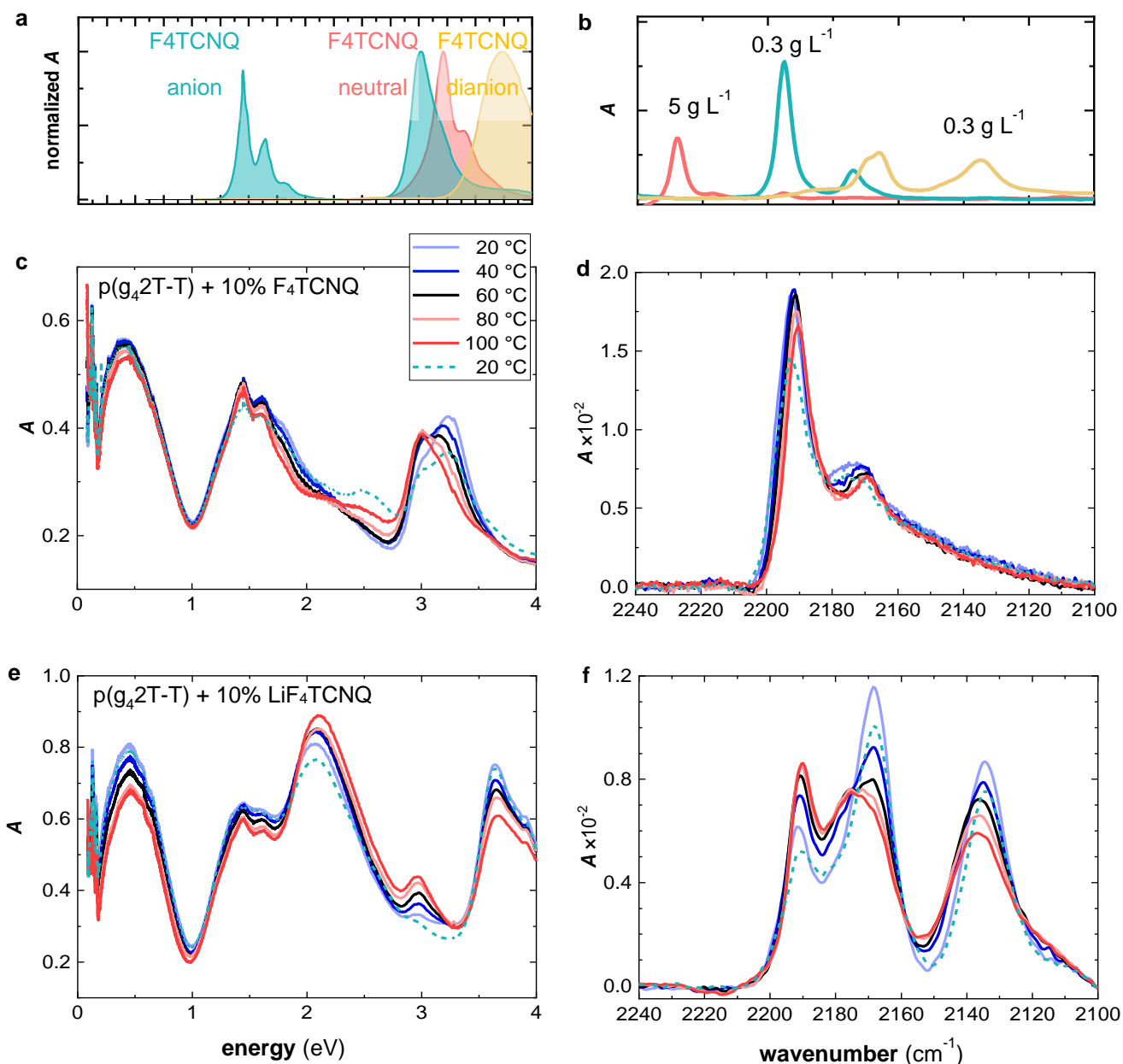
Figure 6.4 UV–vis and FTIR absorption spectra of (a-b) the cyano stretch vibrations of F_4TCNQ neutral, anion and dianion (reprinted with permission from ref [127] published by Springer Nature) and p(g$_4$2T-T) doped with (c-d) F_4TCNQ and (e-f) LiF$_4$TCNQ at different temperatures. Absorbance is denoted by A.

A series of UV-vis and FTIR spectra were recorded by Dr. David Kiefer for p(g$_4$2T-T) doped with 10 mol% F_4TCNQ and LiF$_4$TCNQ at different temperatures to probe the change in the concentration of F_4TCNQ neutral, anion and dianion (Figure 6.4 a-b). The height of the absorption peaks assigned to the cyano stretch vibration is proportional to the concentration of F_4TCNQ anions and dianions.[127] In

spectra of the films doped with 10 mol% F$_4$TCNQ, no dianions can be discerned. (Figure 6.4 c-d). Increasing the temperature leads to a decrease in polaronic absorbance at ~0.4 eV and an increase in neat polymer absorbance at ~2.9 eV (Figure 6.4 c). Simultaneously, the height of the peak assigned to neutral F$_4$TCNQ (~ 3.2 eV) decreases and a peak associated with anions (~3.0 eV) increases. Sublimation of F$_4$TCNQ, reduces the absolute content of the dopant in the film. Therefore, the ratio of anion to neutral concentration increases. This behavior, together with the fact that the mobility of charges increases at higher temperature can explain why the conductivity does not decrease up to 100 °C. After cooling, neutral F$_4$TCNQ is partially regained while the F$_4$TCNQ anion concentration decreases. This is indicated by an increase in the height of the of F$_4$TCNQ neutral absorbance peak as well as a decrease in its anion absorbance peak while the one for neat polymer increases (Figure 6.4 d). Therefore, it is argued that besides sublimation, neutral F$_4$TCNQ is converted to its anion upon heating. Upon heating p(g$_4$2T-T) doped with LiF$_4$TCNQ, the same trend is observed for the polaronic absorbance at 0.45 eV (Figure 6.4 e). Concomitantly, the dianion concentration decreases and anion concentration increases. Since no sublimation takes place in this temperature range (Figure 6.2 b-c), the absorbance peaks of both dianions and anions are almost returned to their initial state upon cooling of the films (Figure 6.4 f).

6.1.4 Electrical Properties of the Blends

To prepare thick films of molecularly doped blends, p(g$_4$2T-T) solution was mixed with EAA copolymer, PCL and PEO solutions at the weight fractions ranging from 10 - 50 wt%. The mixed solutions were then co-processed with 10 mol% LiF$_4$TCNQ (with regard to thiophene rings) and drop cast on glass slides.
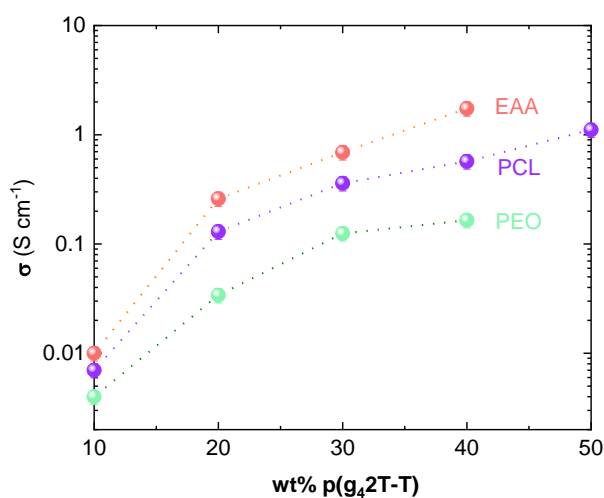
Figure 6.5 Electrical conductivity σ of blends of p(g$_4$2T-T) with PCL, EAA copolymer, PEO and 10 mol% LiF$_4$TCNQ (with regard to thiophene rings) as a function of p(g$_4$2T-T) content.

6.1.5 Melt Processing of the Insulating Polymers

Filaments of the insulating polymers were extruded and used for 3D printing. A homogeneous filament of PEO could only be obtained at 140 °C. PCL and EAA copolymer were both successfully extruded at 100 °C, which is in the temperature range where the conductivity of p($g_4$2T-T) is stable (see Figure 6.3). The resulting PCL and EAA copolymer filaments were used for 3D printing. It was very challenging to 3D print EAA copolymer due to its softness. However, 3D printing of PCL was possible at 110 °C. As a result, further experiments involving melt processing were carried out with the blends of p($g_4$2T-T) and PCL.

6.1.6 p($g_4$2T-T):PCL Blends

To study the microstructure of the p($g_4$2T-T):PCL blend, optical microscopy was carried out. Microscopy images of 2:8 p($g_4$2T-T):PCL (Figure 6.6 a) indicate an even dispersion of p($g_4$2T-T) throughout the matrix with the presence of some agglomerates.

The thermomechanical properties of the p($g_4$2T-T):PCL blends with and without LiF$_4$TCNQ were explored using DMA. Since thick drop-cast films were inhomogeneous in terms of thickness and had the tendency to crack, they were hot-pressed at 100 °C prior to DMA analysis (Figure 6.6 b). The conductivity of the hot-pressed 1:9 and 2:8 p($g_4$2T-T):PCL films doped with 10 mol% LiF$_4$TCNQ were 4×10^{-3} S cm^{-1} and 13×10^{-2} S cm^{-1}. Tensile deformation of the blends indicates a slight decrease in modulus of PCL from ~160 MPa to ~145 MPa and ~130 MPa upon blending with 20 wt% and 10 wt% p($g_4$2T-T), respectively (Figure 6.6 c). The blends co-processed with 10 mol% LiF$_4$TCNQ with regard to thiophene rings feature a higher modulus of $E \approx 200$ MPa and $E \approx 184$ MPa for 1:9 and 2:8 p($g_4$2T-T):PCL blends, respectively (Figure 6.6 c). The increase in elastic modulus of p($g_4$2T-T) as a result of molecular doping will be further discussed in *chapter 8*.
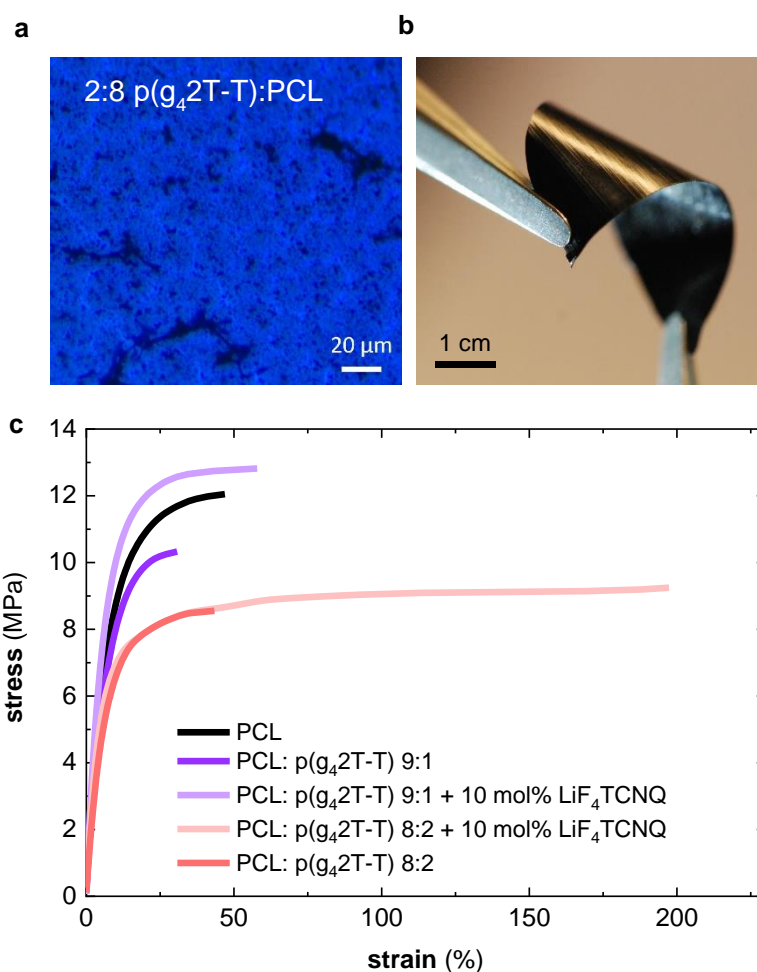
Figure 6.6 (a) Optical microscopy image of a drop-cast film of 2:8 p($g_4$2T-T):PCL, (b) photograph of a hot-pressed 2:8 p($g_4$2T-T):PCL film, and (c) tensile deformation stress-strain curves of pressed films of 2:8 and 1:9 p($g_4$2T-T):PCL with and without 10 mol% of LiF$_4$TCNQ with regard to thiophene rings.

A DMA thermogram of neat PCL shows a loss modulus maximum at ~ -50 °C, corresponding to the T_g of the polymer (Figure 6.7 a). The glass transition of PCL and p($g_4$2T-T) overlap, considering that the T_g of the latter is at -46 °C (Figure 4.2). Therefore, 2:8 p($g_4$2T-T):PCL exhibits only one peak in the loss modulus at -48 °C. Upon doping with LiF$_4$TCNQ, the peak in the loss modulus exhibits a shoulder at -11 °C, which is assigned to the glass transition of doped p($g_4$2T-T). A change in the glass transition temperature of p($g_4$2T-T) as a result of molecular doping will be discussed in *Chapter 8*.
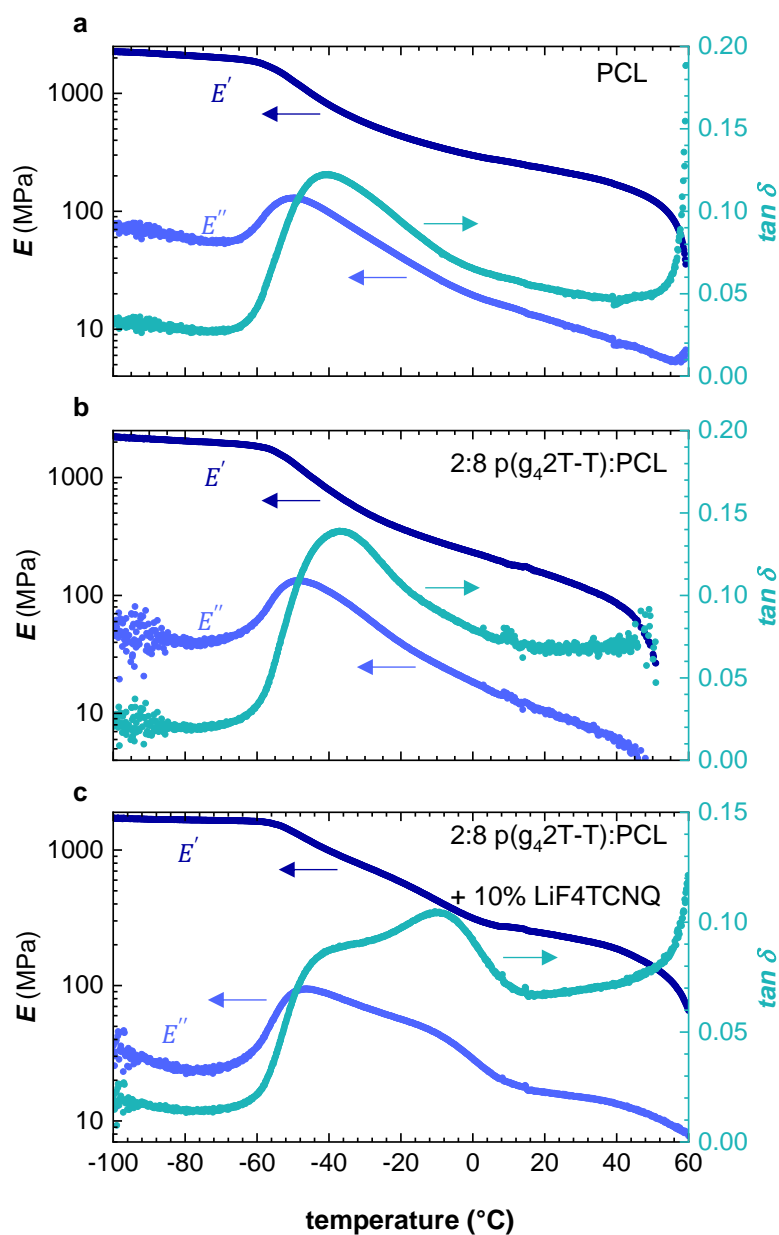
Figure 6.7 DMA thermograms of neat PCL, 2:8 p(g₄2T-T):PCL and 2:8 p(g₄2T-T):PCL doped with 10 mol% LiF₄TCNQ (with regard to thiophene rings).

6.1.7 Melt Extrusion of the Blends

Melt extrusion of 2:8 p(g$_4$2T-T):PCL doped with 10 mol% LiF$_4$TCNQ was carried out. To do so, 400 mg of p(g$_4$2T-T) and 1600 mg of PCL were dissolved in CH$_3$CL and CH$_3$Cl:AcN, respectively, and mixed. A LiF$_4$TCNQ solution in AcN was added to the blend solution and the mixture was dried using a rotary evaporator. The resulting dry blend was cut into pieces and fed into an Xplore

Microcompounder for compounding and extrusion at 100 °C. The extruded filament (shown in Figure 6.8) was unfortunately not electrically conductive. However, dissolution of the filament in 1:1 CH$_3$Cl:ACN and drop-casting resulted in a film with a conductivity of 3×10^{-2} S cm^{-1}, suggesting that the material had not degraded during compounding. To study the microstructure of the filament and drop-cast film, SEM images were recorded. SEM images of the filament revealed the presence of up to 50 µm large p(g$_4$2T-T) domains (Figure 6.8 b-c). It appears that melt processing led to loss of connectivity of the p(g$_4$2T-T) phase, which is required for charge transport. SEM images of the drop-cast film do not show any large domains of p(g$_4$2T-T) (Figure 6.8 d), which is in agreement with the film being electrically conductive.
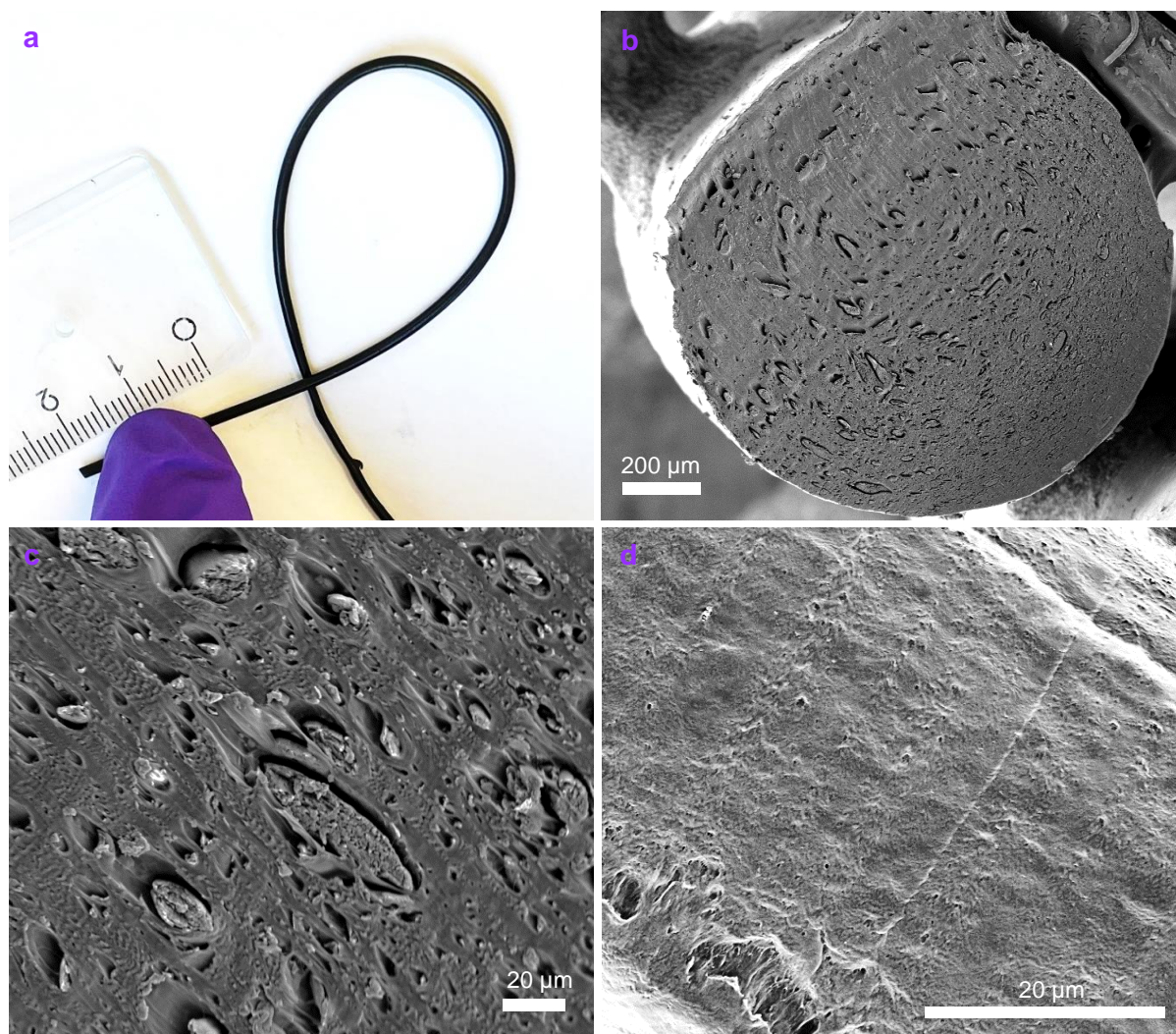
Figure 6.8 (a) Photograph and SEM images (b-c) of the extruded filament of 2:8 p(g$_4$2T-T):PCL doped with 10 mol% LiF$_4$TCNQ and (d) a drop-cast film prepared from a redissolved section of the filament.

6.2 Blend Fibers of p(g₄2T-T) and Polyurethane

For fabrication of unobtrusive electronic devices to be worn close to or inside the body, materials are required that in addition to being biocompatible, match the elastic modulus (for skin, $E = 0.1 - 20$ MPa)[135] of the tissue that they are in contact with. Further, such a stretchable electronic device should be able to withstand reversible deformation up to 55%,[136] that is the extent the skin can be stretched on certain parts of the body *e.g.*, on a knee joint.[13, 136] Sturdy and durable e-textiles should be stable and *reversibly* stretchable, in terms of both mechanical and electrical properties. Electrically conducting fibers are an important building block of e-textiles.
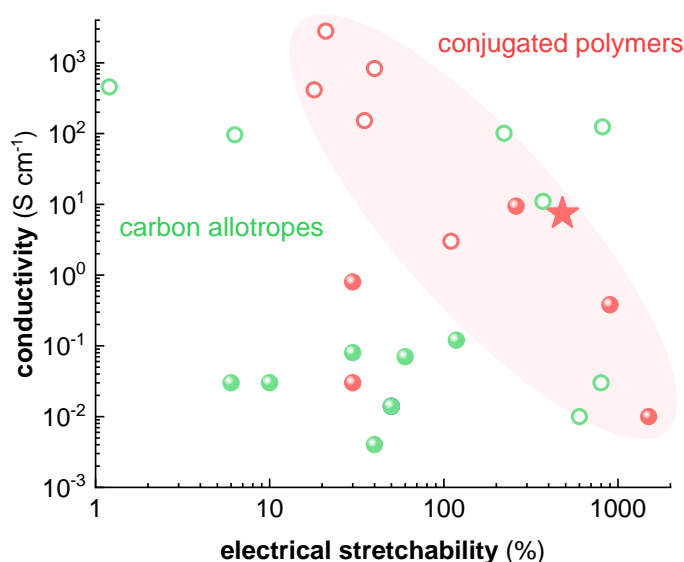
Figure 6.9 Ashby plot showing conductivity vs. electrical stretchability, *i.e.,* maximum stretchability for which the material retains its conductivity, of carbon-based conductive fibers made by blending conjugated polymers (filled pink circles) or compounding carbon allotropes (filled green circles) with stretchable polymers or made by any other means comprising conjugated polymers (empty pink circles) or carbon allotropes (empty green circles). The data was obtained from references [137-147]. The 1:4 p(g₄2T-T):polyurethane (PU) fibers doped with iron(III) p-toluenesulfonate hexahydrate (Fe(Tos)₃.H₂O) in this study are shown as a star. This figure is adapted with permission from ref. [81] published by Wiley.

Conjugated polymers and conducting carbon allotropes as well as metals are generally not stretchable in their pristine form.[148] Therefore, it is of interest to prepare stretchable conducting fibers by combining

an elastomer with a conducting material through blending with other polymers,[79, 80] compounding with nanomaterials [149-153] or other methods such as coating the elastomeric fibers.[142, 143, 154] Figure 6.9 displays the electrical stretchability, *i.e.,* as the maximum strain up to which a material or device remains conductive vs. the conductivity of the un-stretched carbon-based conductive fibers prepared by the aforementioned methods. Polymer blend fibers (filled pink circles in Figure 6.9) tend to feature a higher electrical stretchability compared to their composite fiber counterparts (filled green circles in Figure 6.9).
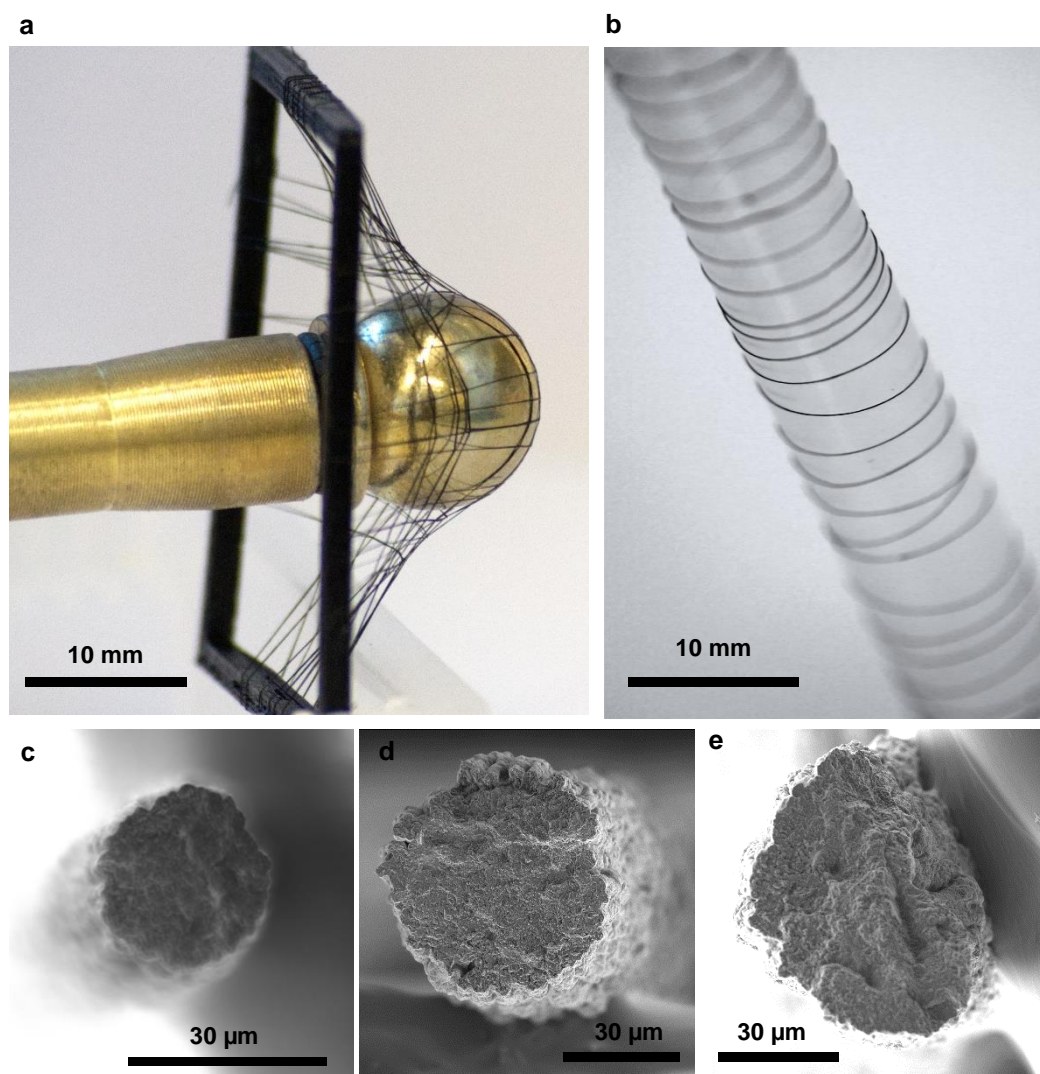
Figure 6.10 Photographs of (a) a stretched weave and (b) a roll of p($g_4$2T-T):PU fibers. SEM images of the cross-section of p($g_4$2T-T):PU fibers (c) F_{thin}, (d) F_{midi} and (e) F_{thick}. This figure is reproduced with permission from ref. [81] published by Wiley.

Highly stretchable materials like rubbers usually have low modulus. It would be advantageous to directly use a conducting material that is inherently soft. Therefore, conducting stretchable fibers (Figure 6.10 a-b) with low modulus were fabricated from a blend of $p(g_42T-T)$ and polyurethane (PU). The former component imparts electrical conductivity and softness, and the latter introduces elasticity and stretchability.

Fibers of 1:4 $p(g_42T-T)$:PU were wet-spun (detailed procedure is described in *paper II*) with three diameters denoted as F_{thin}, F_{midi} and F_{thick} with respective cross-sectional areas of ~640 µm², ~2510 µm² and ~3800 µm² (Figure 6.10 c-e). Neat PU_{thin} and PU_{thick} fibers were also prepared with the same spinning parameters as their blend counterparts

6.2.1 Impact of Doping on the the Electrical and Mechanical properties

In a first set of experiments, the blend fibers were sequentially doped with $Fe(Tos)_3.H_2O$ (see chemical structure in Figurev1.3) in AcN for different lengths of time from 1 h - 48 h (schematic is shown in onset of Figure 6.11 a). The highest conductivity values were obtained for a doping time of 24 h, resulting in (7.4 ± 0.8) S cm⁻¹, (2.4 ± 0.3) S cm⁻¹ and (2.9 ± 0.6) S cm⁻¹ for F_{thin}, F_{midi} and $F_{thick.}$ fibers, respectively (see *paper II* for conductivity values at different doping times).
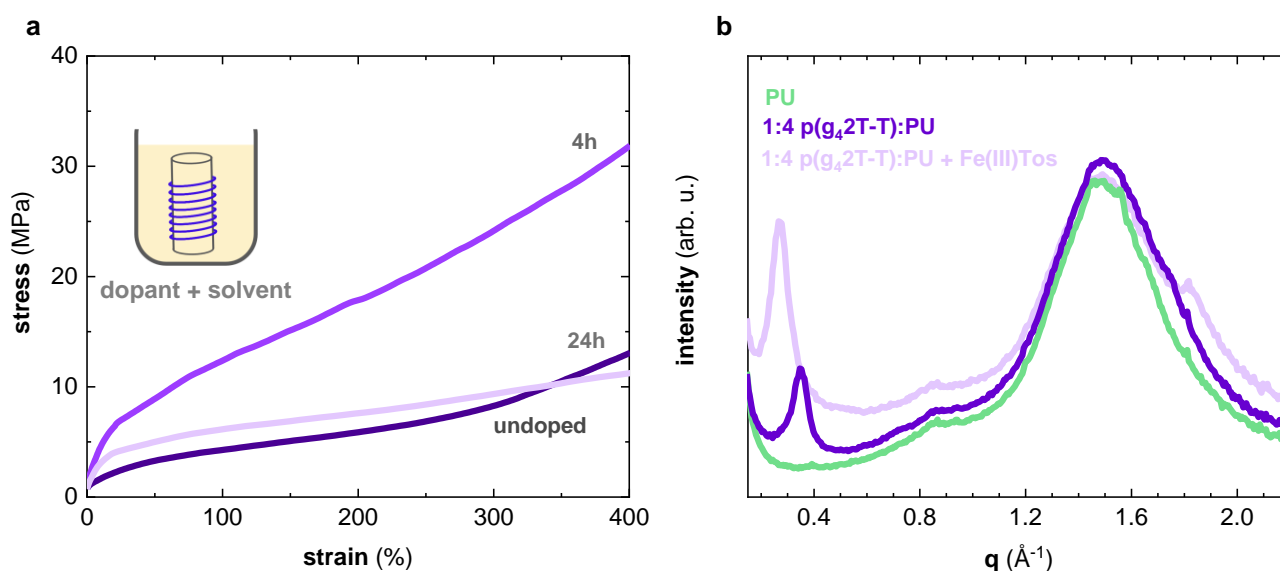
Figure 6.11 (a) Stress/strain curves recorded during tensile deformation of 1:4 $p(g_42T-T)$:PU fiber (F_{thin}) before (purple) and after doping with $Fe(Tos)_3.H_2O$ for 4 h and 24 h up to a strain of 400% without failure. (b) WAXS diffractograms of neat PU (PU_{thick}, green), and $p(g_42T-T)$:PU fibers (F_{midi}) before (dark purple) and after doping with $Fe(Tos)_3.H_2O$ for 24 h (light purple). Reproduced with permission from ref [81] published by Wiley.

Further, the impact of molecular doping on the stiffness of the fibers was studied using tensile deformation up to 400% strain. Stress-strain curves of 1:4 $p(g_42T-T)$:PU fibers (F_{thin}) indicate an increase in Young's modulus from (19 ± 3) MPa to (60 ± 6) MPa after doping for 1 h (Figure 6.11 a). However, a longer doping time resulted in fibers with a Young's modulus of (33 ± 1) MPa (Figure 6.11 a).

To investigate how doping affected the nanostructure of the blend fibers, WAXS was carried out. PU fibers (PU_{thick}) are mostly amorphous, giving rise to a broad halo around 1.6 $\text{Å}^{-1}$ (Figure 6.11 b). The addition of $p(g_42T-T)$ leads to the emergence of a peak at 0.34 Å^{-1} that corresponds to lamellar stacking of the conjugated polymer. Sequential doping of the blend fiber with $Fe(Tos)_3.H_2O$ for 24 h resulted in a more pronounced lamellar stacking peak that had shifted to 0.26 Å^{-1}. Concurrently, a peak at ~1.81 Å^{-1} is observed, which corresponds to π-π stacking.[34, 133] Arguably, the increase in Young's modulus upon molecular doping can be explained with increased π-π stacking of $p(g_42T-T)$.[44] At the same time, longer doping times lead to a further ingression of dopant molecules that distort the nanostructure of the polymer, which may explain the slight decrease in stiffness. The same behavior is observed for $p(g_42T-T)$ doped with H-TFSI acid for which the elastic modulus first increases upon the addition of H-TFSI, followed by a decrease at higher dopant concentrations (see *Chapter 8* for more detail).

6.2.2 Stability of the p(g$_4$2T-T):PU Fibers

In order to determine the electrical stretchability of the doped blend fibers, tensile deformation was carried out and the electrical resistance was recorded at the same time. 1:4 $p(g_42T-T)$:PU fibers (F_{midi}) doped with $Fe(Tos)_3.H_2O$ break at a tensile strain of $\varepsilon_{brea} \approx 480\%$ (Figure 6.12 a). Meanwhile, the resistance relative to the initial value (R/R_0) only marginally changes up to 200% strain and increases by 3 times until failure. Hence the electrical stretchability and strain at break are considered to be the same (480%, Figure 6.12 a).

To Probe the stability of the mechanical and electrical properties of the fibers, the same experiment was carried out on a blend fiber (F_{midi}) that was stored at room temperature in air over 9 months after spinning and doping. It was found that its mechanical properties remained unaffected to a great extent with an $\varepsilon_{break} = 435\%$ (Figure 6.12 b). The electrical resistance of the 9-month-old fiber showed a similar trend upon stretching (Figure 6.12 b). Further, monitoring of the electrical conductivity of 1:4 $p(g_42T-T)$:PU blend fibers (F_{midi} and F_{thick}) doped with $Fe(Tos)_3.H_2O$ (24 h) over 12 months revealed a high electrical stability with a slight drop in conductivity during the first month (Figure 6.12 c).
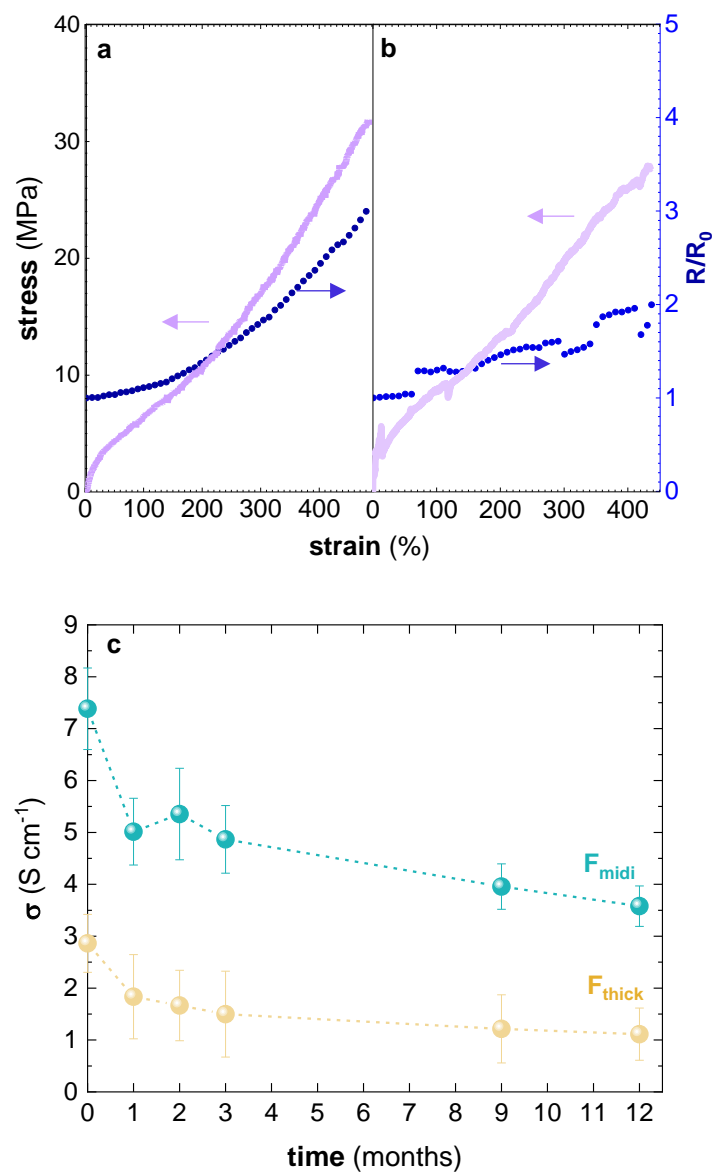
Figure 6.12 Stress/strain curves recorded during tensile deformation of (a) fresh p(g$_4$2T-T):PU fiber (F$_{midi}$) doped with Fe(Tos)$_3$.H$_2$O (light purple) and (b) characterized 9 months after doping, during which time they were stored at room temperature in air. Also shown is the *in situ* recorded change in electrical resistance R/R_0 (blue symbols) during tensile deformation where R_0 is the resistance of the unstretched fiber. (c) Electrical conductivity of p(g$_4$2T-T):PU fibers F$_{midi}$ (green) and F$_{thick}$ (yellow) doped with Fe(Tos)$_3$.H$_2$O monitored during 12 months of storage. Reproduced with permission from ref. [81] published by Wiley.
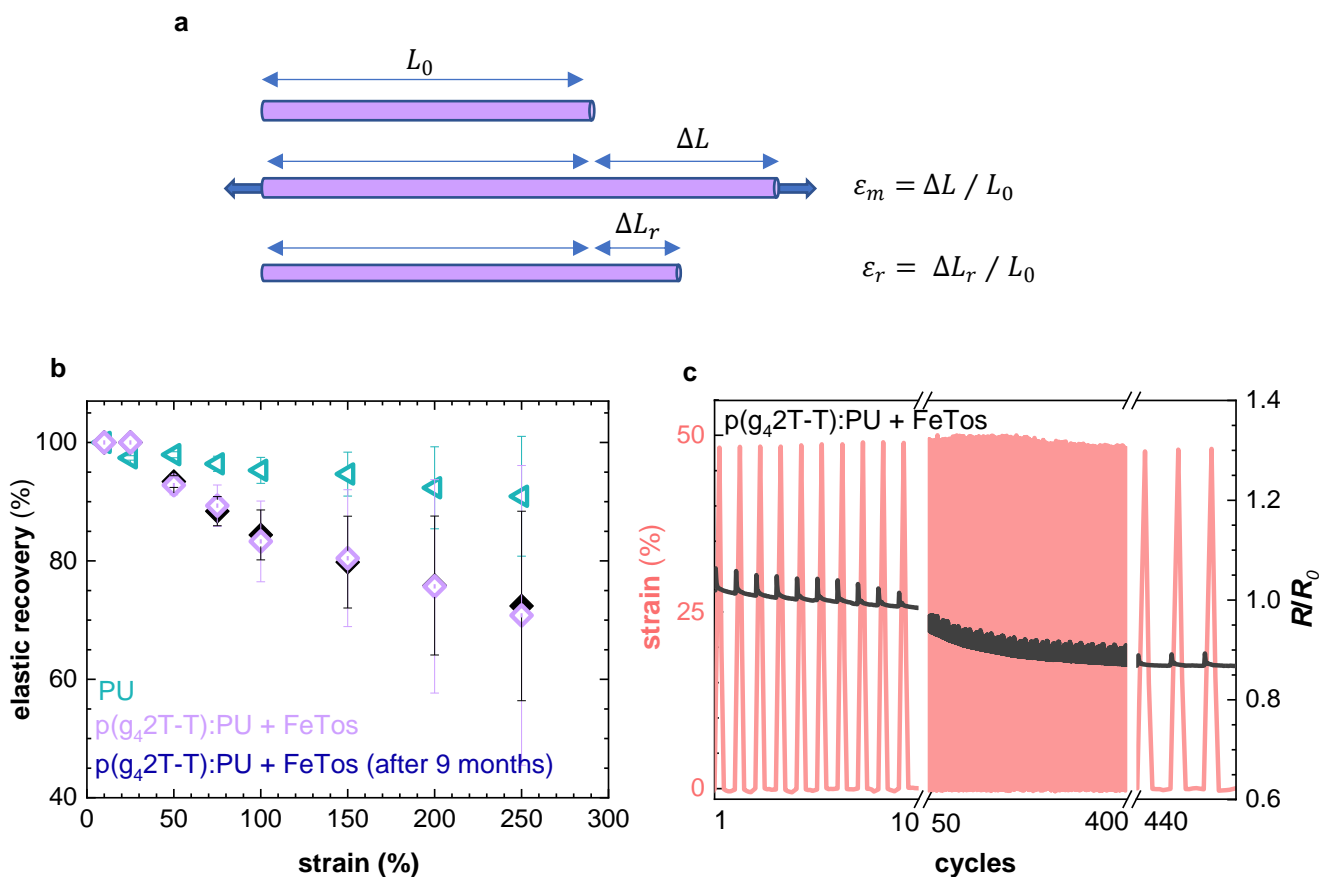
Figure 6.13 (a) Schematic of an elastic recovery experiment: a fiber with initial length of L_0 is stretched by ΔL ($\varepsilon_m = \Delta L / L_0$) and after relaxation the increase in length of the fiber ΔL_r ($\varepsilon_r = \Delta L_r / L_0$) is determined. The elastic recovery is defined as $(\varepsilon_m - \varepsilon_r)/\varepsilon_m$. (b) Elastic recovery for a p($g_4$2T-T):PU fiber (F_{midi}) doped with Fe(Tos)$_3$.H$_2$O recorded shortly after doping (purple diamonds) and after 9 months storage at room temperature in air (blue diamonds) and for the PU fiber (PU$_{thick}$) (green triangles). (c) Cyclic strain testing of p($g_4$2T-T):PU (F_{midi}) fiber with a maximum strain of 50% followed by relaxation for 30 seconds as well as in-situ resistance ratio (R/R_0). Reproduced with permission from ref [81] published by Wiley.

In a further set of experiments, the extent of elastic recovery was probed during relaxation for 30 s after stretching to different strains from 5% to 250%. If the fiber with initial length of L_0 is stretched by ΔL ($\varepsilon_m = \Delta L / L_0$) and after relaxation for 30 seconds the length of the fiber is increased by ΔL_r ($\varepsilon_r = \Delta L_r / L_0$), the elastic recovery will be less than 100% and is defined as $(\varepsilon_m - \varepsilon_r)/\varepsilon_m$ (see the schematic in Figure 6.13 a). More details about the elastic recovery experiment can be found in *paper II*. It is observed that the doped p($g_4$2T-T):PU fibers show ~ 7% loss in elastic recovery up to 50% stretching

(Figure 6.13 b). Of high interest in this context is that doped p($g_4$2T-T):PU fibers stored over 9 months display exactly the same elastic recovery behavior as fresh fibers (Figure 6.13 b).

Cyclic stretching tests (50% strain and subsequent relaxation for 30 s) accompanied by an *in-situ* resistance measurement of the doped blend fibers, F_{midi}, indicates that the change in resistance (R/R_0) at each stretching cycle ($\Delta R/R_0 \approx 0.04$) is stable throughout 453 cycles (Figure 6.13 c). Therefore, p($g_4$2T-T):PU fibers doped with $Fe(Tos)_3.H_2O$ feature a high degree of cyclic stability.

7

NANOCOMPOSITES OF p(g$_4$2T-T) AND NANOCELLULOSE

Cellulose (see chemical structure in Figure 7.1) is the most abundant biopolymer in nature, mostly found in plant cell walls providing mechanical support with its extended chain conformation and microfibrillar morphology. [155] Cellulose microfibrils disintegrated from plant cell walls are called microfibrillated cellulose (MFC). Going further down in the hierarchical structure of the cellulose fibers, MFC consist of cellulose nanofibrils (CNF) that are packed together. Therefore, CNF has a lower lateral dimension (~ 3 - 20 nm)[156] than MFC that can have a width of up to 100 nm in width.[157] The length of MFC and CNF is on the order of several micrometers. Consequently, these fibers have a high aspect ratio. Each cellulose fibril is composed of disordered and crystalline domains. Using acid hydrolysis to remove the disordered regions, cellulose nanocrystals (CNC) with a width from 2 nm to 20 nm and length ranging from 100 nm to 500 nm are obtained,[158] resulting in a modulus of more than 100 GPa.[159, 160] Depending on the acid used, new surface functionalities can be added to CNC. For instance, hydrolysis with sulfuric acid gives rise to the formation of charged sulfate groups on cellulose units.

Due to their high stiffness and strength, cellulose nanomaterials have been widely used for mechanical reinforcement of polymers.[156, 161-163] There are studies that demonstrate by incorporation of nanocellulose into conjugated polymers, can alter the mechanical properties [91, 164] and the electrical performance of the conjugated polymer may also enhance.[165-167]

This chapter describes the initial attempts to combine p(g$_4$2T-T) with different types of nanocellulose for increasing the elastic modulus without compromising the electrical properties.
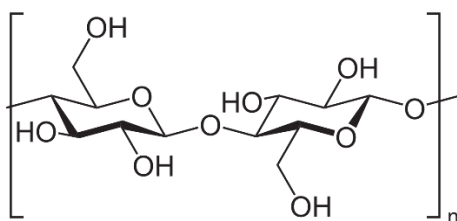
Figure 7.1 Chemical structure of cellulose.

7.1 Materials and Methods

Materials

NaOH-neutralized CNCs from sulfuric acid hydrolysis were obtained as a spray-dried powder from CelluForce, Canada. CNC was dispersed in N,N-dimethylformamide (DMF) at a solid content of 0.004% and 1 wt% using an Ultra Turrax high shear mixer at 14 000 rpm for 10 min.

MFC (Exilva Forte, 2.1 wt% solid content in water) was kindly provided by Borregaard AS, Norway, and solvent exchanged to DMF at concentration of 1.18 wt%.

CNF (2.6 wt% solid content in water) was kindly provided by the research institutes of Sweden (RISE), and solvent exchanged to DMF at the concentration of 0.9 wt%.

The solvent exchange from water to DMF for the obtained MFC and CNF dispersions was carried out by the following procedure: 400 mL of DMF was added to 2g of the respective aqueous cellulose dispersion (MFC or CNF). The mixture was sonicated for 20 min followed by stirring for 30 min. Then, a rotary evaporator at high temperature was used to remove the solvent to the point that cellulose is still wet. The above procedure was repeated several times in order to achieve complete water removal and exchange to DMF.

The synthesis procedure of p(g$_4$2T-T) *batch 1*, which is used throughout the rest of this thesis, is described elsewhere.[34] The second batch of p(g$_4$2T-T) used in this study, denoted as *batch 2*, was synthesized by Dr. Mariza Mone using a previously reported method.[34]

Molecular Weight Determination of the Polymers

The size exclusion chromatography (SEC) for molecular weight distribution of p(g$_4$2T-T) *batch 1* is described in experimental section of *paper I*. SEC for p(g$_4$2T-T) *batch 2* was performed by Jaywant Phopase in Laboratory of Organic Electronics, Linköping university on an Agilent 1260 Infinity II, equipped with a Polargel-M column and a triple detector. The eluent was DMF + 0.1% LiBr and the temperature of 30 °C was used. Poly(methyl methacrylate) (PMMA) standards were used for calibration.

Preparing the Nanocomposites

p(g$_4$2T-T) was dissolved in DMF at 20 g L^{-1} and mixed with cellulose dispersions at the desired ratios.

To dope the composites, PDSA (from Sigma Aldrich, 10 g L^{-1} in AcN) and F$_4$TCNQ (from TCI chemicals, 2 g L^{-1} in AcN) were added to the dispersion of p(g$_4$2T-T) and nanocellulose.

The composites containing MFC and CNF were prepared at 40 °C, while the ones with CNC were made at a higher temperature (100 °C without PDSA and 70°C with PDSA).

Tensile Deformation

Tensile testing was carried out using a Q800 dynamic mechanical analyzer from TA Instruments, at a force rate of 0.005 N min^{-1}. All samples from *batch 2* of p(g$_4$2T-T) were supported by paper frames (see more details in section 2.8).

Electrical Measurements

The electrical conductivity of the nanocomposites was measured using the same method described in experimental section of *paper I*.

7.2 Mechanical Properties of Nanocomposites of p(g$_4$2T-T) and CNC

A CNC dispersion (0.004 wt%) was mixed with p(g$_4$2T-T) *batch 1* ($M_n \approx$ 24 Kg mol^{-1}, PDI $\approx$ 3.3) at a weight ratio of 15:100 and tensile deformation was carried out to analyze the mechanical properties. (Figure 7.2 c). The introduction of 13 wt% CNC slightly increased the modulus from (8 ± 4) MPa to (18 ± 5) MPa (cf. section 3.2). Berg et al. have reported that doping of polyaniline (PANI) improves its interaction with cellulose nanowhiskers due to the introduction of positive charges on the polymer. Further, it is argued that the interaction between doped PANI and hydroxyl groups on cellulose whiskers is the dominant factor for the absorption onto the cellulose whiskers.[91] Since only 1 out of 8 hydroxyl groups of CNC is sulfate functionalized, there is a possible interaction between doped p(g$_4$2T-T) and CNC hydroxyl groups.[91] Therefore, 6 mol% PDSA was added to the composite of 10:100 CNC:p(g$_4$2T-T) (Figure 7.2 a). Stress-strain curves indicate a higher modulus of ~ 45 MPa as a result of doping despite a lower CNC content (9 wt%) compared to the undoped composite. However, the film appeared inhomogeneous and processing at 70°C led to degradation and a color change of the mixture. Therefore, to decrease the processing temperature, the concentration of CNC in DMF was increased to 1 wt%. Further, new nanocomposites with a composition of 10:100 and 1:100 CNC:p(g$_4$2T-T) with addition of 6 mol% PDSA were fabricated (Figure 7.2 b). Tensile deformation reveled that the modulus of the composites is ~15 MPa and ~11 MPa, respectively (Figure 7.2 c). Generally, a uniform dispersion of nanoparticles in the polymer matrix is essential for altering the mechanical properties.[168] The lower modulus that was obtained when increasing the cellulose dispersion concentration from 0.004 wt% to 1 wt% indicates that CNC was not dispersed to the same extent. It is speculated that the minor influence of the CNC content on the modulus in the presence of PDSA arises because of the poor cellulose dispersion.
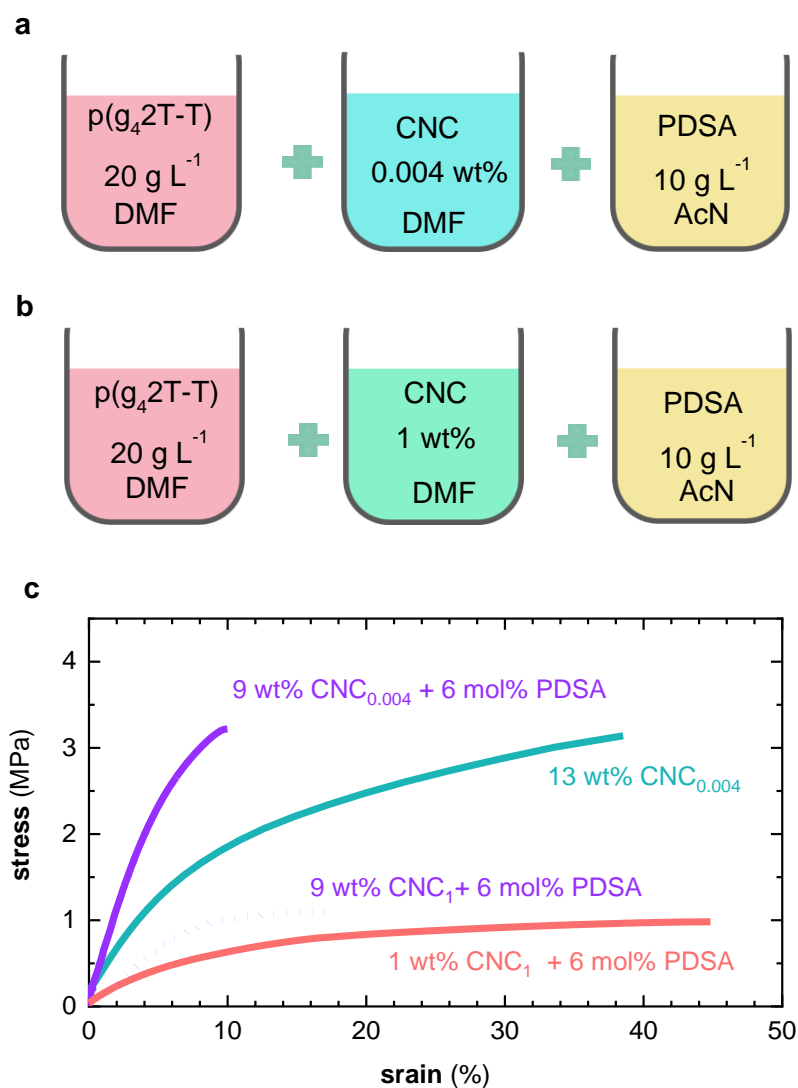
Figure 7.2 Schematic of nanocomposite preparation procedure of p($g_4$2T-T) and CNC at (a) 0.004 wt% and (b) 1 wt% in DMF, followed by doping with PDSA. 0.004 wt% and 1 wt% CNC dispersions in DMF are denoted as $CNC_{0.004}$ and CNC_1, respectively. (c) Stress-strain curves recorded during tensile deformation of the nanocomposites with 13 wt% $CNC_{0.004}$ (green), 9 wt% $CNC_{0.004}$ + 6 mol% PDSA (solid purple), 9 wt% CNC_1 + 6 mol% PDSA (dotted purple) and 1 wt% CNC_1 + 6 mol% PDSA (pink).

7.3 Mechanical Properties of Nanocomposites of p($g_4$2T-T) with MFC and CNF

Nanocomposites with MFC, which has non-functionalized hydroxyl groups, were fabricated. Tensile testing of MFC-based nanocomposites reveals that the modulus is significantly improved and increased

with MFC content. The modulus of a composite containing 13 wt% MFC reaches (204 ± 54) MPa. (Figure 7.3). Even though CNC has a higher crystallinity than MFC, hence higher modulus, larger improvement in the elastic modulus of p($g_4$2T-T) is observed upon introduction of MFC than CNC. This can be associated with the higher aspect ratio of MFC and a better dispersion. While the dispersion of MFC in DMF was stable, the CNC dispersion heavily sedimented with time.
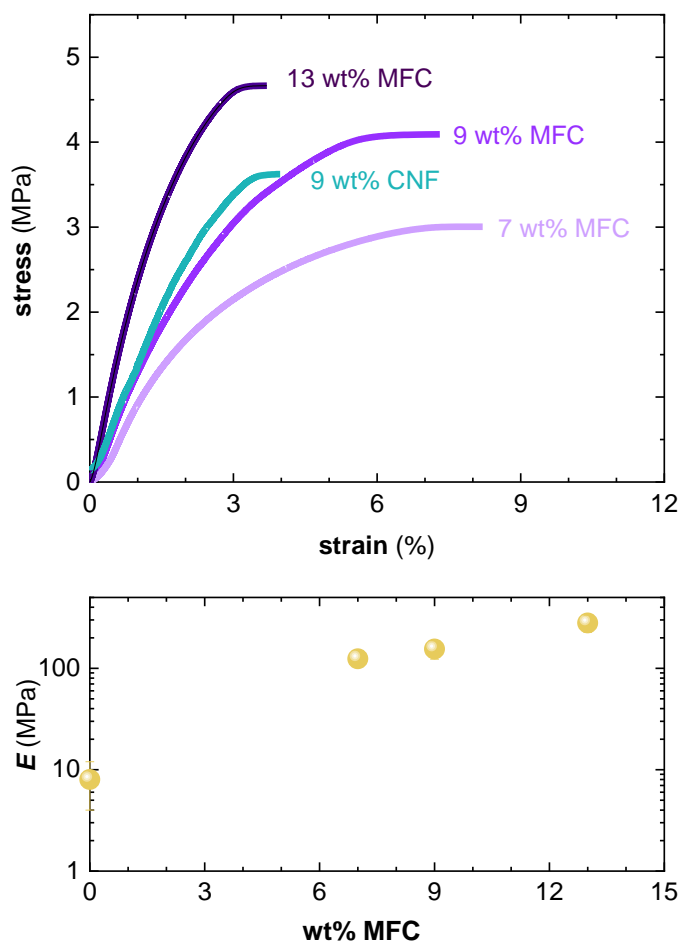
Figure 7.3 (a) Tensile deformation stress-strain curves of p($g_4$2T-T):MFC (purple) and p($g_4$2T-T):CNF nanocomposites (green). (b) Young's modulus of MFC-based nanocomposites as a function of MFC content.

Since CNF theoretically possesses a higher aspect ratio than MFC, a nanocomposite of CNF and p($g_4$2T-T) was prepared, and the mechanical properties were compared with its MFC-based counterpart with the same loading (9 wt%). The modulus of 10:100 MFC: p($g_4$2T-T) is (180 ± 32) MPa, while 10:100 CNF:p($g_4$2T-T) exhibits E ~150 MPa. Since the influence of CNF and MFC on the increase of the composite modulus is similar, it was decided to carry out further experiments with CNF. At the

same time, due to the lack of a sufficient amount of p(g$_4$2T-T) *batch 1*, further experiments were performed using a different batch of the polymer (*batch 2, $M_n \approx$ 21 Kg mol^{-1}, PDI $\approx$ 5.9*), which features a modulus of (1.2 ± 0.1) MPa (Figure 7.3 a). The addition of CNF significantly improved the modulus reaching a value of $E = (32 \pm 7)$ MPa at 13 wt% loading, resulting in a figure of merit $\eta = \log (E_{doped}/E_{neat}) \approx 1.4$ (Figure 7.3 a-b).

7.4 Electrical Conductivity of Nanocomposites of p(g$_4$2T-T) and CNF

To Study the impact of CNF on the electrical conductivity of the polymer, CNF-based nanocomposites with a CNF content ranging from 0 wt% to 13 wt% were doped with 20 mol% F$_4$TCNQ via co-processing. The measured electrical conductivity values hardly change with CNF content (Figure 7.4 c). Hence, the addition of CNF to p(g$_4$2T-T) not only improves the mechanical properties, but also preserves the electrical conductivity of the material doped with F$_4$TCNQ, which is (24 ± 1) S cm^{-1}.
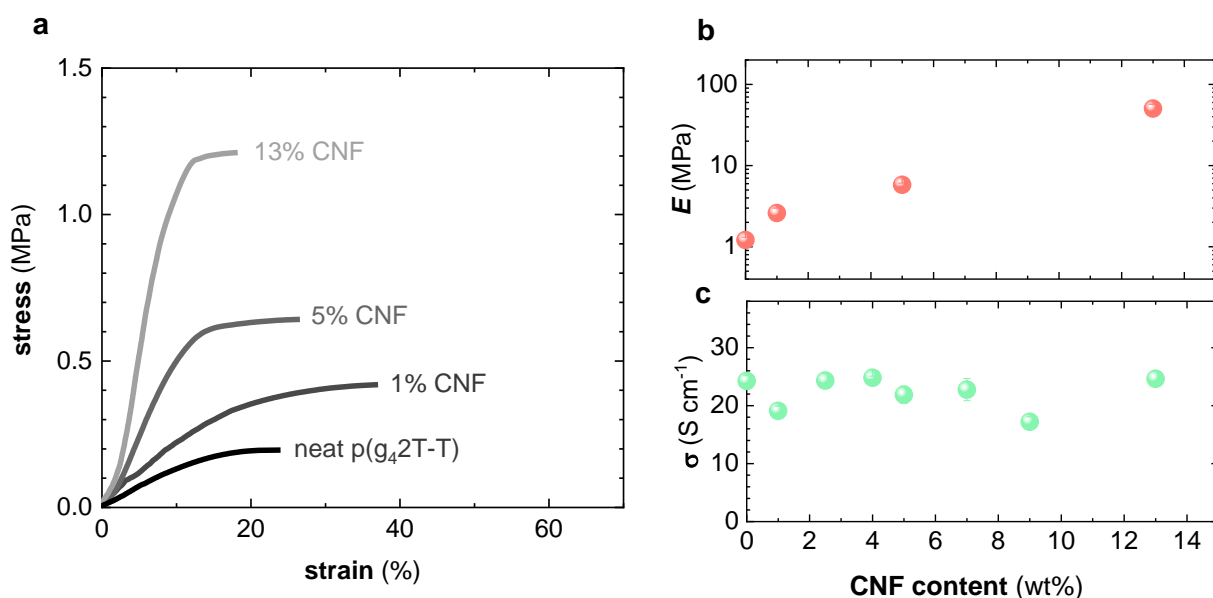
Figure 7.4 (a) Tensile deformation stress-strain plots of neat p(g$_4$2T-T) (*batch 2*) and its nanocomposites with CNF. (b) Young's modulus of the nanocomposites as a function of CNF content. (c) Conductivity of the nanocomposites doped with 20 mol% F$_4$TCNQ as a function of CNF content.

8

IMPACT OF MOLECULAR DOPING ON THE THERMOMECHANICAL PROPERTIES OF p(g$_4$2T-T)

The addition of a stiff reinforcing agent to a polymer, will increase the stiffness to a higher degree in case of a soft matrix compared to a hard counterpart. Therefore, the stiffening effect is more pronounced above T_g.[37] In a similar way, the introduction of molecular dopants has a more pronounced impact on the mechanical properties of softer conjugated polymers for which the T_g is below room temperature. This chapter explores how the mechanical properties of p(g$_4$2T-T) can be fine-tuned using different molecular dopants and discusses the underlying reasons for the observed increase in stiffness.

8.1 p(g$_4$2T-T):F$_4$TCNQ

Doping of p(g$_4$2T-T) with 20 mol% F$_4$TCNQ results in a conductivity of (42 ± 1) S cm^{-1}. To probe the influence of F$_4$TCNQ on the thermomechanical properties of the polymer, DMA and oscillatory shear rheometry have been carried out. Prior to doping, p(g$_4$2T-T) exhibits a maximum in shear loss modulus (G'') at ~ 62 °C, which can be associated with its T_g (Figure 8.1). The shear storage modulus (G') of the polymer at 20 °C is ~8 MPa. The introduction of F$_4$TCNQ shifts the T_g to ~ 3 °C and increases the tensile storage modulus, E', to ~ 1.5 GPa.

Ghosh et al have argued that addition of MgSO$_4$ to PEDOT:PSS leads to ionic type cross-linking of the polymer chains. F$_4$TCNQ is capable of double charge transfer leading to the formation of dianions, which can be expected to form ionic crosslinks between adjacent polymer chains. To study if ionic cross-linking impacts the mechanical properties, tensile deformation was carried out on p(g$_4$2T-T) doped with F$_4$TCNQ and F$_2$TCNQ, the latter of which can only form anions. To allow a fair comparison, samples with a similar oxidation level were proposed. Doping with 6 mol% F$_2$TCNQ gives rise to O$_{ox}$ ≈ 6.4 %. A similar O$_{ox}$ ≈ 5.8 % is obtained for 3 mol % F$_4$TCNQ (more details on calculation of oxidation levels can be found in *paper III*). The FTIR spectra confirm the presence of dianions for

doping with F_4TCNQ, while they are absent in case of doping with F_2TCNQ (Figure 8.2 a). The Young's moduli of p($g_4$2T-T) doped with 3 mol% F_4TCNQ and 6 mol% F_2TCNQ are found to be (24 ± 4) MPa and (31 ± 2) MPa, respectively (Figure 8.2 b). Therefore, the charge of the counterion does not appear to influence the stiffness of the doped polymer. However, the strain at break $\varepsilon_b \approx (50 \pm 10)$ % is larger in case of the latter dopant as compared to F_4TCNQ doped material with $\varepsilon_b \approx (30 \pm 5)$ % (Figure 8.2 b).
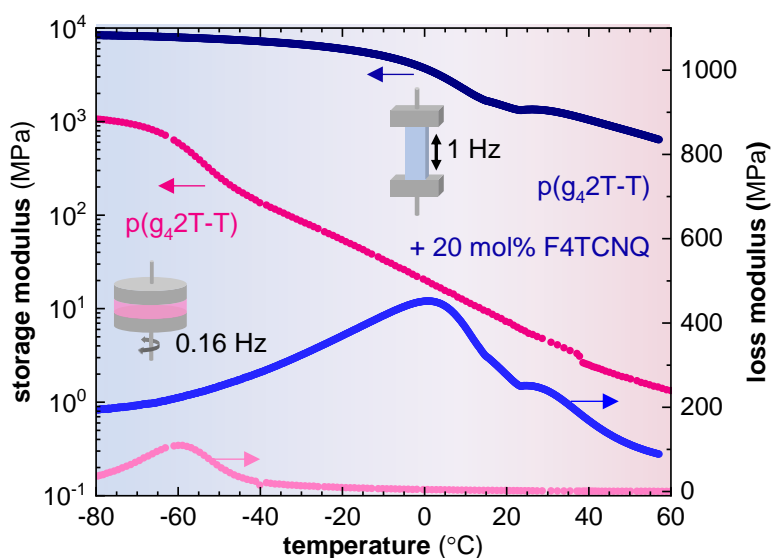
Figure 8.1 (a) Shear storage and loss modulus G' and G'' of p($g_4$2T-T) (shades of pink) as well as (b) tensile storage and loss modulus E' and E'' of p($g_4$2T-T) doped with 20 mol% F_4TCNQ (shades of blue) recorded as a function of temperature. Adapted with permission from ref [44], published by the Royal Society of Chemistry.

The structural changes that occur as a result of molecular doping were explored by performing WAXS on p($g_4$2T-T) co-processed with F_4TCNQ and F_2TCNQ. Upon the addition of 3 mol% F_4TCNQ ($O_{ox} \approx 5.7\%$) a prominent scattering peak emerges at $q_{010} \approx 1.84$ Å^{-1}, indicating π-stacking. A similar peak at $q_{010} \approx 1.79$ Å^{-1} is observed in the presence of 6 mol% F_2TCNQ ($O_{ox} \approx 6.4\%$). Oxidation of the material gives rise to π-stacking. Concurrently, $h00$ diffraction peaks ($h = 1$-3; $q_{100} = 0.36$ Å^{-1}) stemming from lamellar stacking shift to lower scattering vectors $q_{100} \approx 0.3$ Å^{-1} and $q_{100} \approx 0.28$ Å^{-1} for F_4TCNQ and F_2TCNQ, respectively, at $O_{ox} \approx 6\%$, which can be explained with ingression of counterions in between the side chains.
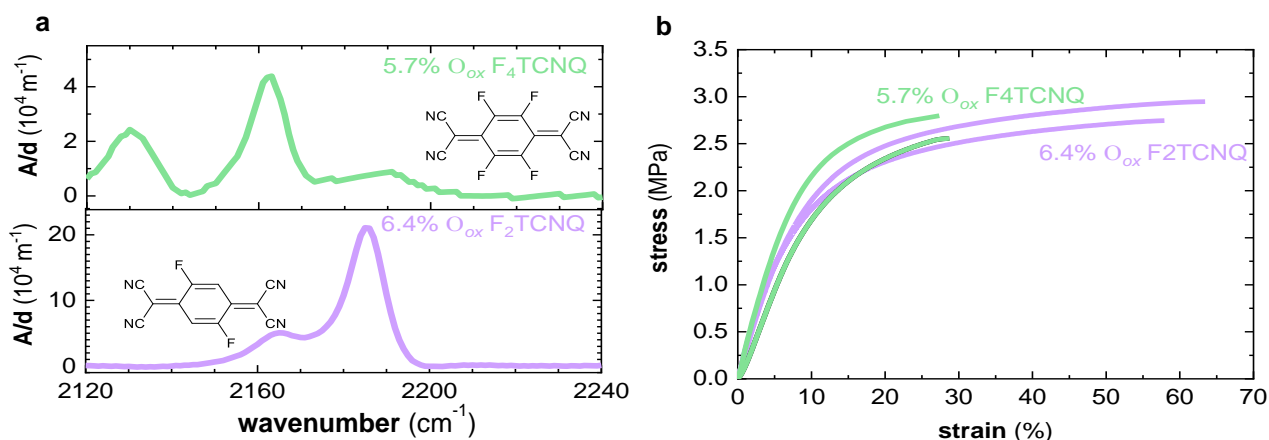
Figure 8.2 (a) Transmission FTIR absorbance spectra, with the absorbance *A* normalized by the film thickness *d*, of p(g$_4$2T-T) doped with 3 mol% F$_4$TCNQ (green; $O_{ox} \approx 5.7$ %) and 6 mol% F$_2$TCNQ (purple; $O_{ox} \approx 6.4$%), (b) stress-strain curves recorded at room temperature by tensile deformation of free-standing samples of p(g$_4$2T-T) doped with 3 mol% F$_4$TCNQ (green) and 6 mol% F$_2$TCNQ (purple). Adapted with permission from ref [44], published by the Royal Society of Chemistry.
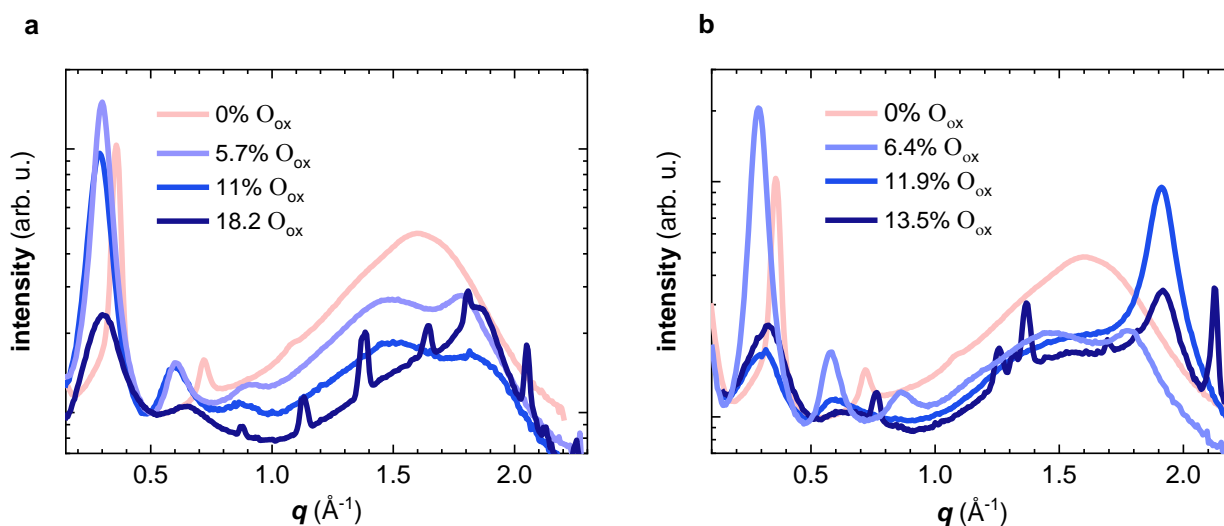
Figure 8.3 (a) X-ray diffractograms of neat p(g$_4$2T-T) (pink) and p(g$_4$2T-T) doped with (a) F$_4$TCNQ and (b) F$_2$TCNQ resulting in the indicated O$_{ox}$. Reprinted with permission from ref [44], published by the Royal Society of Chemistry.

The influence of the oxidation level on the electrical and mechanical properties was studied by carrying out tensile deformation on p(g$_4$2T-T) doped with 3 mol% to 30 mol% F$_4$TCNQ and F$_2$TCNQ (see the corresponding oxidation levels in Table S2 in *paper III*). The Young's moduli and electrical conductivity were plotted as a function of oxidation level (Figure 8.4 a-b). In case of F$_4$TCNQ, both the conductivity and Young's modulus increase at higher oxidation levels. At O$_{ox}$ ≈18% (30 mol% dopant), the conductivity reaches σ = (52 ± 3) S cm^{-1} and the Young's modulus increases to E = (232 ± 16) MPa from E = (8 ± 2) MPa for neat p(g$_4$2T-T), giving rise to a figure of merit $\eta = \log\left(E_{doped}/E_{neat}\right) \approx 1.5$. Instead, the highest conductivity, σ = (26 ± 7) S cm^{-1}, and modulus, E = (377 ± 85) MPa, upon doping with F$_2$TCNQ are achieved at O$_{ox}$ ≈ 12% (20 mol% dopant), followed by a decrease at higher oxidation levels. Therefore, the highest achieved η for F$_2$TCNQ is ~1.7 at O$_{ox}$ ≈ 12%.

As the F$_4$TCNQ doping level increases, the intensity of the π-stacking peak increases. In case of F$_2$TCNQ, a similar trend in terms of π-stacking is observed up to O$_{ox}$ ≈ 12%. For higher oxidation levels, the degree of π-stacking decreases. The π-stacking due to polaron formation stiffens the polymer backbone. Since π-stacking facilitates hopping of charges between adjacent polymer chains as well as the transfer of mechanical force, both E and σ increase with O$_{ox}$ (Figure 8.4 c). However, in the presence of F$_2$TCNQ, as the doping level increases to O$_{ox}$ >12%, doping appears to disrupt the ability of the polymer to π-stack.

The increase in π-stacking upon doping is consistent with the observed increase in T_g and stiffness (see Figure 8.1, 8.3 and 8.4). A higher degree of crystallinity impedes main-chain relaxation of the remaining amorphous fraction. Therefore, a higher T_g is observed.

Figure 8.4 Young's modulus E (black) and conductivity σ of p(g$_4$2T-T) doped with (a) F$_4$TCNQ (yellow) and (b) F$_2$TCNQ (purple), (c) σ vs. E of p(g$_4$2T-T) doped with F$_4$TCNQ (yellow) and F$_2$TCNQ (purple). Adapted with permission from ref [44], published by the Royal Society of Chemistry.
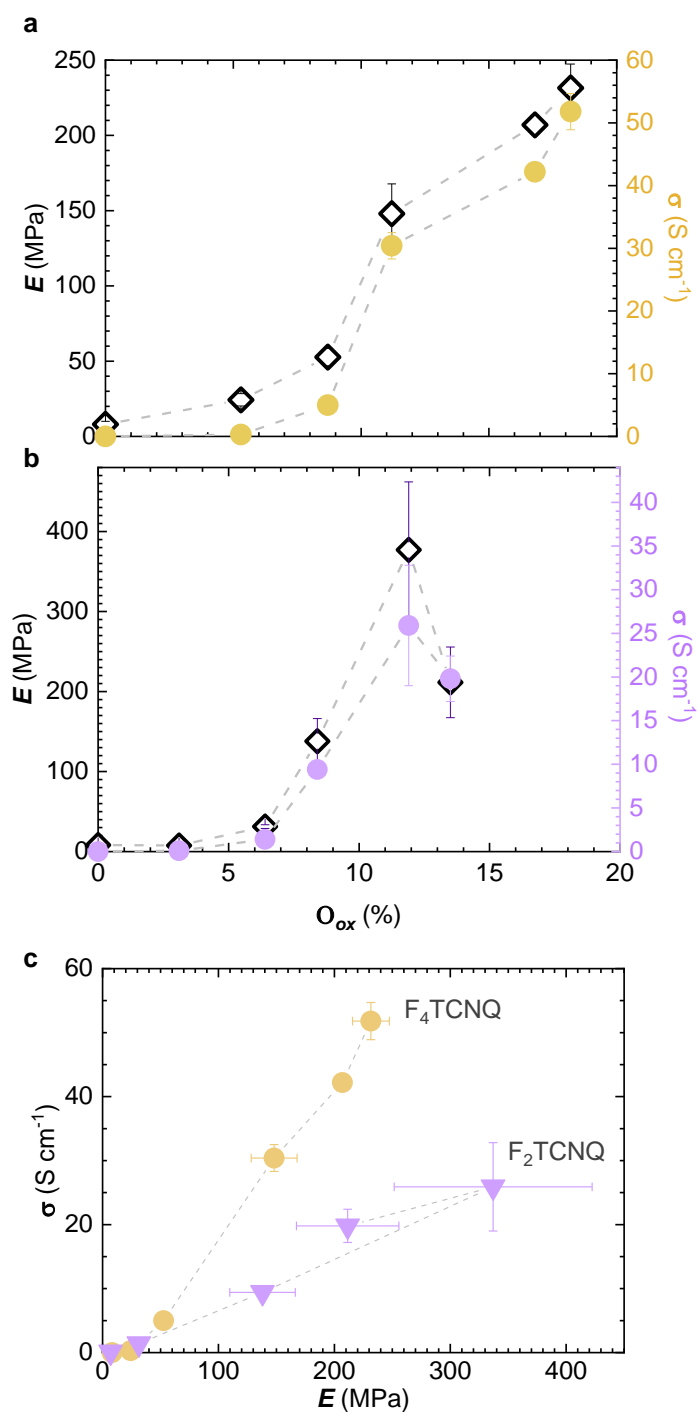
8.2 Do Other Dopants Have the Same Impact on the Mechanical Properties of p(g₄2T-T)?

To explore if the same increase in stiffness of p(g$_4$2T-T) takes place for molecular dopants other than F$_4$TCNQ and F$_2$TCNQ, the polymer was doped with 10 mol% tris(4-bromophenyl)ammoniumyl hexachloroantimonate (Magic Blue), 2,3-dichloro-5,6-dicyano-1,4-benzoquinone (DDQ), 1,3-propanedisulfonic acid (PDSA), and H-TFSI (see the chemical structures in *chapter 1*). The Young's modulus vs. conductivity of doped p(g$_4$2T-T) is displayed in Figure 8.5. The introduction of 10 mol% Magic Blue substantially increases the Young's modulus to (148 ± 20) MPa, resulting in $\eta \approx 1.3$. Meanwhile, the two acid dopants only give rise to a minor increase in stiffness. According to figure 8.5, it is observed that the addition of 10 mol% F$_2$TCNQ and H-TFSI results in very similar conductivity values while the modulus in case of the latter is more than 3 times higher.
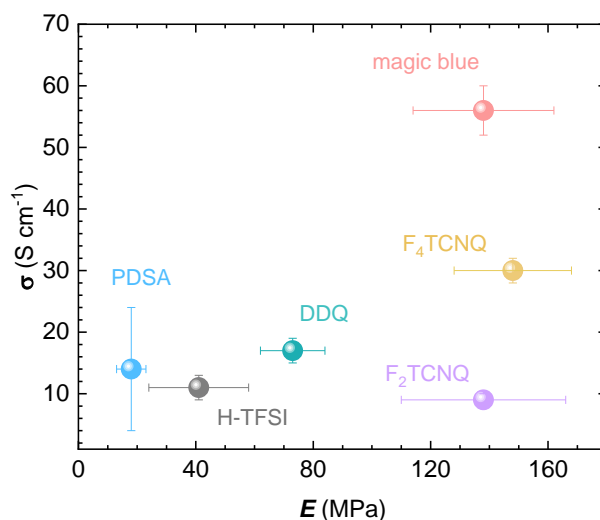
Figure 8.5 Young's moduli *E* and conductivity σ of p(g$_4$2T-T) doped with 10 mol% of the dopants Magic Blue, PDSA, DDQ, H-TFSI, F$_2$TCNQ and F$_4$TCNQ.

8.2.1 p(g₄2T-T):H-TFSI

Intriguingly, p(g$_4$2T-T) doped with 10 mol% H-TFSI features a $T_g \approx$ -56 °C (Figure 8.6), which is significantly lower than the value observed for p(g$_4$2T-T) doped with 20 mol% F$_4$TCNQ (see Figure 8.1). Hence, the use of acid dopants can be used for the design of soft conductors, which are in high demand for wearable electronics.

The T_g of p(g$_4$2T-T) doped with varying concentrations of H-TFSI (4 - 40 mol%) has been studied. At higher H-TFSI concentrations, the T_g slightly increased to -39 °C (Figure 8.6). Hofmann et al, have

shown that ageing of p(g$_4$2T-T) doped with H-TFSI leads to higher conductivity values due to the slow kinetics of acid doping (Figure 8.7 c).[133] Interestingly, at dopant concentrations higher than 20 mol%, a slight difference in T_g of aged and fresh samples is observed (Figure 8.6).
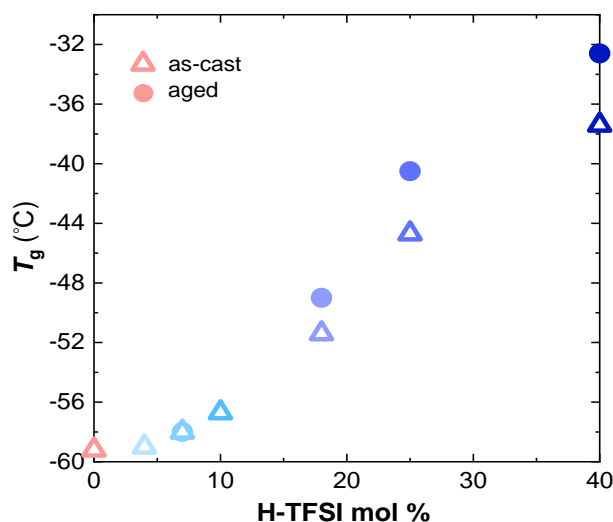
Figure 8.6 T_g (midpoint) as a function of H-TFSI concentration (mol%) measured with DSC at 10 K min^{-1} for as-cast (open triangles) and aged samples (solid circles). DSC measurements were carried out together with Furqan Farooqi and Sandra Hultmark.

Grazing-incidence wide-angle X-ray scattering (GIWAXS) was employed to scrutinize the ordered regions of p(g$_4$2T-T):H-TFSI. A q_{010} peak emerges at ~1.7 Å^{-1} upon the introduction of 4 mol% H-TFSI indicating π-stacking, but its intensity decreases again for a dopant concentration higher than 10 mol% (Figure 8.7 a). Similar to p(g$_4$2T-T) doped with F$_2$TCNQ, doping impedes π-stacking of the backbone. Furthermore, the planar and stiff backbone caused by doping together with intercalation of the dopant between the side chains reduces the crystallinity by hindering the side chains from packing as evidenced by a substantial decrease in lamellar q_{100} peaks. It can be argued that the counterions and the water that is produced during oxygen mediated doping reaction of H-TFSI (eq. 1.7), plasticizes the polymer. Therefore, despite an increase in π-stacking, the main relaxation of the amorphous fraction is not strongly hindered, and hence the T_g only slightly increases.
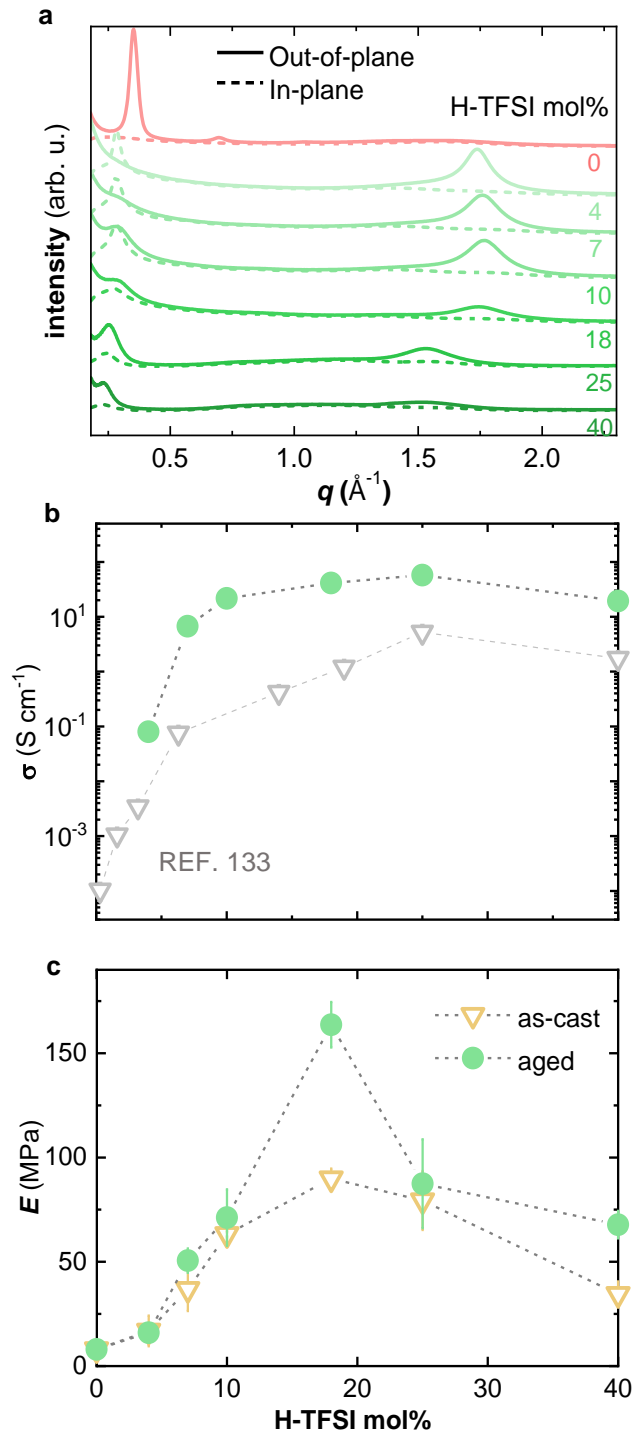
Figure 8.7 (a) In-plane (dashed lines) and out-of-plane (solid lines) GIWAXS diffractograms of p(g₄2T-T) doped with different mol% of H-TFSI. (b) Conductivity σ and (c) Young's modulus E of fresh (open triangles) and aged (solid circles) films of p(g42T-T) co-processed with H-TFSI as a function of dopant concentration. Conductivity data for as-cast samples (grey data points) are obtained from Ref. [133]. GIWAXS analysis was carried out by Sarah Marine. Electrical and mechanical characterizations were performed by Emmy Järsvall and Mariavittoria Craighero, respectively.

Further, the mechanical properties of doped p(g$_4$2T-T) have been probed as a function of H-TFSI concentrations. The conductivity of aged films of p(g$_4$2T-T) co-processed with H-TFSI increased to σ = (22 ± 1) S cm^{-1} at 10 mol% dopant (more details on ageing can be found in the experimental section of *paper IV*). Instead, for samples containing more than 10 mol% dopant, a similar conductivity is observed. The observed trend in electrical conductivity as a function of doping concentration is in agreement with the conductivity of p(g$_4$2T-T):H-TFSI measured 3 days after doping by Hofmann et al.[133]

The stiffness of as-cast films increases up to 18 mol% and then decreases at higher H-TFSI content (Figure 8.7 b). Starting from 7 mol%, the modulus of aged films is improved compared to their fresh counterparts and reaches a maximum of E = (164 ± 11) MPa at 18 mol%. The trend in the change of the elastic modulus of the films is in agreement with the increase of π-stacking up to 10 mol% H-TFSI and deterioration of π-stacking at dopant concentrations higher than 25 mol%.

10

CONCLUSIONS AND OUTLOOK

Several strategies that allow to modulate the mechanical properties of a soft polythiophene with tetraethylene glycol sidechains, p(g$_4$2T-T), have been explored and pertinent structure-property relationships have been discussed in this thesis. The proposed strategies can be harnessed to prepare electrical conductors with desired electrical and mechanical properties.

To begin with, I investigated blending of p(g$_4$2T-T), which was co-processed with a thermally stable dopant LiF$_4$TCNQ, with polycaprolactone to improve the mechanical properties and enable melt processing. Despite the improved stiffness, unfortunately melt extrusion yielded a non-conducting filament due to the formation of large disconnected islands of p(g$_4$2T-T):LiF$_4$TCNQ. However, the films obtained from dissolution of the filament exhibited an electrical conductivity of 3×10^{-2} S cm^{-1}, indicating that the loss of conductivity after melt-extrusion was indeed a result of phase separation and not because of thermal degradation. In further experiments to prevent the phase separation between p(g$_4$2T-T) and polycaprolactone as a result of melting the polycaprolactone phase, the addition of a third component as a compatibilizer could be explored that links the conjugated polymer and the insulator.

The same conjugated polymer was blended with polyurethane at a ratio of 1:4 and wet-spun into stretchable fibers, which exhibited a conductivity of $\sigma \approx 7.4$ S cm^{-1} and high stretchability $\varepsilon_{break} \approx 480\%$ after doping with Fe(Tos)$_3 \cdot$6H$_2$O. The fibers displayed a high elastic recovery. Hence at 50% of strain, a high degree of cyclic stability was observed. Moreover, the fibers feature outstanding stability in terms of mechanical and electrical properties after 9 months of storage under ambient conditions. Based on these results, blending of a soft polar polythiophene with elastomers such as polyurethane is a promising and straight-forward strategy to improve both the stretchability and the degree of elastic recovery of these polymers. The aforementioned properties make these fibers viable for e-textile applications in terms of mechanical and electrical properties. In addition, materials suitable for wearable electronics should be biocompatible if in contact with body. Despite the fact that Fe(Tos)$_3 \cdot$6H$_2$O is less toxic compared to dopants like F$_4$TCNQ, further studies must be carried out to facilitate the selection of bio-compatible dopants for these fibers.

In a further set of experiments, the addition of up to 13 wt% cellulose nanofibrils to p($g_4$2T-T) is shown to improve the stiffness of the material, without comprising the electrical properties after co-processing with F$_4$TCNQ. Since cellulose is a highly hydrophilic material, the impact of moisture on the mechanical and electrical properties of these nanocomposites can be studied and harnessed for the design of electronic devices that change their behaviour at different humidity levels.

Furthermore, I studied a copolymer consisting of soft p($g_4$2T-T) segments and hard urethane blocks. The urethane segments form a partially reversible hydrogen bonding network that considerably reinforces the material. The p[p($g_4$2T-T)-co-U] copolymer showed a Young's modulus and elongation at break of ~ 25 MPa and ~ 95%, respectively. Molecular doping with F$_4$TCNQ indicated that the presence of urethane blocks did not strongly impact the number of charge carriers and their mobility. Further, electrochemical oxidation of p($g_4$2T-T) and the copolymer did not show a significant difference between their ability to take up charge. Based on these results, the introduction of reinforcing blocks is a promising strategy for modulating the mechanical properties of soft conjugated polymers. As a future study, the type and relative length of the reinforcing segments in the copolymer can be further adjusted to modify the mechanical properties with a minimized compromise on the electrical properties of the resulting materials.

Molecular doping was used as a tool to modulate the mechanical properties of p($g_4$2T-T). The influence of different dopants on the electrical, mechanical and structural properties of p($g_4$2T-T) was studied. It was found that molecular doping can be used to modulate the stiffness as well as electrical conductivity. Molecular doping with the dopants F$_4$TCNQ, F$_2$TCNQ and H-TFSI strongly enhanced the degree of p-stacking of the polymer. As a result, the Young's modulus increased up to 232 MPa, 377 MPa and 160 MPa, respectively. However, while in case of the former two dopants the T_g increased to 3 °C, H-TFSI only slightly increased the T_g. The difference in the T_g of the doped p($g_4$2T-T) may be caused by a more pronounced plasticization effect in case of TFSI anions due to their larger molar mass compared to F$_4$TCNQ anions.[169] It was demonstrated that the electrical and mechanical properties can be at least to some extent decoupled through the choice of the dopant. It is feasible that molecular doping can also be used as a tool to decrease the stiffness and T_g of conjugated polymers with a high elastic modulus.

Finally, I have studied the impact of oligoethylene glycol side-chain length on the electrical and thermomechanical properties of soft polythiophenes. p($g_3$2T-T) exhibited a higher electrical conductivity and Young's modulus than p($g_4$2T-T). However, its stretchability was substantially reduced. Meanwhile, p($g_6$2T-T) is excessively soft and sticky. One limitation of my thesis is the use of p($g_4$2T-T) as the only model for soft conjugated polymers. Other soft conjugated polymers need to be studied to confirm if the same structure-property relationships that I have discussed in my thesis also holds for them. Therefore, it would be interesting to employ the demonstrated strategies, in particular

molecular doping, for polythiophenes with different side-chain length as well as polymers with different backbones.

It can be anticipated that the results in this thesis will aid the design of electrical conductors with optimal mechanical and electrical properties for a variety of applications within the field of organic electronics.

ACKNOWLEDGEMENTS

Nazanin, thank you for proof-reading parts of my thesis and being a great friend since we were 18 years-old.

Alicja, thank you for being an amazing friend! You can always read me and have been there for me no matter what. We have laughed and cried together. I'm truly grateful for our friendship.

Ali, thank you for your endless support and love. You can always make me laugh even during the writing period that I was grumpy!

I would also like to express gratitude to my parents for always putting me first. To my mom, Fariba, who inspired me to become an independent woman and my dad, Jafar, for his unconditional support.

BIBLIOGRAPHY

1.   Rasmussen, S. C., The Early History of Polyaniline: Discovery and Origins. *Substantia* **2017,** *1* (2).

2.   Zhou, Y.; Han, S.-T.; Roy, V. A. L., 6 - Nanocomposite Dielectric Materials for Organic Flexible Electronics. In *Nanocrystalline Materials (Second Edition)*, Tjong, S.-C., Ed. Elsevier: Oxford, **2014**; pp 195-220.

3.   Jurchescu, O. D., 13 - Conductivity measurements of organic materials using field-effect transistors (FETs) and space-charge-limited current (SCLC) technique. In *Handbook of Organic Materials for Optical and (Opto)electronic Devices*, Ostroverkhova, O., Ed. Woodhead Publishing: **2013**; pp 377-397.

4.   Puniredd, S. R.; Pisula, W.; Müllen, K., 2 - Influence of film morphology on optical and electronic properties of organic materials. In *Handbook of Organic Materials for Optical and (Opto)electronic Devices*, Ostroverkhova, O., Ed. Woodhead Publishing: **2013**; pp 83-101.

5.   Khodagholy, D.; Malliaras, G. G.; Owens, R. M., 8.05 - Polymer-Based Sensors. In *Polymer Science: A Comprehensive Reference*, Matyjaszewski, K.; Möller, M., Eds. Elsevier: Amsterdam, **2012**; pp 101-128.

6.   Tarver, J. D.; Sezen-Edmonds, M.; Yoo, J. E.; Loo, Y.-L., 5.01 - Organic Electronic Devices With Water-Dispersible Conducting Polymers. In *Comprehensive Nanoscience and Nanotechnology (Second Edition)*, Andrews, D. L.; Lipson, R. H.; Nann, T., Eds. Academic Press: Oxford, **2019**; pp 1-34.

7.   Hynynen, J.; Kiefer, D.; Müller, C., Influence of crystallinity on the thermoelectric power factor of P3HT vapour-doped with F4TCNQ. *RSC Adv.* **2018,** *8* (3), 1593-1599.

8.   Zuo, G.; Abdalla, H.; Kemerink, M., Conjugated Polymer Blends for Organic Thermoelectrics. *Adv. Electron. Mater.* **2019,** *5* (11), 1800821.

9.   Kroon, R.; Ryan, J. D.; Kiefer, D.; Yu, L.; Hynynen, J.; Olsson, E.; Müller, C., Bulk Doping of Millimeter-Thick Conjugated Polymer Foams for Plastic Thermoelectrics. *Adv. Funct. Mater.* **2017,** *27* (47), 1704183.

10.   Zhou, H.; Zhang, Y.; Seifter, J.; Collins, S. D.; Luo, C.; Bazan, G. C.; Nguyen, T.-Q.; Heeger, A. J., High-Efficiency Polymer Solar Cells Enhanced by Solvent Treatment. *Adv. Mater.* **2013,** *25* (11), 1646-1652.

11.   Xie, J.; Gu, P.; Zhang, Q., Nanostructured Conjugated Polymers: Toward High-Performance Organic Electrodes for Rechargeable Batteries. *ACS Energy Lett.* **2017,** *2* (9), 1985-1996.

12.   Mike, J. F.; Lutkenhaus, J. L., Recent advances in conjugated polymer energy storage. *J. Polym. Sci., Part B: Polym. Phys.* **2013,** *51* (7), 468-480.

13.   Someya, T.; Bao, Z.; Malliaras, G. G., The rise of plastic bioelectronics. *Nature* **2016,** *540* (7633), 379-385.

14.   Inal, S.; Rivnay, J.; Suiu, A.-O.; Malliaras, G. G.; McCulloch, I., Conjugated Polymers in Bioelectronics. *Acc. Chem. Res.* **2018,** *51* (6), 1368-1376.

15.   Rivnay, J.; Inal, S.; Collins, B. A.; Sessolo, M.; Stavrinidou, E.; Strakosas, X.; Tassone, C.; Delongchamp, D. M.; Malliaras, G. G., Structural control of mixed ionic and electronic transport in conducting polymers. *Nat. Commun.* **2016,** *7* (1), 11287.

16.   Wang, S.; Xu, J.; Wang, W.; Wang, G. N.; Rastak, R.; Molina-Lopez, F.; Chung, J. W.; Niu, S.; Feig, V. R.; Lopez, J.; Lei, T.; Kwon, S. K.; Kim, Y.; Foudeh, A. M.; Ehrlich, A.; Gasperini, A.; Yun,

Y.; Murmann, B.; Tok, J. B.; Bao, Z., Skin electronics from scalable fabrication of an intrinsically stretchable transistor array. *Nature* **2018,** *555* (7694), 83-88.

17.   Wang, S.; Oh, J. Y.; Xu, J.; Tran, H.; Bao, Z., Skin-Inspired Electronics: An Emerging Paradigm. *Acc. Chem. Res.* **2018,** *51* (5), 1033-1045.

18.   Lund, A.; van der Velden, N. M.; Persson, N.-K.; Hamedi, M. M.; Müller, C., Electrically conducting fibres for e-textiles: An open playground for conjugated polymers and carbon nanomaterials. *Mater. Sci. Eng. R Rep* **2018,** *126*, 1-29.

19.   Volonakis, G.; Logothetidis, S., 2 - Structural and electronic properties of fullerene-based organic materials: Density functional theory-based calculations. In *Handbook of Flexible Organic Electronics*, Logothetidis, S., Ed. Woodhead Publishing: Oxford, **2015**; pp 37-56.

20.   Ray, T. R.; Choi, J.; Bandodkar, A. J.; Krishnan, S.; Gutruf, P.; Tian, L.; Ghaffari, R.; Rogers, J. A., Bio-Integrated Wearable Systems: A Comprehensive Review. *Chem. Rev.* **2019,** *119* (8), 5461-5533.

21.   Yuk, H.; Lu, B.; Zhao, X., Hydrogel bioelectronics. *Chem. Soc. Rev.* **2019,** *48* (6), 1642-1667.

22.   Kaltenbrunner, M.; Sekitani, T.; Reeder, J.; Yokota, T.; Kuribara, K.; Tokuhara, T.; Drack, M.; Schwödiauer, R.; Graz, I.; Bauer-Gogonea, S.; Bauer, S.; Someya, T., An ultra-lightweight design for imperceptible plastic electronics. *Nature* **2013,** *499* (7459), 458-463.

23.   Lee, J. A.; Aliev, A. E.; Bykova, J. S.; de Andrade, M. J.; Kim, D.; Sim, H. J.; Lepró, X.; Zakhidov, A. A.; Lee, J.-B.; Spinks, G. M.; Roth, S.; Kim, S. J.; Baughman, R. H., Woven-Yarn Thermoelectric Textiles. *Adv. Mater.* **2016,** *28* (25), 5038-5044.

24.   Fan, W.; He, Q.; Meng, K.; Tan, X.; Zhou, Z.; Zhang, G.; Yang, J.; Wang, Z. L., Machine-knitted washable sensor array textile for precise epidermal physiological signal monitoring. *Sci. Adv.* **2020,** *6* (11), eaay2840.

25.   Liu, M.; Pu, X.; Jiang, C.; Liu, T.; Huang, X.; Chen, L.; Du, C.; Sun, J.; Hu, W.; Wang, Z. L., Large-Area All-Textile Pressure Sensors for Monitoring Human Motion and Physiological Signals. *Adv. Mater.* **2017,** *29* (41), 1703700.

26.   Oh, J. Y.; Son, D.; Katsumata, T.; Lee, Y.; Kim, Y.; Lopez, J.; Wu, H.-C.; Kang, J.; Park, J.; Gu, X.; Mun, J.; Yin, Y.; Cai, W.; Yun, Y.; Tok, J. B. H.; Bao, Z., Stretchable self-healable semiconducting polymer film for active-matrix strain-sensing array. *Sci. Adv.* **2019,** *5* (11), eaav3097.

27.   Tessarolo, M.; Gualandi, I.; Fraboni, B., Recent Progress in Wearable Fully Textile Chemical Sensors. *Adv. Mater. Technol.* **2018,** *3* (10), 1700310.

28.   Gorman, C. B.; Grubb, R. H., Conjugated Polymers. Springer Science+Business Media Dordrecht: **1991**.

29.   Kroon, R.; Mengistie, D. A.; Kiefer, D.; Hynynen, J.; Ryan, J. D.; Yu, L.; Müller, C., Thermoelectric plastics: from design to synthesis, processing and structure–property relationships. *Chem. Soc. Rev.* **2016,** *45* (22), 6147-6164.

30.   Bubnova, O.; Crispin, X., Towards polymer-based organic thermoelectric generators. *Energy Environ. Sci.* **2012,** *5* (11), 9345-9362.

31.   Conjugated Polymers. In *The Physics of Polymers: Concepts for Understanding Their Structures and Behavior*, Strobl, G., Ed. Springer Berlin Heidelberg: Berlin, Heidelberg, **2007**; pp 287-312.

32.   Mammone, R. J.; MacDiarmid, A. G., p-Doping of (CH) to the metallic regime with gaseous oxygen. Application to oxygen fuel-cell-type electrodes. *J. Chem. Soc., Faraday Trans. 1* **1985,** *81* (1), 105-112.

33.   Yu, L.; Scheunemann, D.; Lund, A.; Kiefer, D.; Müller, C., Sequential doping of solid chunks of a conjugated polymer for body-heat-powered thermoelectric modules. *Appl. Phys. Lett.* **2021,** *119* (18), 181902.

34.   Kroon, R.; Kiefer, D.; Stegerer, D.; Yu, L.; Sommer, M.; Müller, C., Polar Side Chains Enhance Processability, Electrical Conductivity, and Thermal Stability of a Molecularly p-Doped Polythiophene. *Adv. Mater.* **2017,** *29* (24), 1700930.

35.   Yuen, J. D.; Dhoot, A. S.; Namdas, E. B.; Coates, N. E.; Heeney, M.; McCulloch, I.; Moses, D.; Heeger, A. J., Electrochemical Doping in Electrolyte-Gated Polymer Transistors. *J. Am. Chem. Soc.* **2007,** *129* (46), 14367-14371.

36.   Jacobs, I. E.; Lin, Y.; Huang, Y.; Ren, X.; Simatos, D.; Chen, C.; Tjhe, D.; Statz, M.; Lai, L.; Finn, P. A.; Neal, W. G.; D'Avino, G.; Lemaur, V.; Fratini, S.; Beljonne, D.; Strzalka, J.; Nielsen, C. B.; Barlow, S.; Marder, S. R.; McCulloch, I.; Sirringhaus, H., High-Efficiency Ion-Exchange Doping of Conducting Polymers. *Adv. Mater. n/a* (n/a), 2102988.

37.   Nielsen, L. E.; Landel, R. F., Mechanical properties of polymers and composites. 2nd ed.; Marcel Dekker: New York, **1993**.

38.   Richeton, J.; Ahzi, S.; Vecchio, K. S.; Jiang, F. C.; Adharapurapu, R. R., Influence of temperature and strain rate on the mechanical behavior of three amorphous polymers: Characterization and modeling of the compressive yield stress. *Int. J. Solids Struct.* **2006,** *43* (7), 2318-2335.

39.   Gedde, U. W., Mechanical Properties of Materials, An Introductory Text. KTH: Stockholm, **2005**.

40.   Panwar, V.; Pal, K., Chapter 12 - Dynamic Mechanical Analysis of Clay–Polymer Nanocomposites. In *Clay-Polymer Nanocomposites*, Jlassi, K.; Chehimi, M. M.; Thomas, S., Eds. Elsevier: **2017**; pp 413-441.

41.   Gedde, U. W.; Hedenqvist, M. S., Fundamental Polymer Science. 2nd ed.; Springer: **2019**.

42.   Krevelen, D. W. V., Properties of Polymers. 4th ed.; Elsevier: **1972**.

43.   Müller, C., On the Glass Transition of Polymer Semiconductors and Its Impact on Polymer Solar Cell Stability. *Chem. Mater.* **2015,** *27* (8), 2740-2754.

44.   Zokaei, S.; Kim, D.; Järsvall, E.; Fenton, A. M.; Weisen, A. R.; Hultmark, S.; Nguyen, P. H.; Matheson, A. M.; Lund, A.; Kroon, R.; Chabinyc, M. L.; Gomez, E. D.; Zozoulenko, I.; Müller, C., Tuning of the elastic modulus of a soft polythiophene through molecular doping. *Mater. Horiz.* **2022,** *9* (1), 433-443.

45.   Xie, R.; Weisen, A. R.; Lee, Y.; Aplan, M. A.; Fenton, A. M.; Masucci, A. E.; Kempe, F.; Sommer, M.; Pester, C. W.; Colby, R. H.; Gomez, E. D., Glass transition temperature from the chemical structure of conjugated polymers. *Nat. Commun.* **2020,** *11* (1), 893.

46.   Balar, N.; Siddika, S.; Kashani, S.; Peng, Z.; Rech, J. J.; Ye, L.; You, W.; Ade, H.; O'Connor, B. T., Role of Secondary Thermal Relaxations in Conjugated Polymer Film Toughness. *Chem. Mater.* **2020,** *32* (15), 6540-6549.

47.   Zhang, S.; Alesadi, A.; Selivanova, M.; Cao, Z.; Qian, Z.; Luo, S.; Galuska, L.; Teh, C.; Ocheje, M. U.; Mason, G. T.; St. Onge, P. B. J.; Zhou, D.; Rondeau-Gagné, S.; Xia, W.; Gu, X., Toward the Prediction and Control of Glass Transition Temperature for Donor–Acceptor Polymers. *Adv. Funct. Mater.* **2020,** *30* (27), 2002221.

48.   Kaltenbrunner, M.; White, M. S.; Głowacki, E. D.; Sekitani, T.; Someya, T.; Sariciftci, N. S.; Bauer, S., Ultrathin and lightweight organic solar cells with high flexibility. *Nat. Commun.* **2012,** *3* (1), 770.

49.   Lipomi, D. J.; Tee, B. C. K.; Vosgueritchian, M.; Bao, Z., Stretchable Organic Solar Cells. *Adv. Mater.* **2011,** *23* (15), 1771-1775.

50.   Root, S. E.; Savagatrup, S.; Printz, A. D.; Rodriquez, D.; Lipomi, D. J., Mechanical Properties of Organic Semiconductors for Stretchable, Highly Flexible, and Mechanically Robust Electronics. *Chem. Rev.* **2017,** *117* (9), 6467-6499.

51.   Wang, M.; Baek, P.; Akbarinejad, A.; Barker, D.; Travas-Sejdic, J., Conjugated polymers and composites for stretchable organic electronics. *J. Mater. Chem. C* **2019,** *7* (19), 5534-5552.

52.   Ashizawa, M.; Zheng, Y.; Tran, H.; Bao, Z., Intrinsically stretchable conjugated polymer semiconductors in field effect transistors. *Prog. Polym. Sci.* **2020,** *100*, 101181.

53.   Peng, R.; Pang, B.; Hu, D.; Chen, M.; Zhang, G.; Wang, X.; Lu, H.; Cho, K.; Qiu, L., An ABA triblock copolymer strategy for intrinsically stretchable semiconductors. *J. Mater. Chem. C* **2015,** *3* (15), 3599-3606.

54.   Baek, P.; Aydemir, N.; An, Y.; Chan, E. W. C.; Sokolova, A.; Nelson, A.; Mata, J. P.; McGillivray, D.; Barker, D.; Travas-Sejdic, J., Molecularly Engineered Intrinsically Healable and Stretchable Conducting Polymers. *Chem. Mater.* **2017,** *29* (20), 8850-8858.

55.   Chen, A. X.; Kleinschmidt, A. T.; Choudhary, K.; Lipomi, D. J., Beyond Stretchability: Strength, Toughness, and Elastic Range in Semiconducting Polymers. *Chem. Mater.* **2020,** *32* (18), 7582-7601.

56.   Sugiyama, F.; Kleinschmidt, A. T.; Kayser, L. V.; Alkhadra, M. A.; Wan, J. M. H.; Chiang, A. S. C.; Rodriquez, D.; Root, S. E.; Savagatrup, S.; Lipomi, D. J., Stretchable and Degradable Semiconducting Block Copolymers. *Macromolecules* **2018,** *51* (15), 5944-5949.

57.   Zhao, Y.; Zhao, X.; Zang, Y.; Di, C.-a.; Diao, Y.; Mei, J., Conjugation-Break Spacers in Semiconducting Polymers: Impact on Polymer Processability and Charge Transport Properties. *Macromolecules* **2015,** *48* (7), 2048-2053.

58.   Gasperini, A.; Bivaud, S.; Sivula, K., Controlling conjugated polymer morphology and charge carrier transport with a flexible-linker approach. *Chem. Sci.* **2014,** *5* (12), 4922-4927.

59.   Savagatrup, S.; Zhao, X.; Chan, E.; Mei, J.; Lipomi, D. J., Effect of Broken Conjugation on the Stretchability of Semiconducting Polymers. *Macromol. Rapid Commun.* **2016,** *37* (19), 1623-1628.

60.   Schroeder, B. C.; Chiu, Y.-C.; Gu, X.; Zhou, Y.; Xu, J.; Lopez, J.; Lu, C.; Toney, M. F.; Bao, Z., Non-Conjugated Flexible Linkers in Semiconducting Polymers: A Pathway to Improved Processability without Compromising Device Performance. *Adv. Electron. Mater.* **2016,** *2* (7), 1600104.

61.   Mun, J.; Wang, G.-J. N.; Oh, J. Y.; Katsumata, T.; Lee, F. L.; Kang, J.; Wu, H.-C.; Lissel, F.; Rondeau-Gagné, S.; Tok, J. B.-H.; Bao, Z., Effect of Nonconjugated Spacers on Mechanical Properties of Semiconducting Polymers for Stretchable Transistors. *Adv. Funct. Mater.* **2018,** *28* (43), 1804222.

62.   Oh, J. Y.; Rondeau-Gagné, S.; Chiu, Y.-C.; Chortos, A.; Lissel, F.; Wang, G.-J. N.; Schroeder, B. C.; Kurosawa, T.; Lopez, J.; Katsumata, T.; Xu, J.; Zhu, C.; Gu, X.; Bae, W.-G.; Kim, Y.; Jin, L.; Chung, J. W.; Tok, J. B. H.; Bao, Z., Intrinsically stretchable and healable semiconducting polymer for organic transistors. *Nature* **2016,** *539* (7629), 411-415.

63.   Zheng, Y.; Ashizawa, M.; Zhang, S.; Kang, J.; Nikzad, S.; Yu, Z.; Ochiai, Y.; Wu, H.-C.; Tran, H.; Mun, J.; Zheng, Y.-Q.; Tok, J. B. H.; Gu, X.; Bao, Z., Tuning the Mechanical Properties of a Polymer Semiconductor by Modulating Hydrogen Bonding Interactions. *Chem. Mater.* **2020,** *32* (13), 5700-5714.

64.   Savagatrup, S.; Printz, A. D.; Rodriquez, D.; Lipomi, D. J., Best of Both Worlds: Conjugated Polymers Exhibiting Good Photovoltaic Behavior and High Tensile Elasticity. *Macromolecules* **2014,** *47* (6), 1981-1992.

65.   Smith, Z. C.; Wright, Z. M.; Arnold, A. M.; Sauvé, G.; McCullough, R. D.; Sydlik, S. A., Increased Toughness and Excellent Electronic Properties in Regioregular Random Copolymers of 3-Alkylthiophenes and Thiophene. *Adv. Electron. Mater.* **2017,** *3* (1), 1600316.

66.	Pankaj, S.; Hempel, E.; Beiner, M., Side-Chain Dynamics and Crystallization in a Series of Regiorandom Poly(3-alkylthiophenes). *Macromolecules* **2009,** *42* (3), 716-724.

67.	Savagatrup, S.; Makaram, A. S.; Burke, D. J.; Lipomi, D. J., Mechanical Properties of Conjugated Polymers and Polymer-Fullerene Composites as a Function of Molecular Structure. *Adv. Funct. Mater.* **2014,** *24* (8), 1169-1181.

68.	Liu, D.; Ding, Z.; Wu, Y.; Liu, S. F.; Han, Y.; Zhao, K., In Situ Study of Molecular Aggregation in Conjugated Polymer/Elastomer Blends toward Stretchable Electronics. *Macromolecules* **2022,** *55* (1), 297-308.

69.	McGrail, B. T.; Sehirlioglu, A.; Pentzer, E., Polymer Composites for Thermoelectric Applications. *Angew. Chem. Int. Ed.* **2015,** *54* (6), 1710-1723.

70.	Ford, M. J.; Wang, M.; Patel, S. N.; Phan, H.; Segalman, R. A.; Nguyen, T.-Q.; Bazan, G. C., High Mobility Organic Field-Effect Transistors from Majority Insulator Blends. *Chem. Mater.* **2016,** *28* (5), 1256-1260.

71.	Goffri, S.; Müller, C.; Stingelin-Stutzmann, N.; Breiby, D. W.; Radano, C. P.; Andreasen, J. W.; Thompson, R.; Janssen, R. A. J.; Nielsen, M. M.; Smith, P.; Sirringhaus, H., Multicomponent semiconducting polymer systems with low crystallization-induced percolation threshold. *Nat. Mater.* **2006,** *5* (12), 950-956.

72.	Sparrowe, D.; Baklar, M.; Stingelin, N., Low-temperature printing of crystalline:crystalline polymer blend transistors. *Org. Electron.* **2010,** *11* (7), 1296-1300.

73.	Lu, G.; Blakesley, J.; Himmelberger, S.; Pingel, P.; Frisch, J.; Lieberwirth, I.; Salzmann, I.; Oehzelt, M.; Di Pietro, R.; Salleo, A.; Koch, N.; Neher, D., Moderate doping leads to high performance of semiconductor/insulator polymer blend transistors. *Nat. Commun.* **2013,** *4* (1), 1588.

74.	Wang, S.; Fabiano, S.; Himmelberger, S.; Puzinas, S.; Crispin, X.; Salleo, A.; Berggren, M., Experimental evidence that short-range intermolecular aggregation is sufficient for efficient charge transport in conjugated polymers. *Proc. Natl. Acad. Sci. U.S.A.* **2015,** *112* (34), 10599-10604.

75.	Zeglio, E.; Vagin, M.; Musumeci, C.; Ajjan, F. N.; Gabrielsson, R.; Trinh, X. T.; Son, N. T.; Maziz, A.; Solin, N.; Inganäs, O., Conjugated Polyelectrolyte Blends for Electrochromic and Electrochemical Transistor Devices. *Chem. Mater.* **2015,** *27* (18), 6385-6393.

76.	Ferenczi, T. A. M.; Müller, C.; Bradley, D. D. C.; Smith, P.; Nelson, J.; Stingelin, N., Organic Semiconductor:Insulator Polymer Ternary Blends for Photovoltaics. *Adv. Mater.* **2011,** *23* (35), 4093-4097.

77.	Kiefer, D.; Yu, L.; Fransson, E.; Gómez, A.; Primetzhofer, D.; Amassian, A.; Campoy-Quiles, M.; Müller, C., A solution-doped polymer semiconductor: insulator blend for thermoelectrics. *Adv. Sci.* **2017,** *4* (1), 1600203.

78.	Lu, G.; Bu, L.; Li, S.; Yang, X., Bulk Interpenetration Network of Thermoelectric Polymer in Insulating Supporting Matrix. *Adv. Mater.* **2014,** *26* (15), 2359-2364.

79.	Granero, A. J.; Wagner, P.; Wagner, K.; Razal, J. M.; Wallace, G. G.; in het Panhuis, M., Highly Stretchable Conducting SIBS-P3HT Fibers. *Adv. Funct. Mater.* **2011,** *21* (5), 955-962.

80.	Seyedin, M. Z.; Razal, J. M.; Innis, P. C.; Wallace, G. G., Strain-Responsive Polyurethane/PEDOT:PSS Elastomeric Composite Fibers with High Electrical Conductivity. *Adv. Funct. Mater.* **2014,** *24* (20), 2957-2966.

81.	Zokaei, S.; Craighero, M.; Cea, C.; Kneissl, L. M.; Kroon, R.; Khodagholy, D.; Lund, A.; Müller, C., Electrically Conducting Elastomeric Fibers with High Stretchability and Stability. *Small* **2022,** *18* (5), 2102813.

82.   Xu, J.; Wang, S.; Wang, G.-J. N.; Zhu, C.; Luo, S.; Jin, L.; Gu, X.; Chen, S.; Feig, V. R.; To, J. W. F.; Rondeau-Gagné, S.; Park, J.; Schroeder, B. C.; Lu, C.; Oh, J. Y.; Wang, Y.; Kim, Y.-H.; Yan, H.; Sinclair, R.; Zhou, D.; Xue, G.; Murmann, B.; Linder, C.; Cai, W.; Tok, J. B.-H.; Chung, J. W.; Bao, Z., Highly stretchable polymer semiconductor films through the nanoconfinement effect. *Science* **2017,** *355*, 59.

83.   Choi, D.; Kim, H.; Persson, N.; Chu, P.-H.; Chang, M.; Kang, J.-H.; Graham, S.; Reichmanis, E., Elastomer–Polymer Semiconductor Blends for High-Performance Stretchable Charge Transport Networks. *Chem. Mater.* **2016,** *28* (4), 1196-1204.

84.   Zhang, G.; Lee, S.; Gutiérrez-Meza, E.; Buckley, C.; McBride, M.; Valverde-Chávez, D. A.; Kwon, Y. H.; Savikhin, V.; Xiong, H.; Dunn, T. J.; Toney, M. F.; Yuan, Z.; Silva, C.; Reichmanis, E., Robust and Stretchable Polymer Semiconducting Networks: From Film Microstructure to Macroscopic Device Performance. *Chem. Mater.* **2019,** *31* (17), 6530-6539.

85.   Zhang, S.; Cheng, Y.-H.; Galuska, L.; Roy, A.; Lorenz, M.; Chen, B.; Luo, S.; Li, Y.-T.; Hung, C.-C.; Qian, Z.; St. Onge, P. B. J.; Mason, G. T.; Cowen, L.; Zhou, D.; Nazarenko, S. I.; Storey, R. F.; Schroeder, B. C.; Rondeau-Gagné, S.; Chiu, Y.-C.; Gu, X., Tacky Elastomers to Enable Tear-Resistant and Autonomous Self-Healing Semiconductor Composites. *Adv. Funct. Mater.* **2020,** *30* (27), 2000663.

86.   Nikzad, S.; Wu, H.-C.; Kim, J.; Mahoney, C. M.; Matthews, J. R.; Niu, W.; Li, Y.; Wang, H.; Chen, W.-C.; Toney, M. F.; He, M.; Bao, Z., Inducing Molecular Aggregation of Polymer Semiconductors in a Secondary Insulating Polymer Matrix to Enhance Charge Transport. *Chem. Mater.* **2020,** *32* (2), 897-905.

87.   Tchmutin, I. A.; Ponomarenko, A. T.; Krinichnaya, E. P.; Kozub, G. I.; Efimov, O. N., Electrical properties of composites based on conjugated polymers and conductive fillers. *Carbon* **2003,** *41* (7), 1391-1395.

88.   Liu, Y.; Hao, W.; Yao, H.; Li, S.; Wu, Y.; Zhu, J.; Jiang, L., Solution Adsorption Formation of a π-Conjugated Polymer/Graphene Composite for High-Performance Field-Effect Transistors. *Adv. Mater.* **2018,** *30* (3), 1705377.

89.   Cheon, H. J.; Shin, S. Y.; Tran, V. V.; Park, B.; Yoon, H.; Chang, M., Preparation of conjugated polymer/reduced graphene oxide nanocomposites for high-performance volatile organic compound sensors. *Chem. Eng. J.* **2021,** *425*, 131424.

90.   Zhao, D.; Zhang, Q.; Chen, W.; Yi, X.; Liu, S.; Wang, Q.; Liu, Y.; Li, J.; Li, X.; Yu, H., Highly Flexible and Conductive Cellulose-Mediated PEDOT:PSS/MWCNT Composite Films for Supercapacitor Electrodes. *ACS Appl. Mater. Interfaces* **2017,** *9* (15), 13213-13222.

91.   van den Berg, O.; Schroeter, M.; Capadona, J. R.; Weder, C., Nanocomposites based on cellulose whiskers and (semi)conducting conjugated polymers. *J. Mater. Chem.* **2007,** *17* (26), 2746-2753.

92.   Dong, B. X.; Liu, Z.; Onorato, J. W.; Ma, T.; Strzalka, J.; Bennington, P.; Luscombe, C. K.; Ober, C. K.; Nealey, P. F.; Patel, S. N., Ionic Dopant-Induced Ordering Enhances the Thermoelectric Properties of a Polythiophene-Based Block Copolymer. *Adv. Funct. Mater.* **2021,** *31* (51), 2106991.

93.   Hynynen, J.; Järsvall, E.; Kroon, R.; Zhang, Y.; Barlow, S.; Marder, S. R.; Kemerink, M.; Lund, A.; Müller, C., Enhanced Thermoelectric Power Factor of Tensile Drawn Poly(3-hexylthiophene). *ACS Macro Lett.* **2019,** *8* (1), 70-76.

94.   Mun, J.; Kang, J.; Zheng, Y.; Luo, S.; Wu, Y.; Gong, H.; Lai, J.-C.; Wu, H.-C.; Xue, G.; Tok, J. B.-H.; Bao, Z., F4-TCNQ as an Additive to Impart Stretchable Semiconductors with High Mobility and Stability. *Adv. Electron. Mater.* **2020,** *6* (6), 2000251.

95.   Tokito, S.; Smith, P.; Heeger, A. J., Highly conductive and stiff fibres of poly (2, 5-dimethoxy-p-phenylenevinylene) prepared from soluble precursor polymer. *Polymer* **1991,** *32* (3), 464-470.

96.   Tokito, S.; Smith, P.; Heeger, A. J., Mechanical and electrical properties of poly-(2, 5-thienylene vinylene) fibers. *Synth. Met.* **1990,** *36* (2), 183-194.

97.   Cao, Y.; Smith, P.; Heeger, A. J., Mechanical and electrical properties of polyacetylene films oriented by tensile drawing. *Polymer* **1991,** *32* (7), 1210-1218.

98.   Zheng, Y.; Wang, G. J. N.; Kang, J.; Nikolka, M.; Wu, H. C.; Tran, H.; Zhang, S.; Yan, H.; Chen, H.; Yuen, P. Y., An intrinsically stretchable high-performance polymer semiconductor with low crystallinity. *Adv. Funct. Mater.* **2019,** *29* (46), 1905340.

99.   Kroon, R.; Hofmann, A. I.; Yu, L.; Lund, A.; Müller, C., Thermally Activated in Situ Doping Enables Solid-State Processing of Conducting Polymers. *Chem. Mater.* **2019,** *31* (8), 2770-2777.

100.   Moulton, J.; Smith, P., Electrical and mechanical properties of oriented poly(3-alkylthiophenes): 2. Effect of side-chain length. *Polymer* **1992,** *33* (11), 2340-2347.

101.   Moulton, J.; Smith, P., Electrical and mechanical properties of oriented poly (3-alkylthiophenes) I. Doping-enhanced stiffness of poly (3-octylthiophene). *Synth. Met.* **1991,** *40* (1), 13-22.

102.   Sharma, A.; Pan, X.; Bjuggren, J. M.; Gedefaw, D.; Xu, X.; Kroon, R.; Wang, E.; Campbell, J. A.; Lewis, D. A.; Andersson, M. R., Probing the Relationship between Molecular Structures, Thermal Transitions, and Morphology in Polymer Semiconductors Using a Woven Glass-Mesh-Based DMTA Technique. *Chem. Mater.* **2019,** *31* (17), 6740-6749.

103.   Sharma, A.; Pan, X.; Campbell, J. A.; Andersson, M. R.; Lewis, D. A., Unravelling the Thermomechanical Properties of Bulk Heterojunction Blends in Polymer Solar Cells. *Macromolecules* **2017,** *50* (8), 3347-3354.

104.   Xiao, M.; Sadhanala, A.; Abdi-Jalebi, M.; Thomas, T. H.; Ren, X.; Zhang, T.; Chen, H.; Carey, R. L.; Wang, Q.; Senanayak, S. P.; Jellett, C.; Onwubiko, A.; Moser, M.; Liao, H.; Yue, W.; McCulloch, I.; Nikolka, M.; Sirringhaus, H., Linking Glass-Transition Behavior to Photophysical and Charge Transport Properties of High-Mobility Conjugated Polymers. *Adv. Funct. Mater.* **2021,** *31* (7), 2007359.

105.   Rivnay, J.; Inal, S.; Salleo, A.; Owens, R. M.; Berggren, M.; Malliaras, G. G., Organic electrochemical transistors. *Nat. Rev. Mater.* **2018,** *3* (2), 17086.

106.   Savva, A.; Cendra, C.; Giugni, A.; Torre, B.; Surgailis, J.; Ohayon, D.; Giovannitti, A.; McCulloch, I.; Di Fabrizio, E.; Salleo, A.; Rivnay, J.; Inal, S., Influence of Water on the Performance of Organic Electrochemical Transistors. *Chem. Mater.* **2019,** *31* (3), 927-937.

107.   Moser, M.; Savagian, L. R.; Savva, A.; Matta, M.; Ponder, J. F.; Hidalgo, T. C.; Ohayon, D.; Hallani, R.; Reisjalali, M.; Troisi, A.; Wadsworth, A.; Reynolds, J. R.; Inal, S.; McCulloch, I., Ethylene Glycol-Based Side Chain Length Engineering in Polythiophenes and its Impact on Organic Electrochemical Transistor Performance. *Chem. Mater.* **2020,** *32* (15), 6618-6628.

108.   Song, C. K.; Eckstein, B. J.; Tam, T. L. D.; Trahey, L.; Marks, T. J., Conjugated Polymer Energy Level Shifts in Lithium-Ion Battery Electrolytes. *ACS Appl. Mater. Interfaces* **2014,** *6* (21), 19347-19354.

109.   Moia, D.; Giovannitti, A.; Szumska, A. A.; Maria, I. P.; Rezasoltani, E.; Sachs, M.; Schnurr, M.; Barnes, P. R. F.; McCulloch, I.; Nelson, J., Design and evaluation of conjugated polymers with polar side chains as electrode materials for electrochemical energy storage in aqueous electrolytes. *Energy Environ. Sci.* **2019,** *12* (4), 1349-1357.

110.   Volkov, A. V.; Sun, H.; Kroon, R.; Ruoko, T.-P.; Che, C.; Edberg, J.; Müller, C.; Fabiano, S.; Crispin, X., Asymmetric Aqueous Supercapacitor Based on p- and n-Type Conducting Polymers. *ACS Appl. Energy Mater.* **2019,** *2* (8), 5350-5355.

111.   Brebels, J.; Manca, J. V.; Lutsen, L.; Vanderzande, D.; Maes, W., High dielectric constant conjugated materials for organic photovoltaics. *J. Mater. Chem. A* **2017,** *5* (46), 24037-24050.

112.   Kiefer, D.; Giovannitti, A.; Sun, H.; Biskup, T.; Hofmann, A.; Koopmans, M.; Cendra, C.; Weber, S.; Anton Koster, L. J.; Olsson, E.; Rivnay, J.; Fabiano, S.; McCulloch, I.; Müller, C., Enhanced n-

Doping Efficiency of a Naphthalenediimide-Based Copolymer through Polar Side Chains for Organic Thermoelectrics. *ACS Energy Lett.* **2018,** *3* (2), 278-285.

113.   Liu, J.; Qiu, L.; Alessandri, R.; Qiu, X.; Portale, G.; Dong, J.; Talsma, W.; Ye, G.; Sengrian, A. A.; Souza, P. C. T.; Loi, M. A.; Chiechi, R. C.; Marrink, S. J.; Hummelen, J. C.; Koster, L. J. A., Enhancing Molecular n-Type Doping of Donor–Acceptor Copolymers by Tailoring Side Chains. *Adv. Mater.* **2018,** *30* (7), 1704630.

114.   Meng, B.; Liu, J.; Wang, L., Oligo(ethylene glycol) as side chains of conjugated polymers for optoelectronic applications. *Polym. Chem.* **2020,** *11* (7), 1261-1270.

115.   Ohayon, D.; Nikiforidis, G.; Savva, A.; Giugni, A.; Wustoni, S.; Palanisamy, T.; Chen, X.; Maria, I. P.; Di Fabrizio, E.; Costa, P. M. F. J.; McCulloch, I.; Inal, S., Biofuel powered glucose detection in bodily fluids with an n-type conjugated polymer. *Nat. Mater.* **2020,** *19* (4), 456-463.

116.   Giovannitti, A.; Sbircea, D.-T.; Inal, S.; Nielsen, C. B.; Bandiello, E.; Hanifi, D. A.; Sessolo, M.; Malliaras, G. G.; McCulloch, I.; Rivnay, J., Controlling the mode of operation of organic transistors through side-chain engineering. *Proc. Natl. Acad. Sci. U.S.A.* **2016,** *113* (43), 12017.

117.   Nielsen, C. B.; Giovannitti, A.; Sbircea, D.-T.; Bandiello, E.; Niazi, M. R.; Hanifi, D. A.; Sessolo, M.; Amassian, A.; Malliaras, G. G.; Rivnay, J.; McCulloch, I., Molecular Design of Semiconducting Polymers for High-Performance Organic Electrochemical Transistors. *J. Am. Chem. Soc.* **2016,** *138* (32), 10252-10259.

118.   Giovannitti, A.; Nielsen, C. B.; Sbircea, D.-T.; Inal, S.; Donahue, M.; Niazi, M. R.; Hanifi, D. A.; Amassian, A.; Malliaras, G. G.; Rivnay, J.; McCulloch, I., N-type organic electrochemical transistors with stability in water. *Nat. Commun.* **2016,** *7* (1), 13066.

119.   Savva, A.; Hallani, R.; Cendra, C.; Surgailis, J.; Hidalgo, T. C.; Wustoni, S.; Sheelamanthula, R.; Chen, X.; Kirkus, M.; Giovannitti, A.; Salleo, A.; McCulloch, I.; Inal, S., Balancing Ionic and Electronic Conduction for High-Performance Organic Electrochemical Transistors. *Adv. Funct. Mater.* **2020,** *30* (11), 1907657.

120.   Moser, M.; Gladisch, J.; Ghosh, S.; Hidalgo, T. C.; Ponder Jr., J. F.; Sheelamanthula, R.; Thiburce, Q.; Gasparini, N.; Wadsworth, A.; Salleo, A.; Inal, S.; Berggren, M.; Zozoulenko, I.; Stavrinidou, E.; McCulloch, I., Controlling Electrochemically Induced Volume Changes in Conjugated Polymers by Chemical Design: from Theory to Devices. *Adv. Funct. Mater.* **2021,** *31* (26), 2100723.

121.   He, Y.; Kukhta, N. A.; Marks, A.; Luscombe, C. K., The effect of side chain engineering on conjugated polymers in organic electrochemical transistors for bioelectronic applications. *J. Mater. Chem. C* **2022,** *10* (7), 2314-2332.

122.   Zokaei, S.; Kroon, R.; Gladisch, J.; Paulsen, B. D.; Sohn, W.; Hofmann, A. I.; Persson, G.; Stamm, A.; Syrén, P.-O.; Olsson, E.; Rivnay, J.; Stavrinidou, E.; Lund, A.; Müller, C., Toughening of a Soft Polar Polythiophene through Copolymerization with Hard Urethane Segments. *Adv. Sci.* **2021,** *8* (2), 2002778.

123.   Balar, N.; Rech, J. J.; Siddika, S.; Song, R.; Schrickx, H. M.; Sheikh, N.; Ye, L.; Megret Bonilla, A.; Awartani, O.; Ade, H.; You, W.; O'Connor, B. T., Resolving the Molecular Origin of Mechanical Relaxations in Donor–Acceptor Polymer Semiconductors. *Adv. Funct. Mater.* **2022,** *32* (4), 2105597.

124.   Szycher, M., Szycher's Handbook of Polyurethanes. 2nd ed.; CRC Press: **1991**; p 1112.

125.   Chittibabu, K. G.; Balasubramanian, S.; Kim, W. H.; Cholli, A. L.; Kumar, J.; Tripathy, S. K., Synthesis and Properties of a Soluble Polythiophene Derivative with a Urethane Side Chain. *J. Macromol. Sci. A* **1996,** *33* (9), 1283-1300.

126.   Zokaei, S.; Kroon, R.; Gladisch, J.; Paulsen, B. D.; Sohn, W.; Hofmann, A. I.; Persson, G.; Stamm, A.; Syrén, P.-O.; Olsson, E.; Rivnay, J.; Stavrinidou, E.; Lund, A.; Müller, C., Toughening of a Soft Polar Polythiophene through Copolymerization with Hard Urethane Segments. *Adv. Sci.* **2021,** *8* (2), 2002778.

127.   Kiefer, D.; Kroon, R.; Hofmann, A. I.; Sun, H.; Liu, X.; Giovannitti, A.; Stegerer, D.; Cano, A.; Hynynen, J.; Yu, L.; Zhang, Y.; Nai, D.; Harrelson, T. F.; Sommer, M.; Moulé, A. J.; Kemerink, M.; Marder, S. R.; McCulloch, I.; Fahlman, M.; Fabiano, S.; Müller, C., Double doping of conjugated polymers with monomer molecular dopants. *Nat. Mater.* **2019,** *18* (2), 149-155.

128.   Fanous, J.; Schweizer, M.; Schawaller, D.; Buchmeiser, M. R., Crystalline and Conductive Poly(3-hexylthiophene) Fibers. *Macromol. Mater. Eng.* **2012,** *297* (2), 123-127.

129.   Brandão, L.; Viana, J.; Bucknall, D. G.; Bernardo, G., Solventless processing of conjugated polymers—A review. *Synth. Met.* **2014,** *197*, 23-33.

130.   Österholm, J. E.; Laakso, J.; Nyholm, P.; Isotalo, H.; Stubb, H.; Inganäs, O.; Salaneck, W. R., Melt and solution processable poly(3-alkylthiophenes) and their blends. *Synth. Met.* **1989,** *28* (1), 435-444.

131.   Laakso, J.; Österholm, J. E.; Nyholm, P., Conducting polymer blends. *Synth. Met.* **1989,** *28* (1), 467-471.

132.   Hase, H.; O'Neill, K.; Frisch, J.; Opitz, A.; Koch, N.; Salzmann, I., Unraveling the Microstructure of Molecularly Doped Poly(3-hexylthiophene) by Thermally Induced Dedoping. *J. Phys. Chem. C* **2018,** *122* (45), 25893-25899.

133.   Hofmann, A. I.; Kroon, R.; Yu, L.; Müller, C., Highly stable doping of a polar polythiophene through co-processing with sulfonic acids and bistriflimide. *J. Mater. Chem. C* **2018,** *6* (26), 6905-6910.

134.   Lu, X.; Ng, H. Y.; Xu, J.; He, C., Electrical conductivity of polyaniline–dodecylbenzene sulphonic acid complex: thermal degradation and its mechanism. *Synth. Met.* **2002,** *128* (2), 167-178.

135.   Silver, F. H.; Freeman, J. W.; DeVore, D., Viscoelastic properties of human skin and processed dermis. *Skin Res. Technol.* **2001,** *7*, 18-23.

136.   Yamada, T.; Hayamizu, Y.; Yamamoto, Y.; Yomogida, Y.; Izadi-Najafabadi, A.; Futaba, D. N.; Hata, K., A stretchable carbon nanotube strain sensor for human-motion detection. *Nat. Nanotechnol.* **2011,** *6* (5), 296-301.

137.   Hofmann, A. I.; Ostergren, I.; Kim, Y.; Fauth, S.; Craighero, M.; Yoon, M. H.; Lund, A.; Muller, C., All-Polymer Conducting Fibers and 3D Prints via Melt Processing and Templated Polymerization. *ACS Appl. Mater. Interfaces* **2020,** *12* (7), 8713-8721.

138.   Gao, Q.; Wang, M.; Kang, X.; Zhu, C.; Ge, M., Continuous wet-spinning of flexible and water-stable conductive PEDOT: PSS/PVA composite fibers for wearable sensors. *Compos. Commun.* **2020,** *17*, 134-140.

139.   He, Z.; Byun, J.-H.; Zhou, G.; Park, B.-J.; Kim, T.-H.; Lee, S.-B.; Yi, J.-W.; Um, M.-K.; Chou, T.-W., Effect of MWCNT content on the mechanical and strain-sensing performance of Thermoplastic Polyurethane composite fibers. *Carbon* **2019,** *146*, 701-708.

140.   Fan, Q.; Zhang, X.; Qin, Z., Preparation of Polyaniline/Polyurethane Fibers and Their Piezoresistive Property. *J. Macromol. Sci., Part B* **2012,** *51* (4), 736-746.

141.   Tian, G.; Zhou, J.; Xin, Y.; Tao, R.; Jin, G.; Lubineau, G., Copolymer-enabled stretchable conductive polymer fibers. *Polymer* **2019,** *177*, 189-195.

142.   Jiang, S.; Zhang, H.; Song, S.; Ma, Y.; Li, J.; Lee, G. H.; Han, Q.; Liu, J., Highly Stretchable Conductive Fibers from Few-Walled Carbon Nanotubes Coated on Poly(m-phenylene isophthalamide) Polymer Core/Shell Structures. *ACS Nano* **2015,** *9* (10), 10252-10257.

143.   Sun, F.; Tian, M.; Sun, X.; Xu, T.; Liu, X.; Zhu, S.; Zhang, X.; Qu, L., Stretchable Conductive Fibers of Ultrahigh Tensile Strain and Stable Conductance Enabled by a Worm-Shaped Graphene Microlayer. *Nano Lett.* **2019,** *19* (9), 6592-6599.

144.   Zhou, J.; Li, E. Q.; Li, R.; Xu, X.; Ventura, I. A.; Moussawi, A.; Anjum, D. H.; Hedhili, M. N.; Smilgies, D.-M.; Lubineau, G.; Thoroddsen, S. T., Semi-metallic, strong and stretchable wet-spun conjugated polymer microfibers. *J. Mater. Chem. C* **2015,** *3* (11), 2528-2538.

145.   Kim, Y.; Lund, A.; Noh, H.; Hofmann, A. I.; Craighero, M.; Darabi, S.; Zokaei, S.; Park, J. I.; Yoon, M.-H.; Müller, C., Robust PEDOT:PSS Wet-Spun Fibers for Thermoelectric Textiles. *Macromol. Mater. Eng* . **2020,** *305* (3), 1900749.

146.   Wang, M.; Gao, Q.; Gao, J.; Zhu, C.; Chen, K., Core–shell PEDOT:PSS/SA composite fibers fabricated via a single-nozzle technique enable wearable sensor applications. *J. Mater. Chem. C* **2020,** *8* (13), 4564-4571.

147.   Seyedin, S.; Zhang, P.; Naebe, M.; Qin, S.; Chen, J.; Wang, X.; Razal, J. M., Textile strain sensors: a review of the fabrication technologies, performance evaluation and applications. *Mater. Horiz.* **2019,** *6* (2), 219-249.

148.   Ding, Y.; Xu, W.; Wang, W.; Fong, H.; Zhu, Z., Scalable and Facile Preparation of Highly Stretchable Electrospun PEDOT:PSS@PU Fibrous Nonwovens toward Wearable Conductive Textile Applications. *ACS Appl. Mater. Interfaces* **2017,** *9* (35), 30014-30023.

149.   Lee, S.; Shin, S.; Lee, S.; Seo, J.; Lee, J.; Son, S.; Cho, H. J.; Algadi, H.; Al-Sayari, S.; Kim, D. E.; Lee, T., Ag Nanowire Reinforced Highly Stretchable Conductive Fibers for Wearable Electronics. *Adv. Funct. Mater.* **2015,** *25* (21), 3114-3121.

150.   Bilotti, E.; Zhang, R.; Deng, H.; Baxendale, M.; Peijs, T., Fabrication and property prediction of conductive and strain sensing TPU/CNT nanocomposite fibres. *J. Mater. Chem.* **2010,** *20* (42).

151.   Lu, Y.; Jiang, J.; Yoon, S.; Kim, K. S.; Kim, J. H.; Park, S.; Kim, S. H.; Piao, L., High-Performance Stretchable Conductive Composite Fibers from Surface-Modified Silver Nanowires and Thermoplastic Polyurethane by Wet Spinning. *ACS Appl. Mater. Interfaces* **2018,** *10* (2), 2093-2104.

152.   Ma, R.; Kang, B.; Cho, S.; Choi, M.; Baik, S., Extraordinarily High Conductivity of Stretchable Fibers of Polyurethane and Silver Nanoflowers. *ACS Nano* **2015,** *9* (11), 10876-10886.

153.   He, Z.; Zhou, G.; Byun, J.-H.; Lee, S.-K.; Um, M.-K.; Park, B.; Kim, T.; Lee, S. B.; Chou, T.-W., Highly stretchable multi-walled carbon nanotube/thermoplastic polyurethane composite fibers for ultrasensitive, wearable strain sensors. *Nanoscale* **2019,** *11* (13), 5884-5890.

154.   Zhao, X.; Chen, F.; Li, Y.; Lu, H.; Zhang, N.; Ma, M., Bioinspired ultra-stretchable and anti-freezing conductive hydrogel fibers with ordered and reversible polymer chain alignment. *Nat. Commun.* **2018,** *9* (1), 3579.

155.   Henriksson, M.; Berglund, L. A.; Isaksson, P.; Lindström, T.; Nishino, T., Cellulose Nanopaper Structures of High Toughness. *Biomacromolecules* **2008,** *9* (6), 1579-1585.

156.   Svagan, A. J.; Azizi Samir, M. A. S.; Berglund, L. A., Biomimetic Polysaccharide Nanocomposites of High Cellulose Content and High Toughness. *Biomacromolecules* **2007,** *8* (8), 2556-2563.

157.   Henriksson, M.; Berglund, L. A., Structure and properties of cellulose nanocomposite films containing melamine formaldehyde. *J. Appl. Polym. Sci.* **2007,** *106* (4), 2817-2824.

158.   Janeni, J.; Adassooriya, N. M., Chapter 3 - Nanocellulose biopolymer-based biofilms: Applications and challenges. In *Biopolymer-Based Nano Films*, Rai, M.; dos Santos, C. A., Eds. Elsevier: **2021**; pp 43-62.

159.   Sehaqui, H.; Liu, A.; Zhou, Q.; Berglund, L. A., Fast Preparation Procedure for Large, Flat Cellulose and Cellulose/Inorganic Nanopaper Structures. *Biomacromolecules* **2010,** *11* (9), 2195-2198.

160.   Shankaran, D. R., Chapter 14 - Cellulose Nanocrystals for Health Care Applications. In *Applications of Nanomaterials*, Mohan Bhagyaraj, S.; Oluwafemi, O. S.; Kalarikkal, N.; Thomas, S., Eds. Woodhead Publishing: **2018**; pp 415-459.

161.   Awal, A.; Rana, M.; Sain, M., Thermorheological and mechanical properties of cellulose reinforced PLA bio-composites. *Mech. Mater.* **2015,** *80*, 87-95.

162.   Wang, B.; Torres-Rendon, J. G.; Yu, J.; Zhang, Y.; Walther, A., Aligned Bioinspired Cellulose Nanocrystal-Based Nanocomposites with Synergetic Mechanical Properties and Improved Hygromechanical Performance. *ACS Appl. Mater. Interfaces* **2015,** *7* (8), 4595-4607.

163.   Fernandes, S. C. M.; Freire, C. S. R.; Silvestre, A. J. D.; Pascoal Neto, C.; Gandini, A.; Berglund, L. A.; Salmén, L., Transparent chitosan films reinforced with a high content of nanofibrillated cellulose. *Carbohydr. Polym.* **2010,** *81* (2), 394-401.

164.   Atifi, S.; Hamad, W. Y., Emulsion-polymerized flexible semi-conducting CNCs–PANI–DBSA nanocomposite films. *RSC Adv.* **2016,** *6* (70), 65494-65503.

165.   Tkalya, E.; Ghislandi, M.; Thielemans, W.; van der Schoot, P.; de With, G.; Koning, C., Cellulose Nanowhiskers Templating in Conductive Polymer Nanocomposites Reduces Electrical Percolation Threshold 5-Fold. *ACS Macro Lett.* **2013,** *2* (2), 157-163.

166.   Mendez, J. D.; Weder, C., Synthesis, electrical properties, and nanocomposites of poly(3,4-ethylenedioxythiophene) nanorods. *Polym. Chem.* **2010,** *1* (8), 1237-1244.

167.   Mihranyan, A.; Nyholm, L.; Bennett, A. E. G.; Strømme, M., A Novel High Specific Surface Area Conducting Paper Material Composed of Polypyrrole and Cladophora Cellulose. *J. Phys. Chem. B* **2008,** *112* (39), 12249-12255.

168.   Suetsugu, Y., State of Dispersion – Mechanical Properties Correlation in Small Particle Filled Polymer Composites. *Int. Polym. Proc.* **1990,** *5* (3), 184-190.

169.   Stolwijk, N. A.; Heddier, C.; Reschke, M.; Wiencierz, M.; Bokeloh, J.; Wilde, G., Salt-Concentration Dependence of the Glass Transition Temperature in PEO–NaI and PEO–LiTFSI Polymer Electrolytes. *Macromolecules* **2013,** *46* (21), 8580-8588.